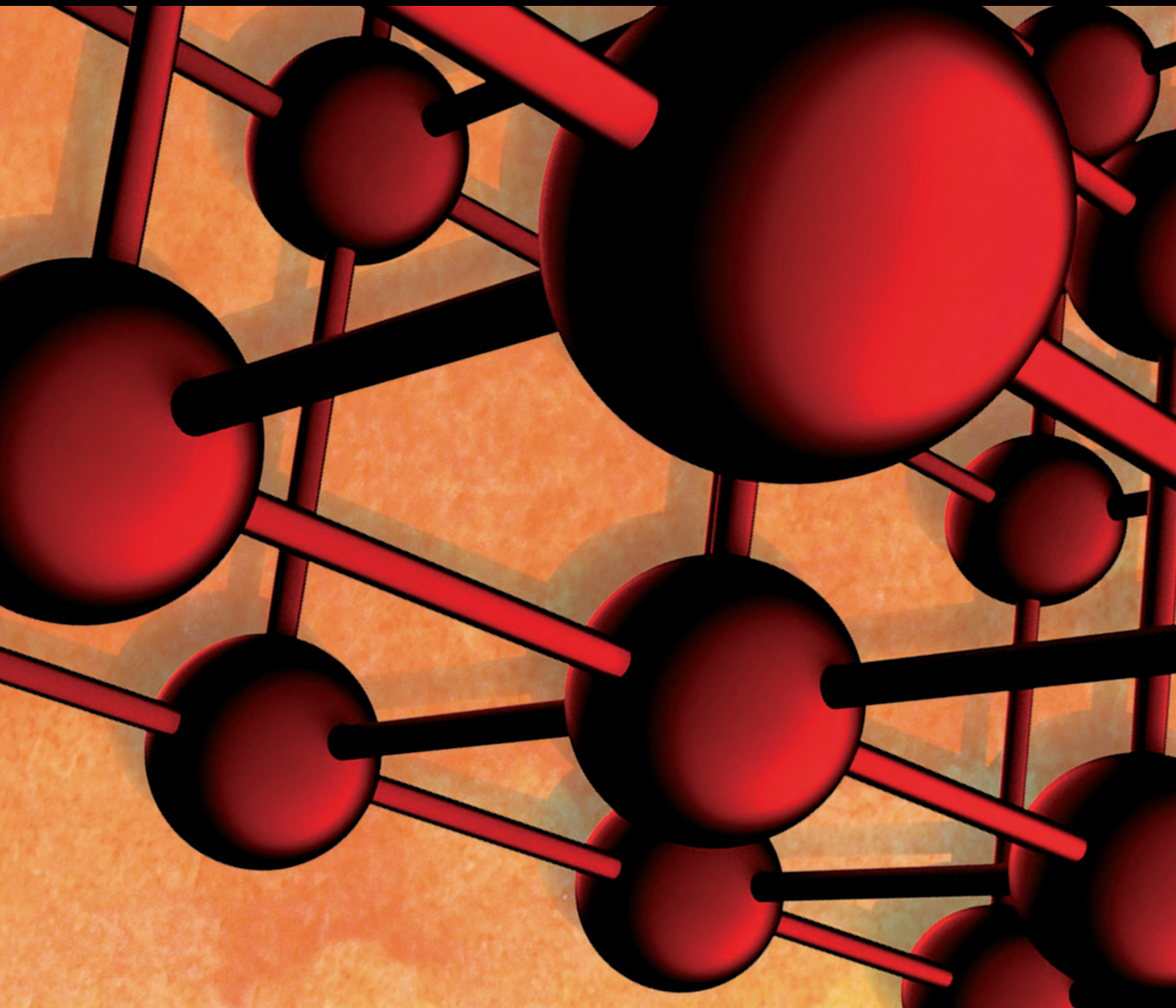# Sustainable Asphalt Pavements Using Alternative Binders

Lead Guest Editor: Ramadhansyah Putra Jaya
Guest Editors: Haryati Yaacob, Mohd Rosli Mohd Hasan, and Xu Yang
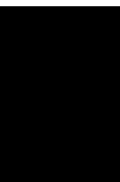
Sustainable Asphalt Pavements Using Alternative Binders

Sustainable Asphalt Pavements Using Alternative Binders

Lead Guest Editor: Ramadhansyah Putra Jaya
Guest Editors: Haryati Yaacob, Mohd Rosli Mohd Hasan, and Xu Yang

Achraf Ghorbal (iD), Tunisia
Georgios I. Giannopoulos (iD), Greece
Ivan Giorgio (iD), Italy
Andrea Grilli (iD), Italy
Vincenzo Guarino (iD), Italy
Daniel Guay, Canada
Jenö Gubicza (iD), Hungary
Xuchun Gui (iD), China
Benoit Guiffard (iD), France
Zhixing Guo, China
Ivan Gutierrez-Urrutia (iD), Japan
Weiwei Han (iD), Republic of Korea
Simo-Pekka Hannula, Finland
A. M. Hassan (iD), Egypt
Akbar Heidarzadeh, Iran
Yi Huang (iD), United Kingdom
Joshua Ighalo, Nigeria
Saliha Ilican (iD), Turkey
Md Mainul Islam (iD), Australia
Ilia Ivanov (iD), USA
Jijo James (iD), India
Hafsa Jamshaid (iD), Pakistan
Hom Kandel (iD), USA
Kenji Kaneko, Japan
Rajesh Kannan A (iD), Democratic People's
Republic of Korea
Mehran Khan (iD), Hong Kong
Akihiko Kimura, Japan
Ling B. Kong (iD), Singapore
Pramod Koshy, Australia
Hongchao Kou (iD), China
Alexander Kromka, Czech Republic
Abhinay Kumar, India
Avvaru Praveen Kumar (iD), Ethiopia
Sachin Kumar, India
Paweł Kłosowski (iD), Poland
Wing-Fu Lai (iD), Hong Kong
Luciano Lamberti, Italy
Fulvio Lavecchia (iD), Italy
Laurent Lebrun (iD), France
Joon-Hyung Lee (iD), Republic of Korea
Cristina Leonelli, Italy
Chenggao Li (iD), China
Rongrong Li (iD), China
Yuanshi Li, Canada

Guang-xing Liang (iD), China
Barbara Liguori (iD), Italy
Jun Liu (iD), China
Yunqi Liu, China
Rong Lu, China
Zhiping Luo (iD), USA
Fernando Lusquiños (iD), Spain
Himadri Majumder (iD), India
Dimitrios E. Manolakos (iD), Greece
Necmettin Maraşlı (iD), Turkey
Alessandro Martucci (iD), Italy
Roshan Mayadunne (iD), Australia
Mamoun Medraj (iD), Canada
Shazim A. Memon (iD), Kazakhstan
Pratima Meshram (iD), India
Mohsen Mhadhbi (iD), Tunisia
Philippe Miele, France
Andrey E. Miroshnichenko, Australia
Ajay Kumar Mishra (iD), South Africa
Hossein Moayedi (iD), Vietnam
Dhanesh G. Mohan (iD), United Kingdom
Sakar Mohan (iD), India
Namdev More, USA
Tahir Muhmood (iD), China
Faisal Mukhtar (iD), Pakistan
Dr. Tauseef Munawar (iD), Pakistan
Roger Narayan (iD), USA
Saleem Nasir (iD), Pakistan
Elango Natarajan, Malaysia
Rufino M. Navarro, Spain
Miguel Navarro-Cia (iD), United Kingdom
Behzad Nematollahi (iD), Australia
Peter Niemz, Switzerland
Hiroshi Noguchi, Japan
Dariusz Oleszak (iD), Poland
Laurent Orgéas (iD), France
Togay Ozbakkaloglu, United Kingdom
Marián Palcut (iD), Slovakia
Davide Palumbo (iD), Italy
Gianfranco Palumbo (iD), Italy
Murlidhar Patel, India
Zbyšek Pavlík (iD), Czech Republic
Alessandro Pegoretti (iD), Italy
Gianluca Percoco (iD), Italy
Andrea Petrella, Italy

Contents

Hindawi

Research Article

The Influence of Nano Titanium as Bitumen Modifier in Stone Mastic Asphalt

Khairil Azman Masri [1,2] **Nur Syafiqah Shamimi Mohd Zali,**[1]
Ramadhansyah Putra Jaya,[1] **Mazlan Abu Seman,**[1] **and Mohd Rosli Mohd Hasan**[3]

¹*Department of Civil Engineering, College of Engineering, Universiti Malaysia Pahang, 26300 Gambang, Kuantan,*
 Pahang, Malaysia
²*Earth Resources and Sustainability Centre (ERAS), Universiti Malaysia Pahang, 26300 Gambang, Kuantan, Pahang, Malaysia*
³*School of Civil Engineering, Universiti Sains Malaysia, Engineering Campus, 14300 Nibong Tebal, Pulau Pinang, Malaysia*

Correspondence should be addressed to Khairil Azman Masri; khairilazman@ump.edu.my

Nanomaterials are emerging as one of the methods to improve the pavement industry. Due to that, this study explores the influence of nano TiO_2 modified binder and mixture with 60/70 grade bitumen. The first stage discovers the physical properties of bitumen by undergoing penetration and softening point tests. Then, the nano TiO_2 modified binder is evaluated in terms of its morphological and chemical properties. To verify the modified binder design, the mechanical performance of stone mastic asphalt (SMA) is assessed in terms of volumetric properties. From the results, 5% nano TiO_2 modified binder shows significant improvement in terms of penetration and softening point. The results also show that the 3% nano TiO_2 modified binder contributes the highest improvement in terms of its chemical properties and the morphological properties. Based on the morphological properties' evaluation, FTIR and XRD observed a sharp peak of nano TiO_2 while the bitumen containing nano TiO_2 is well distributed when SEM-EDX was applied. In addition, the volumetric properties of SMA also significantly improve with the addition of nano TiO_2. It can be said that the addition of nano TiO_2 is able to enhance the overall properties of bitumen.

1. Introduction

Stone mastic asphalt has widely been used in countries such as Unites States, Europe, and Asian countries like Malaysia [1]. The need to use SMA is due to the increasing traffic users over the years which make SMA a suitable choice since it is known to withstand high loads [2]. SMA originated from Germany only consists of coarse aggregates and bitumen as a filler in which the mix is held by the strong elastic properties of the binder [3]. However, with modernisation and new technology introductions, the SMA has been incorporated with many materials in such ways that the materials can improve the SMA properties. A modification to the mixture is one of the methods introduced. Some suggested changes include adding materials as an additive, rejuvenators, or even stabilizers. The focus would be on the aftereffect of the

mechanical effect that the materials have on the SMA, but binder modification has not been further researched in depth [4].

Nanomaterials are chemical compounds or products that are processed and used on a very small scale. The size of nanomaterials is between 1 to 100 nanometres (nm) [5]. They previously have been used in the healthcare industry, beauty products, and biology-related field, and it is priorly used in construction also before embarking to the pavement industry [6]. Nanomaterials have many types of applications depending on their respective type and size. Some of the commonly used nano materials that are always encountered are nano clay, nano silica, nano-sized metals such as copper, zinc, and aluminium oxide [7]. Aging is a concern of asphalt mixtures, and there are two types of it which are thermal oxidative aging and photo oxidative aging [8]. This is where

Properties	Descriptions
Colour	White
Purity	99.9%
Primary particle size	20 nm
Structure	Anatase, Rutile, Brookite
Melting point	1843°C
Boiling point	2972°C
Relative density at 25°C	4.26 g/cm3

the surface modified nanomaterials such as nano silica, nano zinc oxide, and nano TiO$_2$ act as they could improve the antiaging behaviour of asphalt [9].

Nano clay is naturally occurring minerals, and its purity could affect the final nanocomposite properties. Due to their low cost of production, it is commonly used as it has potential to improve mechanical and thermal binder properties [10]. Nano silica properties such as its good stability, affordable cost, high surface area, chemical purity, and good dispersing ability have made it one of the most used materials over the years in improving the mechanical performance of asphalt such as aging, fatigue, and cracking [11].

Among the mentioned nanomaterials, nano TiO$_2$ was chosen due to its properties such as higher reactivity with bitumen due to its small size [12]. It possesses photocatalytic properties which could help in eliminating hazardous gases like nitrogen monoxide [13]. This promotes the environmentally friendly area of the asphalt pavement. Nano TiO$_2$ also improve the asphalt aging properties [14]. Furthermore, nano TiO$_2$ could reduce binder drain down properties by increasing the adhesion between aggregates and bitumen when added into the mix as the nano particles fill the voids that is present and make the structure more compact [15].

This study is aimed to investigate the binder modification by incorporating it with nano titanium and its effect to the SMA. Different percentages of nano TiO$_2$ starting from 1 to 5% will be mixed with the bitumen and will further be accessed. Among the test that will be done on the samples would be the traditional bitumen test which are penetration test and softening point. Then, the sample would be further analysed in terms of morphology and chemical aspects by Fourier transform method analysis (FTIR), scanning electron microscope (SEM-EDX), and X-ray diffraction analysis (XRD). The volumetric properties of SMA are also investigated after the nano TiO$_2$ modified bitumen is included in the SMA mix. The test results show that 3% nano TiO$_2$ modified bitumen has improved the bitumen in terms of its physical properties, rheology, morphology, and chemical characteristics. The volumetric properties of SMA also experience positive enhancement due to the binder modification.

2. Materials and Methods

2.1. Nano Titanium.
The sizes of nano TiO$_2$ are between 10 to 15 nanometres and in white powder form supplied by the local supplier. Table 1 shows the properties of nano TiO$_2$ used for experimental works. Based on Table 1, the usage of nano TiO$_2$ is suitable for bitumen modification due to its high melting and boiling point as well as its structure.

2.2. Bitumen.
The bitumen currently utilised has a 60/70 penetration grade. Table 2 shows the properties of the asphalt binder used in the experimental works.

2.2.1. Preparation of Nano TiO$_2$ Modified Binder.
A mechanical mixer was used to prepare the nano TiO$_2$ modified binder at 1500 rpm and 160°C for 60 minutes. A

predetermined amount of bitumen was obtained and put in the oven for approximately 1.5 to 2 hours until it melted. About 500 g of bitumen was then weighted before mixing with 1 to 5% nano TiO$_2$. The mixture was mixed for 30 minutes while adding the nano TiO$_2$ gradually and further 30 minutes of additional mixing to ensure its homogeneity.

2.3. Experimental Methods

2.3.1. Stone Mastic Asphalt (SMA) Sample Preparation.
SMA samples were prepared according to the Malaysian standard specification JKR/SPJ/S4, by incorporating 6.16% optimum binder content [16] and compacted using a Marshall compactor with 50 blows on each face. Figure 1 represents the aggregate grading used to fabricate asphalt mixture specimens. Sieve analysis was performed to obtain the required aggregated mass based on the targeted specification. The SMA aggregate grading is shown in Figure 1.

2.3.2. Morphological Tests for the Bitumen

(1) Fourier Transform Infrared (FTIR) Spectroscopy. Fourier Transform infrared (FTIR) spectroscopy is an analytical technique used to identify organic, polymeric, and, in some cases, inorganic materials. The technique uses infrared light to scan test samples and observe chemical properties. The qualitative analysis identifies characteristic absorption peaks for the functional group of interest, such as polymer components, carbon, and sulphur oxidation products [17]. In this study, the attenuated total reflectance Fourier-transform infrared (ATR-FTIR) spectroscopy was used to evaluate the modified binder. The sample was prepared by cooling off the bitumen-nano TiO$_2$ mixture before being compacted into a small sphere and placed on a small microscopic slide.

(2) X-Ray Diffraction (XRD). X-ray diffraction or XRD is a nondestructive test method used to analyse the structure of crystalline materials. XRD analysis identifies crystalline phases present in a material, revealing chemical composition information. X-rays are directed toward samples by applying the voltage, and reflected X-rays are gathered by the detector [18]. The phase identification of bitumen was analysed using XRD at [°2θ] theta. Samples were prepared by cooling the bitumen mixture and made into small solid spheres. XRD graph peaks were produced after the testing was finished.

TABLE 2: Properties of 60/70 grade bitumen.

Properties	Descriptions	Material used
Specific gravity @25°C	1.01/1.06 kg/cm^3	1.03
Penetration @25°C	60–70 mm	65
Softening point @25°C	49–56°C	53
Ductility @25°C	100 cm	100
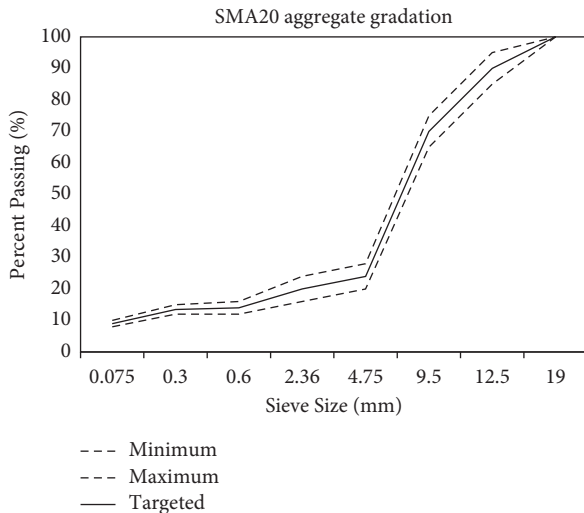
FIGURE 1: The SMA aggregate grading.

2.3.3. Scanning Electron Microscopy with Energy Dispersive X-ray Analysis (SEM-EDX). Scanning electron microscopy (SEM) with energy dispersive X-ray analysis (EDX) provides detailed high-resolution images of the sample by reprojecting a focused electron beam across the surface and detecting secondary or backscattered electron signal. Sample preparation involves cooling the bitumen until it hardens before scrapped into a small portion and observed under the microscope at desired magnifications. Further analysis using EDX was performed to identify the elements present in bitumen samples.

2.3.4. Physical Tests for Bitumen

(1) Softening Point. Bitumen was melted and poured into a pair of rings placed on a plate covered with Vaseline. After the specimen cooled, the ring was suspended in distilled water at 5 ± 2°C for 15 minutes. Steel balls were also placed on the surface of the bitumen in the ring. Then, the bath liquid was stirred and heated at a rate of 5 ± 2°C per minute. A thermometer was placed in the middle of the ring holder, levelled with the bottom of the ring. When the ball passed and dropped into the base plate, the temperature was recorded.

(2) Penetration Test. Specimens were prepared in a sample container and placed in a water bath at room temperature for 1 to 1.5 hours before the test. Then, the penetrometer dial reading was set to zero. The penetration needle was cleaned and fixed into the holder and guide. For a normal test, the precisely dimensioned needle was loaded to 100 ± 0.05 g. Next, the needle was slowly lowered until the tip makes contact with its image on the sample's surface at right angles. The needle holder was released to penetrate the bitumen for 5 ± 0.1s at a constant temperature of 25 ± 0.1°C. The penetration was measured in millimetre (mm).

2.3.5. Volumetric Properties of SMA. This test was conducted on eight samples with two samples each for 0%, 2%, 3%, and 4%. Before testing, the samples were conditioned by placing them in a water bath at a temperature of 60°C for 30 minutes. Then, the samples were placed on a Marshall stability machine and subjected to a force sufficient to break the sample to determine the Marshall Stability. Volumetric properties obtained such as density, stability, flow, and stiffness were recorded.

The following tests were conducted according to the flowchart provided Figure 2.

3. Results and Discussion

3.1. Fourier Transform Infrared Spectroscopy. Figure 3(a) shows the IR spectrum of the original bitumen experiencing a N-H stretching at 3395.75 cm^{-1}. This peak is observed at the 3100–3500 cm^{-1} region which it could be seen that it appears as a wide and broad-shaped spectrum with medium strength. The spectrum then becomes longer and shorter as more nano TiO$_2$ is added. The two peaks at 2923.75 cm^{-1} and 2852.09 cm^{-1} which later appears are related to the C-H symmetric stretching (-CH2) and the C-H asymmetric vibrations (-CH3 and -CH2) due to the presence of hydrocarbon chain segments that usually exist in the bitumen. Figure 3(b) shows some of the functional groups for the bitumen.

Next, from Figure 3(c), it shows that all of the nano TiO$_2$ modified bitumen have almost the same peaks, but at 3% nano TiO$_2$ modified bitumen, there is a new absorption bond that is observed. That is when nano TiO$_2$ is included the original region of 3100–3500 cm^{-1} which then makes the N-H bonds does not appear anymore. It is instead replaced with the two peaks at the 2851–3100 cm^{-1} region which are 2923.14 cm^{-1} and 2851.96 cm^{-1}. These peaks appear as there are interactions between the C-H and O-H bonds of the nano titanium with the bitumen mix; these bonds are stretching with medium strength. The results are consistent with a study by Lin et al.

Going into the 1700 cm^{-1} region, a remarkable peak at 1700.49 cm^{-1} is observed at the carboxylic region indicating that oxidation happens in this region and carbonyl group (C = O) is present. Next, the two peaks observed at 1462.37 cm^{-1} and 1376.67 cm^{-1} are assigned to the O-H bond which experiences bending with medium strength. In which this 1376.67 cm^{-1} peak is a response to the phenol group. Lastly, the 721.20 cm^{-1} peak is due to the presence of C double bond (C = C) in the nano TiO$_2$ modified bitumen sample.
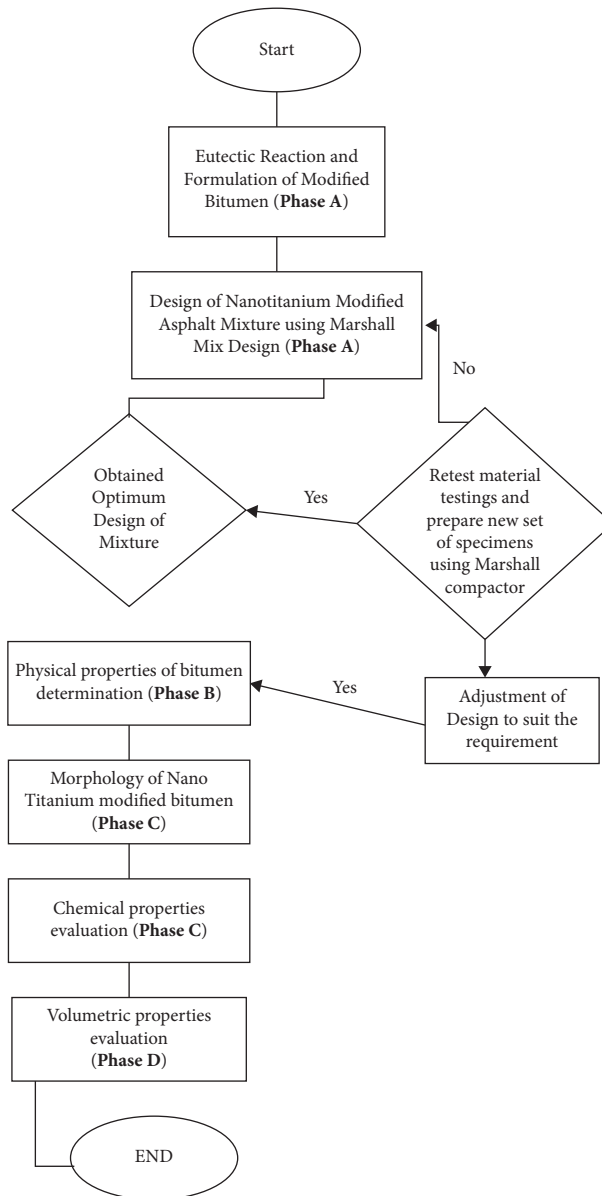
FIGURE 2: Flowchart of the research approach.

3.2. X-Ray Diffraction (XRD). Figures 4 and 5 depict the result of XRD on the unmodified and modified bitumen with nano TiO_2 sample. A close check on the nano TiO_2 powder is also done revealing that the nano titanium is of crystallised structure since sharp peaks are produced along the 25–75-degree peaks. The peak for the virgin bitumen is observed between 20–25 degree which has the peak 23.96 and 26.27 degrees as these peaks are due to the aliphatic chains and layers of condensed saturated rings since it is plain bitumen and is completely amorphous.

After the addition of nano TiO_2 in the bitumen, all of the samples show that the peak intensity rises, and this indicates that the nano TiO_2 particles have successfully incorporated themselves into the bitumen since the starting peak is higher than the starting peak for the original bitumen. The result trend is consistent with a study by Razavi and Kavussi [18].

The highest starts from 2%, followed by 3%, 5%, 4%, and 1%. But only 2% and 3% show that the peak intensity continues to develop up until 60 and 63 degrees, respectively. 3% is chosen as the bitumen continues to develop furthest with the influence of nano TiO_2. This shows that a little amount of nano TiO_2 such as 2% is able to contribute to the inner structure improvement of virgin bitumen.

3.3. Scanning Electron Microscopy with Energy Dispersive X-Ray Analysis (SEM-EDX). Figure 6 shows the morphology of the bitumen both before and after being added with nano titanium powder. Again, SEM analysis is performed to see the condition of the nano titanium when mixed with bitumen. For the unmodified bitumen, the black stripe is the bitumen in the liquid state, and since the sample is semisolid,

IR Spectral Interpretation results for: ***bitumen
Date: Tue Jan 05 10:41:29 2021 (GMT+08:00)

***bitumen
Aliphatic Primary Amines
Aliphatic Hydrocarbons
Primary Aliphatic Alcohols
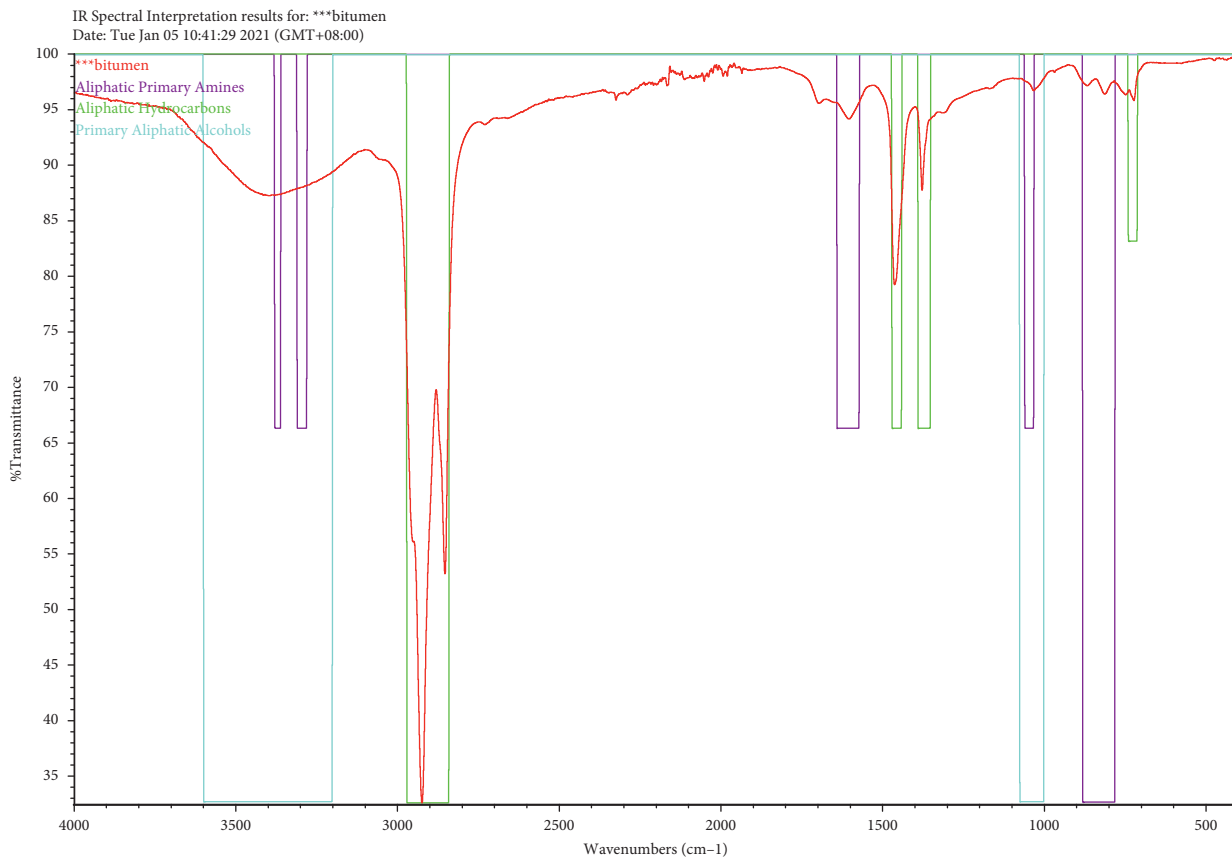
(a)
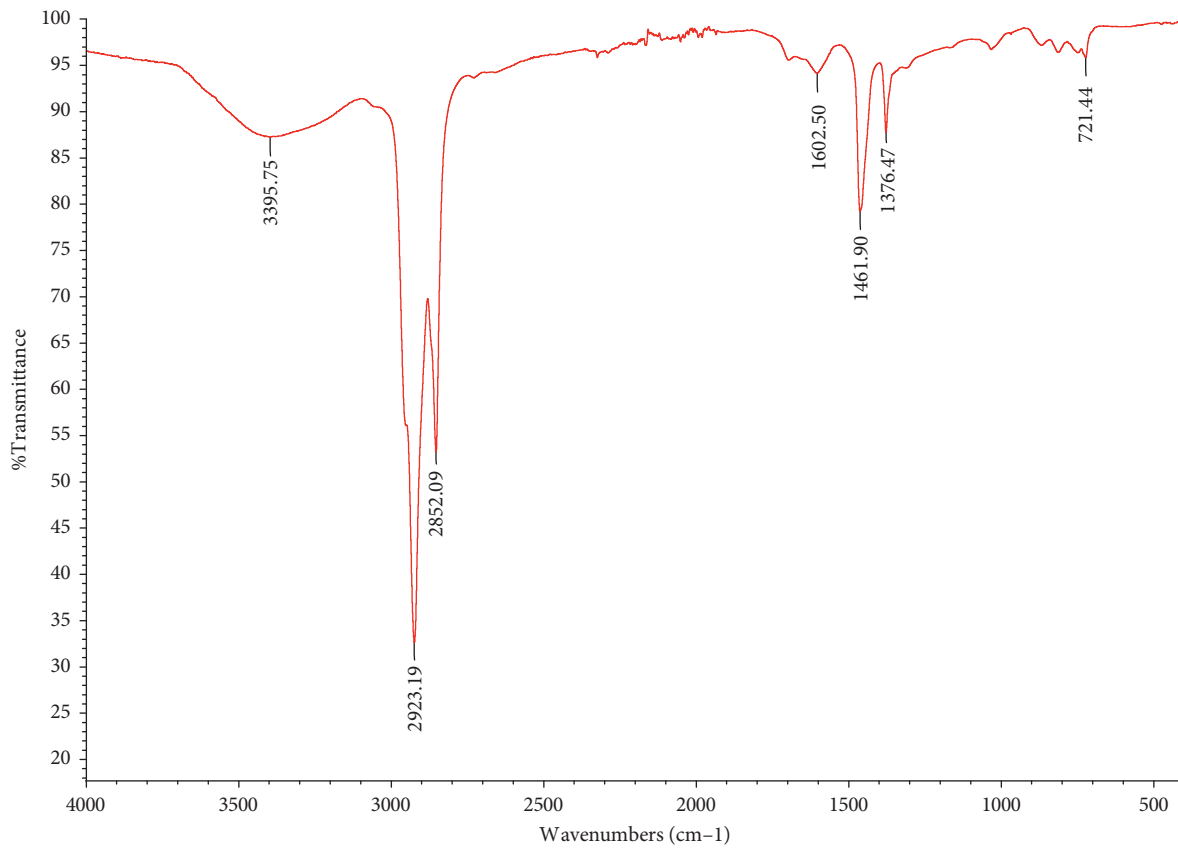
(b)

FIGURE 3: Continued.

(c)
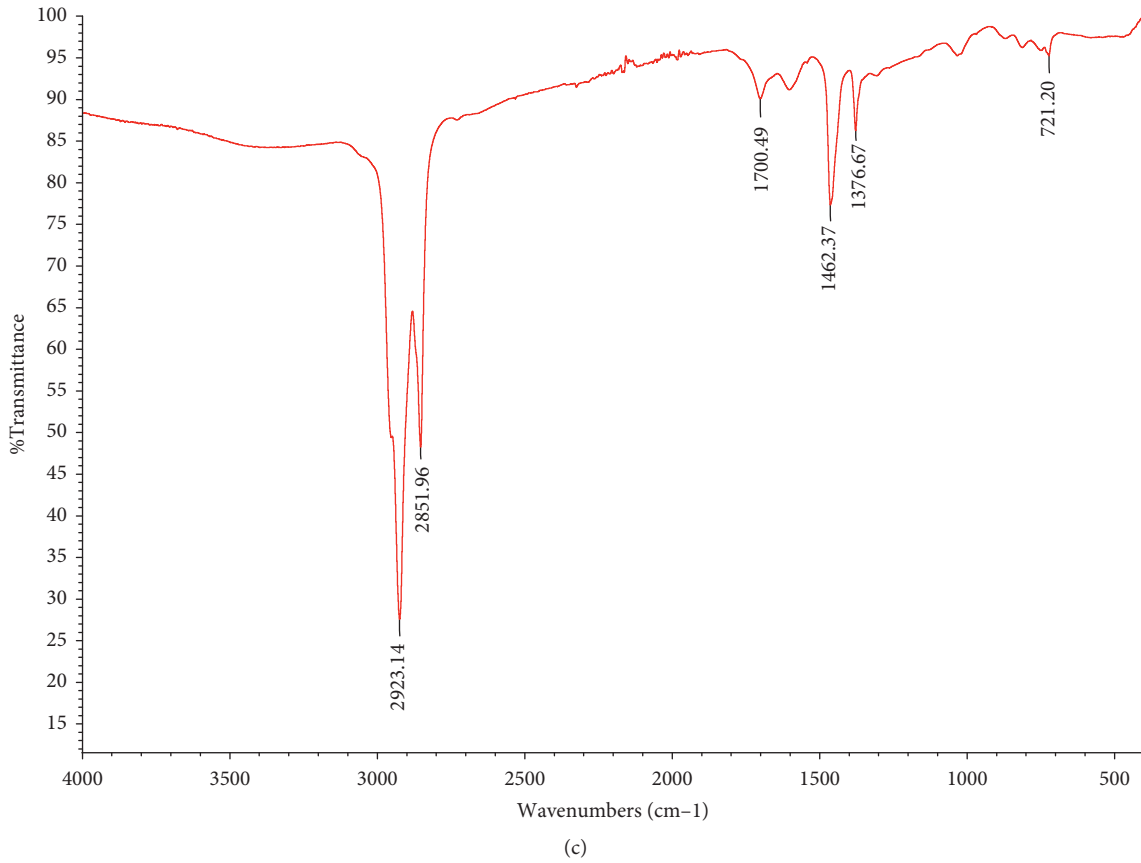
Figure 3: (a) Transmittance peaks of unmodified bitumen. (b) Transmittance (%) vs. wavenumber (cm^{-1}) spectral interpretation of unmodified bitumen. (c) Transmittance peaks of 3% nano TiO_2 modified bitumen.
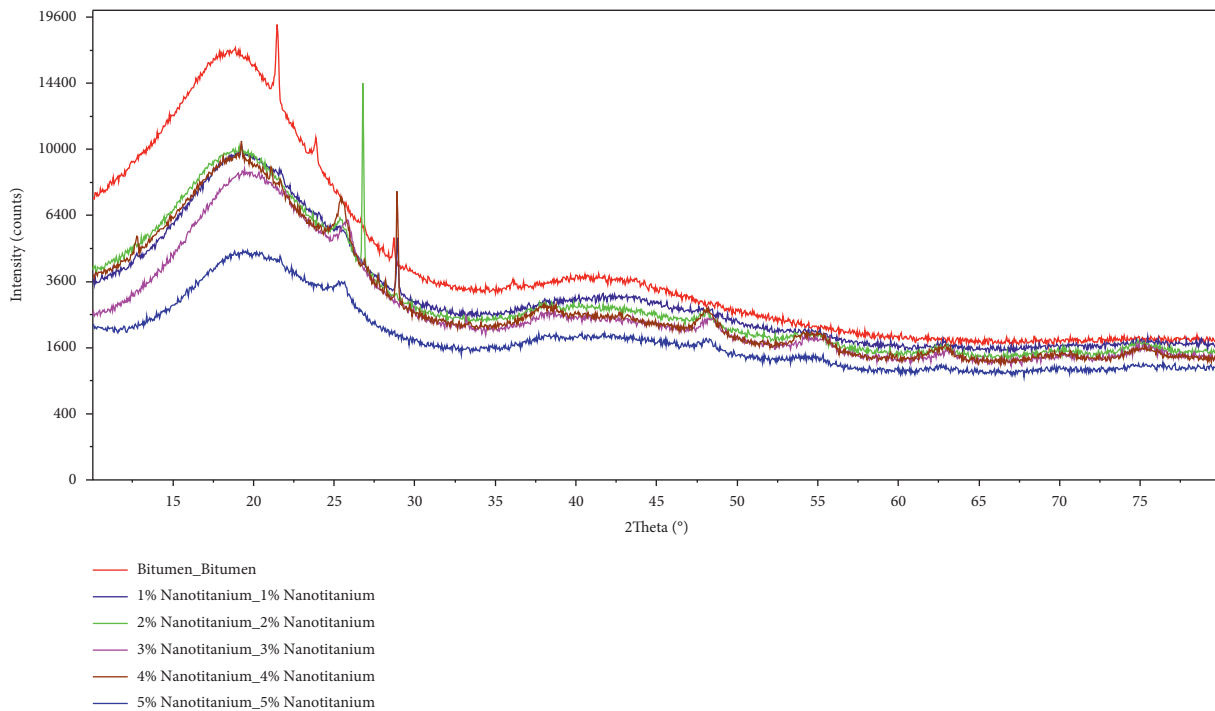
Figure 4: XRD for nano TiO_2 modified binder.
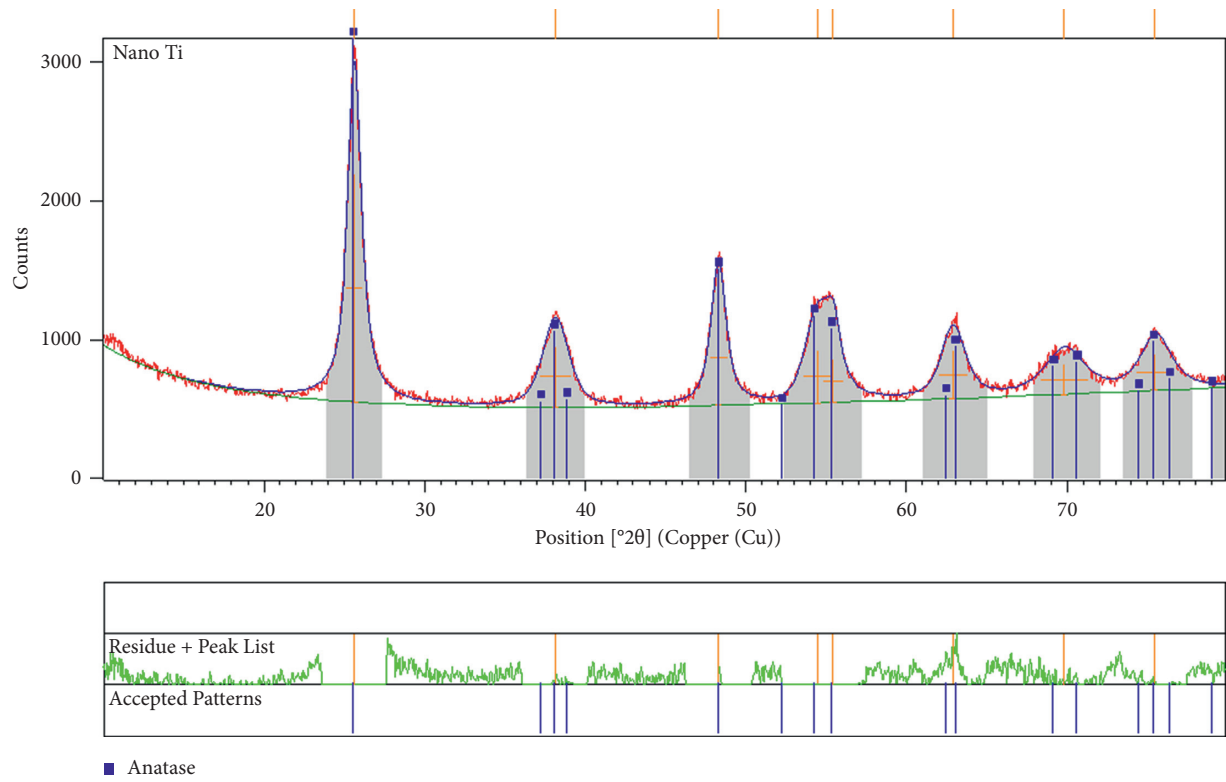
Figure 5: XRD peaks of Nano TiO$_2$ powder.
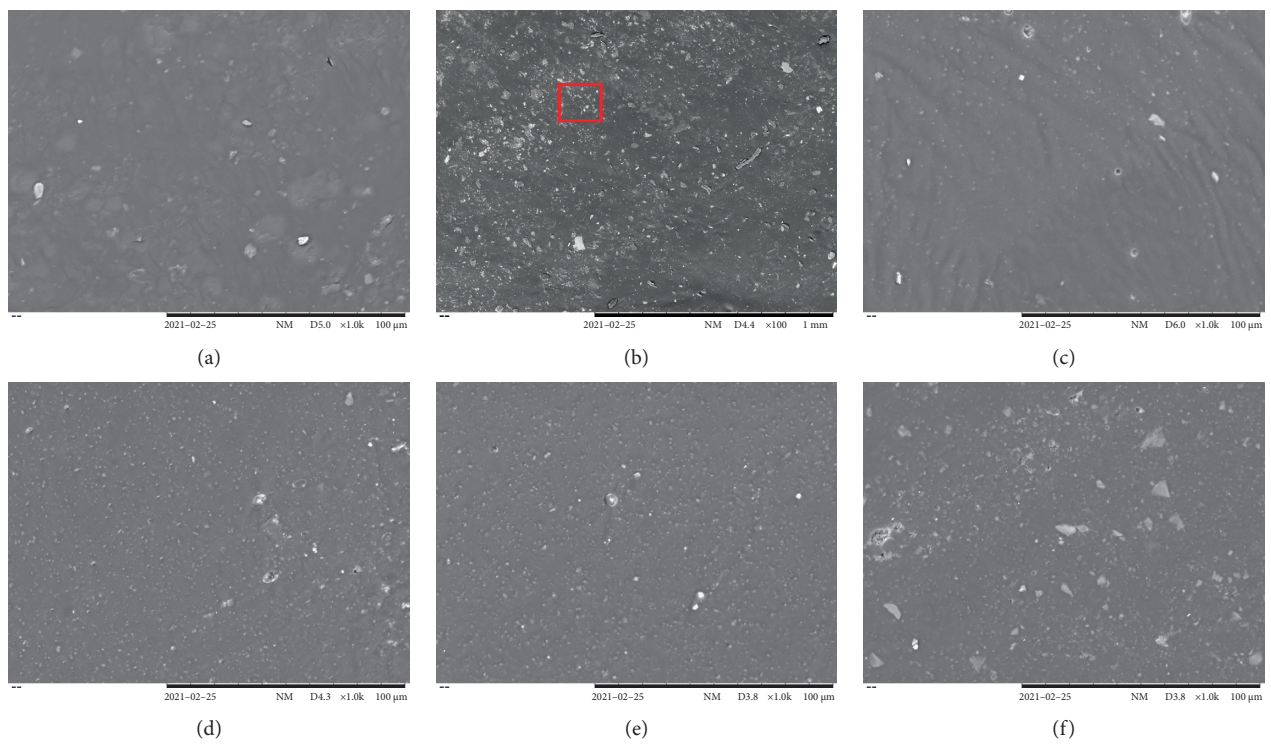
Figure 6: SEM images of modified and unmodified bitumen samples.

TABLE 3: Unmodified and modified bitumen elements.

Nano titanium (%)	Carbon		Oxygen		Sulphur		Titanium	
	Weight (%)	Atomic (%)	Weight (%)	Atomic (%)	Weight (%)	Atomic (%)	Weight (%)	Atomic (%)
0	76.36	84.83	12.32	10.28	5.68	2.36		
1	96.49	98.69	—	—	3.25	1.24	0.26	0.07
2	91.70	96.94			6.56	2.60	1.75	0.46
3	96.11	98.99			3.50	1.50	3.89	1.00
4	86.06	91.5	8.00	6.39	3.62	1.44	3.88	1.05
5	84.94	91.88	6.22	5.05	4.96	2.01	3.88	1.05

there seems to be a melted bitumen state and dry bitumen from the image.

The images generated from Figure 6 show the 0%, 1%, 2%,3%, 4%, and 5% addition of nano TiO_2. The images generated show that some nano TiO_2 powder is still not blended well into the bitumen and the white spots are the powders that has not been able to mix with the bitumen. This can be further verified with reference to the previous Table 1 (properties of nano TiO_2). With the increasing amount of nano TiO_2, the bitumen has difficulty in blending well with the nano TiO_2 which then produces insoluble white lumps that is observed with increasing nano TiO_2 powder. Meanwhile, 3% nano TiO_2 modified bitumen can mix thoroughly and have lesser white streaks or clumps. However, the dispersion is still acceptable, and the improvement is verified based on the obtained results.

Next, EDX analysis is also carried out on the samples; from the elements observed from Table 3 and Figures 7(a)–7(f), it is most likely that the white flakes or clumps observed are from the aluminium or calcium residue composed in the bitumen. The visibility is due to the amount of those elements that still exists inside the nano TiO_2 modified sample. The elements from table confirm that the most abundant elements are carbon and oxygen. Other elements that are obtained include aluminium, sulphur, and calcium. The results are consistent with a few recent studies performed by Snehal et al. [11], Arshad et al. [19], and Babagoli [15].

The unmodified bitumen shows all the elements mentioned before, but when nano TiO_2 is added with various content, the chemical composition changes according to the amount of nano TiO_2 added. Hence, the optimum nano TiO_2 content in terms of SEM-EDX analysis is at 3% nano TiO_2 modified bitumen followed by 5%, 4%, 2%, and 1%, as shown in Table 3. Only two elements are present: carbon and oxygen, which mainly made up the sample alongside nano TiO_2 showing that the nano TiO_2 is mostly blended with the bitumen. Overall, 3% specimen has the most influence on the chemical composition changes and enhancement of virgin bitumen.

3.4. Softening Point. As shown in Figure 8, the softening point is the highest at 0% nano TiO_2 at 44.4°C compared to 5% nano TiO_2 which only record at 41.8°C. Further addition of nano TiO_2 makes the softening points drop lower than the initial reading recorded. The high softening point at 0% implies that the resistance of the bitumen to the heat is increased and shows that there is a low probability that the

bitumen will soften under high temperatures which is a resemblance of the hot weather. However, 4°C is not a large difference, and usually in summer seasons, the temperature on pavement surface is larger than 50°C, so with this bitumen, the risk of rutting exists always. This makes the bitumen less vulnerable when temperature changes. Rutting is one of the deformations happening related to temperature, and with this increase in softening point, the rutting would be reduced. The readings recorded are having the same trend as previous research by Crucho et al. [20] in which the increasing content of nano material added results in lower softening point.

3.5. Penetration Test. The results in Figure 9 show that bitumen penetration varies with different nano TiO_2 percentages. The penetration for nano TiO_2 mixture between 1 to 5% are 73 dmm, 61.5 dmm, 60.5 dmm, 55.5 dmm, 54.5 dmm, and 54 dmm, respectively. The consistency of bitumen is harder at 3% to 5% nano TiO_2 compared with 0% nano TiO_2 sample. This result is consistent with the earlier study on nano silica that observed a decrease in penetration tests [20]. These results are also reflected in the nano TiO_2 usage in the binder, which is similar to the utilisation of nanomaterials. This is caused by the increased viscosity of bitumen, as evident from the penetration value at increasing nano titanium percentages. Essentially, nano TiO_2 addition caused bitumen to be more consistent and harder. Thus, improving rutting resistance produces much stiffer bitumen which affects the resistance to fatigue cracking.

3.6. Volumetric Properties

3.6.1. Stability. Figure 10 shows the density and stability of the modified binder against nano TiO_2 percentages between 0 to 4%. The stability of the mixture is mostly influenced by the cohesion and internal friction of the matrix, which supports the coarse aggregates [21]. Figure 10 shows a comparable trend for density and stability, especially for the 3% nano TiO_2 addition. For this particular sample, the density is 2.238 g/cm^3, while the maximum stability is 5945 N compared to 5879 N for 0% nano TiO_2 addition. It is found that increasing nano TiO_2 amount also increases the stability and density. However, nano TiO_2 addition beyond 3% does not increase both parameters. This indicates that the usage of 3% nano TiO_2 in SMA mixture is more effective in enhancing density and stability. These contribute to less

Spectrum details

Project: New project Spectrum name: Spectrum 1

Electron Image

Image Width: 351.4 μm

100 μm

Acquisition conditions

Acquisition time (s) : 30.0 Process time : 5

Accelerating voltage (kV) : 15.0

Full Scale 162 cts Cursor: 0.000 keV

Quantification Settings

Quantification method : All elements (normalised) Coating element : None

Summary results

Element	Weight %	Weight % σ	Atomic %
Carbon	76.361	3.052	84.832
Oxygen	12.322	3.166	10.277
Aluminum	4.031	0.526	1.993
Sulfur	5.677	0.962	2.363
Calcium	1.608	0.580	0.535

(a)

FIGURE 7: Continued.

Spectrum details

Project: New project   Spectrum name: Spectrum 1

Electron Image

Image Width: 175.7 μm

80 μm
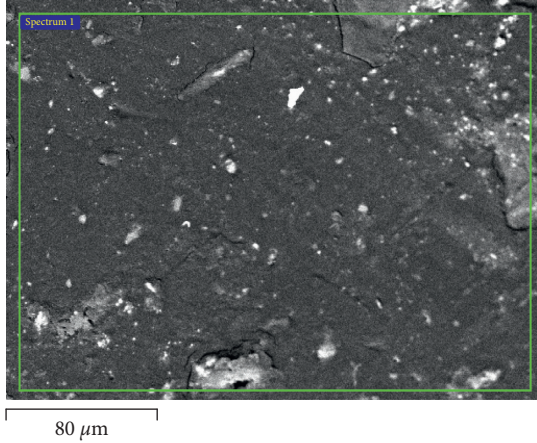
Acquisition conditions

Acquisition time (s) :   29.9   Process time :   5

Accelerating voltage (kV) :   15.0
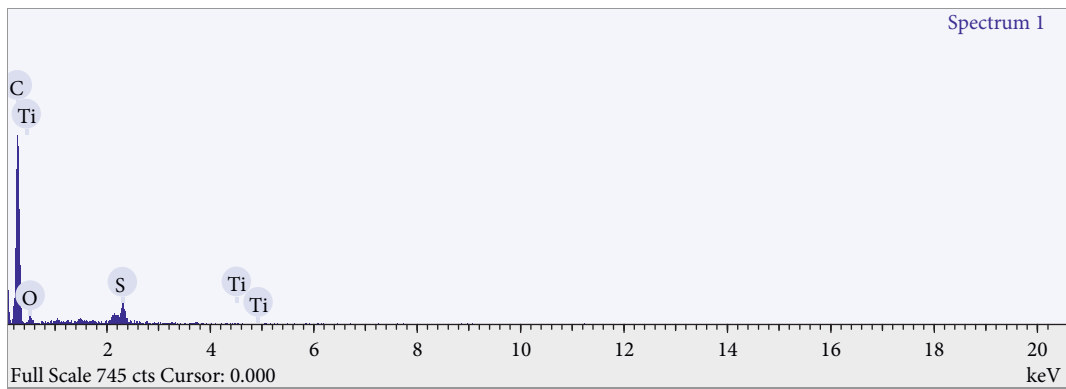
Quantification Settings

Quantification method :   All elements (normalised)   Coating element :   None

Summary results

Element	Weight %	Weight % σ	Atomic %
Carbon	96.490	0.469	98.689
Oxygen	0.000	0.000	0.000
Sulfur	3.246	0.395	1.244
Titanium	0.264	0.261	0.068

(b)

Figure 7: Continued.

Spectrum details

Project:	New project	Spectrum name:	Spectrum 1

Electron Image

Image Width: 351.4 μm

100 μm

Acquisition conditions

Acquisition time (s) :	29.9	Process time :	5
Accelerating voltage (kV) :	15.0		

Full Scale 296 cts Cursor: 0.000

Quantification Settings

Quantification method :	All elements (normalised)	Coating element :	None

Summary results

Element	Weight %	Weight % σ	Atomic %
Carbon	91.695	1.105	96.940
Sulfur	6.559	0.914	2.598
Titanium	1.745	0.656	0.463

(c)

FIGURE 7: Continued.

Spectrum details

Project:	New project	Spectrum name:	Spectrum 1

Electron Image

Image Width: 351.4 μm

100 μm

Acquisition conditions

Acquisition time (s) :	30.0	Process time :	5
Accelerating voltage (kV) :	15.0		

Full Scale 113 cts Cursor: 0.000   keV
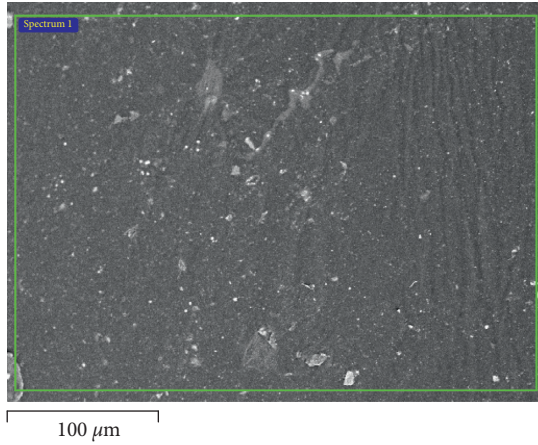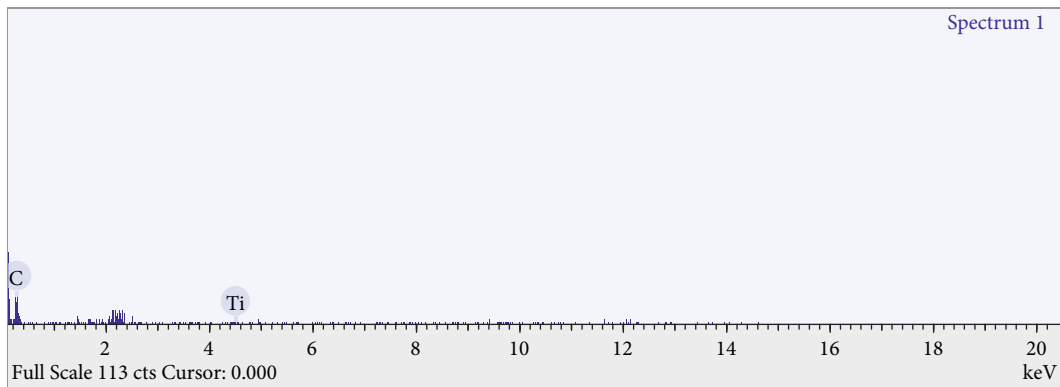
Quantification Settings

Quantification method :	All elements (normalised)	Coating element :	None

Summary results

Element	Weight %	Weight % σ	Atomic %
Carbon	96.107	4.005	98.994
Titanium	3.893	4.005	1.006

(d)

Figure 7: Continued.

Spectrum details

Project:	New project	Spectrum name:	Spectrum 1

Electron Image

Image Width: 351.4 μm

100 μm

Acquisition conditions

Acquisition time (s) :	30.0	Process time :	5
Accelerating voltage (kV) :	15.0		

Quantification Settings

Quantification method :	All elements (normalised)	Coating element :	None

Summary results

Element	Weight %	Weight % σ	Atomic %
Carbon	86.055	1.011	91.499
Oxygen	8.001	1.039	6.387
Aluminum	0.250	0.073	0.118
Sulfur	3.624	0.192	1.444
Titanium	2.070	0.183	0.552

(e)

FIGURE 7: Continued.

Spectrum details

Project: New project   Spectrum name: Spectrum 1

Electron Image

Image Width: 351.4 μm

Spectrum 1

100 μm

Acquisition conditions

Acquisition time (s) :   29.9   Process time :   5

Accelerating voltage (kV) :   15.0

Spectrum 1

C
Ti

S

Ti

O   Ti

2   4   6   8   10   12   14   16   18   20
keV

Full Scale 1966 cts Cursor: 0.000
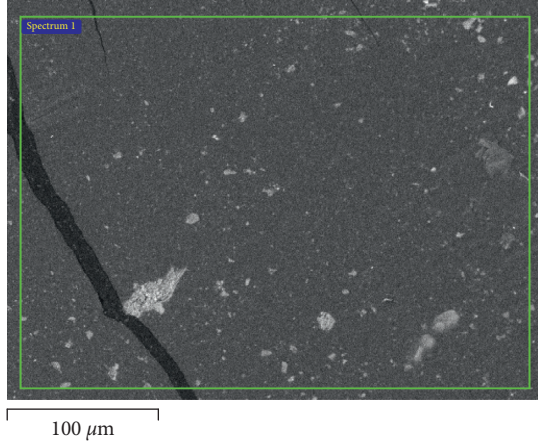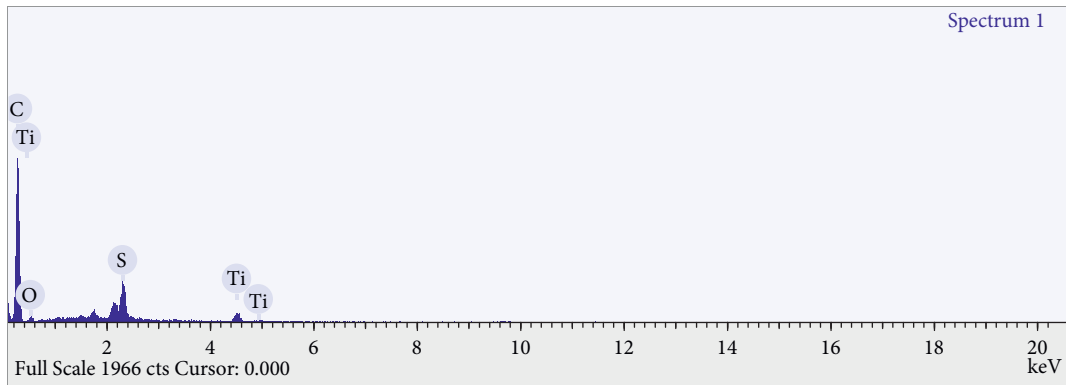
Quantification Settings

Quantification method :   All elements (normalised)   Coating element :   None

Summary results

Element	Weight %	Weight % σ	Atomic %
Carbon	84.938	1.218	91.884
Oxygen	6.221	1.270	5.053
Sulfur	4.962	0.274	2.011
Titanium	3.879	0.277	1.052

(f)

FIGURE 7: (a) Control Sample. (b) 1% nano TiO_2 modified bitumen. (c) 2% nano TiO_2 modified bitumen. (d) 3% nano TiO_2 modified bitumen. (e) 4% nano TiO_2 modified bitumen. (f) 5% nano TiO_2 modified bitumen.

permanent deformation in SMA [22]. Figure 11 shows the stability and flow for various nano titanium percentages. 0% nano TiO_2 yields the highest flow, although further nano TiO_2 addition reduces the flow value.

3.6.2. Flow. Figures 12 and 13 show the flow performance of asphalt mixtures with different nano TiO_2 percentages. The flow value indicates the flexibility of asphalt mixtures [23]. The modified SMA20 mixture produces an inconsistent flow value
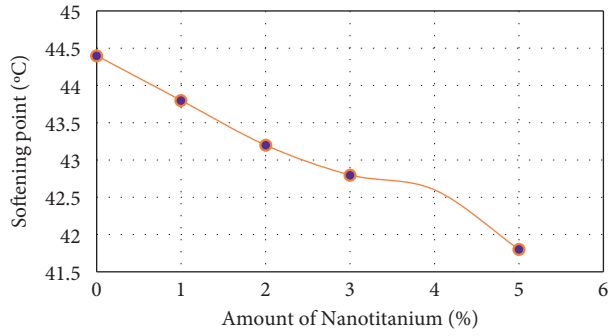
FIGURE 8: The softening point of nano TiO$_2$ modified bitumen.
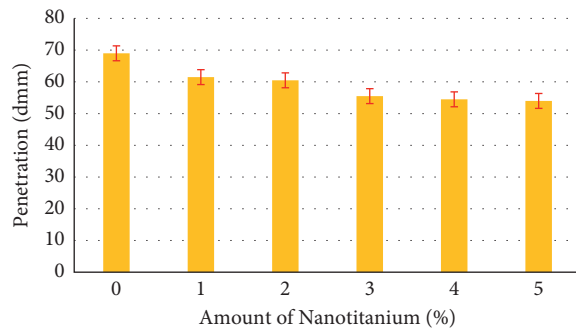
FIGURE 9: Penetration values of nano TiO$_2$ modified binder.
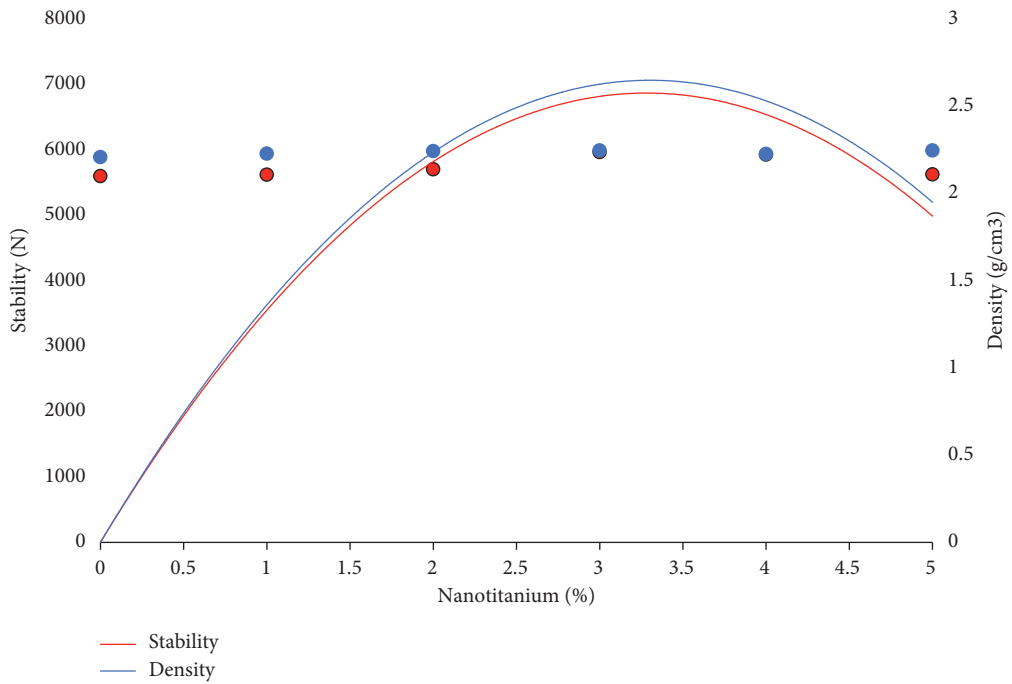
— Stability
— Density

FIGURE 10: Stability and density against nano TiO$_2$ percentages.
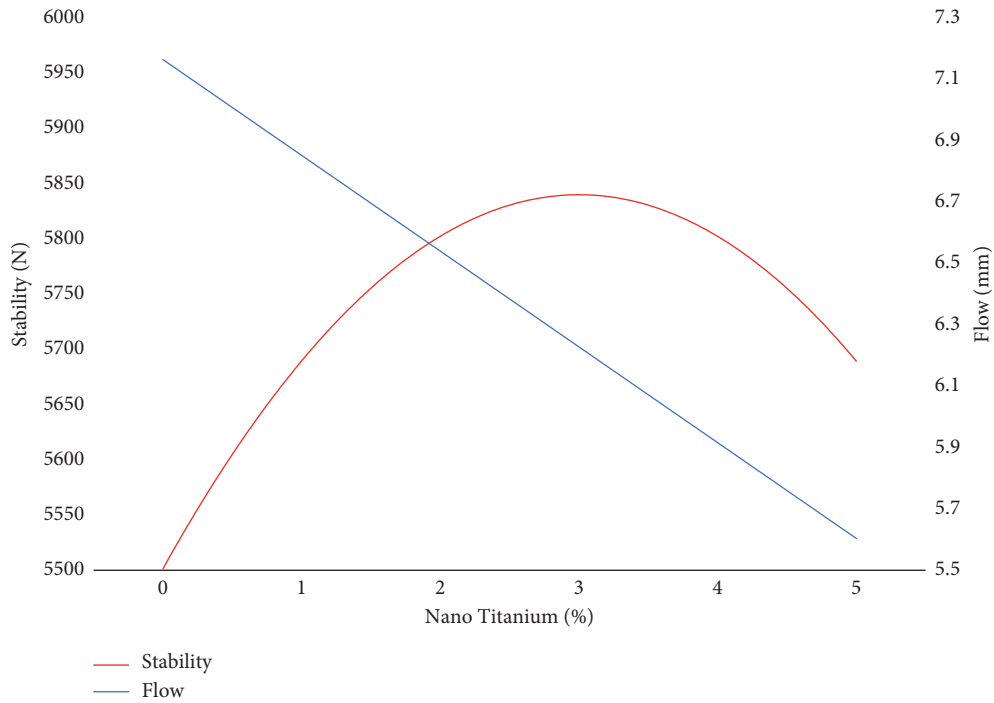
FIGURE 11: Stability and flow against nano TiO$_2$ percentages.
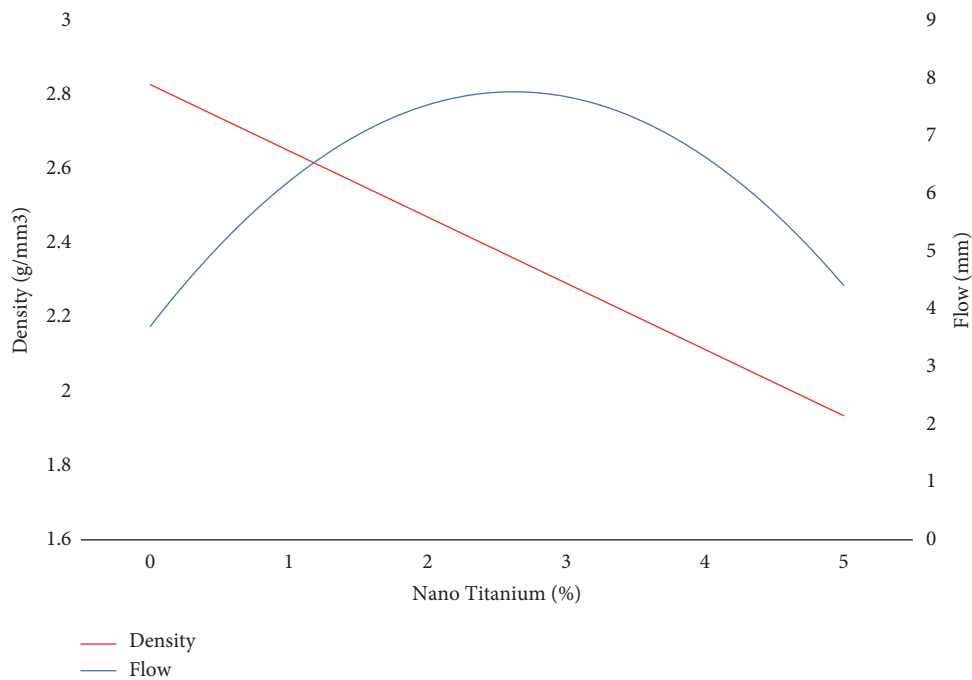
FIGURE 12: Density and flow against nano TiO$_2$ percentage.

with the inclusion of nano TiO$_2$. The flow at 3% nano TiO$_2$ complements both the density and stiffness. 0% nano TiO$_2$ produces a relatively higher flow value (7 mm) than the requirement by the Public Work Department (between 3 to 5 mm). The addition of nano TiO$_2$ reduces the flow, indicating that nano TiO$_2$ could influence the flow properties to a more accustomed value.

3.6.3. *Stiffness*. Figures 14 and 15 exhibits the stiffness of SMA mixtures against various nano TiO$_2$ percentages. The highest stiffness value is obtained by the 3% nano TiO$_2$ addition (965.67 N/mm), compared to 833.3 N/mm for 0% nano TiO$_2$ which is a 14.8% improvement. This shows that nano TiO$_2$ addition improves the stiffness characteristic of asphalt mixture.
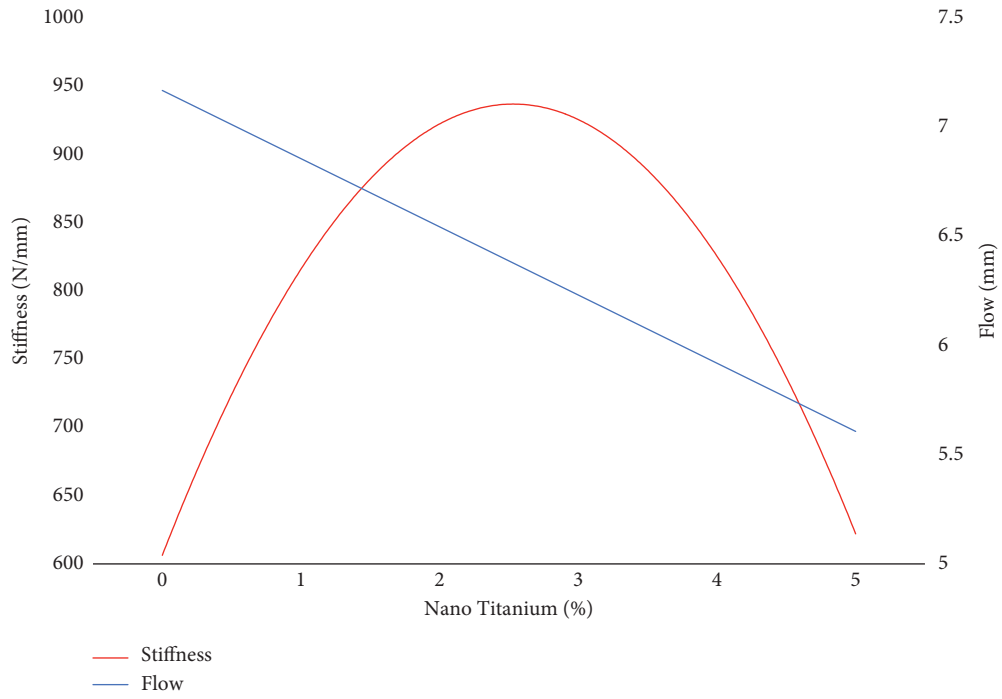
FIGURE 13: Stiffness and flow against nano TiO$_2$ percentages.
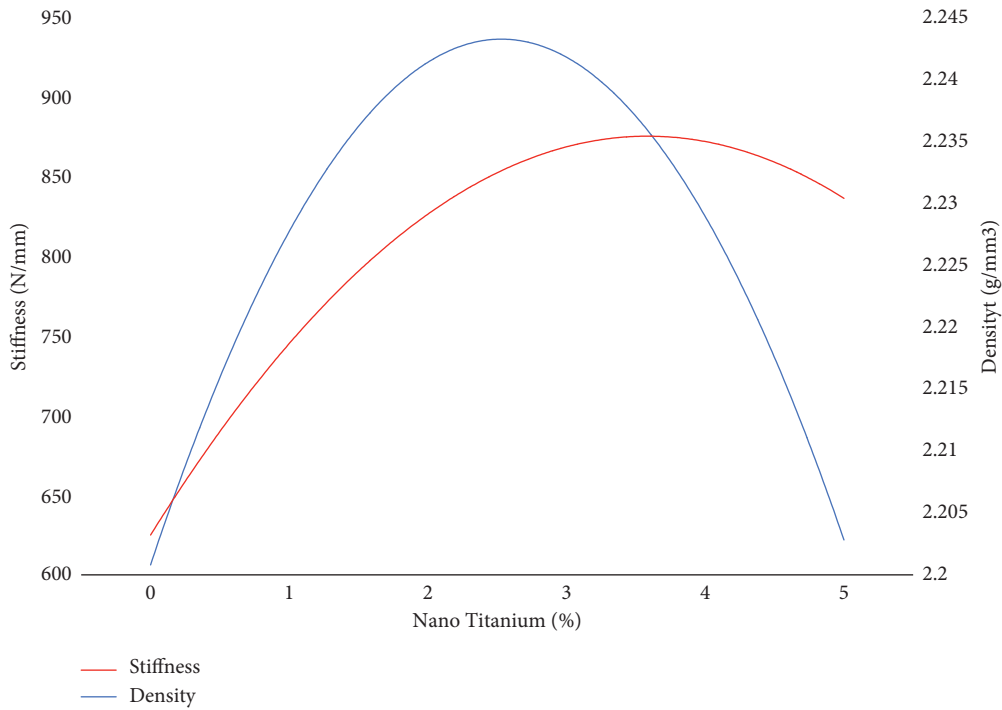
FIGURE 14: Stiffness and density against nano TiO$_2$ percentages.
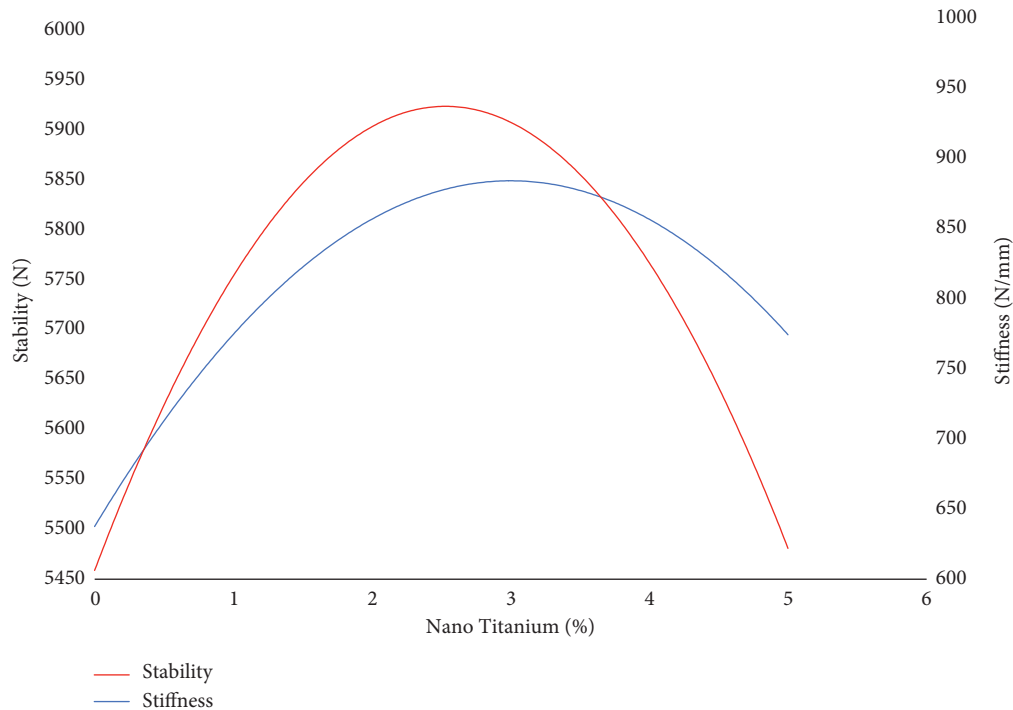
FIGURE 15: Stability and stiffness against nano TiO$_2$ percentages.

4. Conclusion

The nano TiO$_2$ modified binder significantly improves the microstructural, chemical, and physical properties of bitumen, as well as enhancing the mechanical properties of the SMA mixture. The details are as follows:

(a) From FTIR results, the change in chemical bonds happens when the nano TiO$_2$ is added into the bitumen showing that the nano TiO$_2$ successfully blends into the bitumen.

(b) XRD analysis peaks are higher and further compared to the virgin bitumen which has lower peak starting. This proved the existence of nano TiO$_2$ in the virgin bitumen.

(c) SEM-EDX results show that bitumen mixture particles are well dispersed depending on the nano TiO$_2$ percentages. The 3% addition of nano TiO$_2$ reveals that it is able to merge the nano TiO$_2$ particles fully into the bitumen.

(d) The penetration and softening point show a consistent trend similar to previous research studies as discussed earlier showing that 3% to 5% nano modification contributes the optimum value.

(e) Improvements of the physical, morphological, and chemical characteristics also enhance the mechanical performance of SMA as evident from volumetric properties.

The density, stability, flow, and stiffness properties of the 3% nano TiO$_2$ addition mixture are better than the 0% nano TiO$_2$ due to the addition of the modified nano TiO$_2$ binder. Therefore, it can be concluded that overall, 3% nano TiO$_2$ addition enhances the mechanical properties of SMA. Finally, the improvement of nano TiO$_2$ modified binder directly enhances the quality of SMA performance in terms of its volumetric properties [22].

Data Availability

All the data used to support the findings of this study are included within the article.

Conflicts of Interest

The authors declare that they have no conflicts of interest with other entities or researchers.

Acknowledgments

References

[1] A. Ameli, J. Maher, A. Mosavi, N. Nabipour, R. Babagoli, and N. Norouzi, "Performance evaluation of binders and stone matrix asphalt (SMA) mixtures modified by ground tire rubber (GTR), waste polyethylene terephthalate (PET) and anti stripping agents (ASAs)," *Construction and Building Materials*, vol. 251, Article ID 118932, 2020.

[2] S. Eskandarsefat, G. Dondi, and C. Sangiorgi, "Recycled and rubberized SMA modified mixtures: A comparison between polymer modified bitumen and modified fibres," *Construction and Building Materials*, vol. 202, pp. 681–691, 2019.

[3] N. E. Jasni, K. A. Masri, P. J. Ramadhansyah et al., "Mechanical performance of stone mastic asphalt incorporating steel fiber," *IOP Conference Series: Materials Science and Engineering*, vol. 712, no. 1, Article ID 012026, 2020.

[4] J. Choudhary, B. Kumar, and A. Gupta, "Utilization of solid waste materials as alternative fillers in asphalt mixes: A review," *Construction and Building Materials*, vol. 234, Article ID 117271, 2020.

[5] P. Caputo, M. Porto, R. Angelico, V. Loise, P. Calandra, and C. O. Rossi, "Bitumen and asphalt concrete modified by nanometer-sized particles: Basic concepts, the state of the art and future perspectives of the nanoscale approach," *Advances in Colloid and Interface Science*, vol. 285, Article ID 102283, 2020.

[6] S. A. Mazari, E. Ali, R. Abro et al., "Nanomaterials: applications, waste-handling, environmental toxicities, and future challenges - A review," *Journal of Environmental Chemical Engineering*, vol. 9, no. 2, 2021.

[7] M. Motamedi, G. Shafabakhsh, and M. Azadi, "Evaluation of fatigue and rutting properties of asphalt binder and mastic modified by synthesized polyurethane," *Journal of Traffic and Transportation Engineering (English Edition)*, vol. 8, no. 6, pp. 1036–1048, 2021.

[8] H. Hong, H. Zhang, and S. Zhang, "Effect of multi-dimensional nanomaterials on the aging behavior of asphalt by atomic force microscope," *Construction and Building Materials*, vol. 260, Article ID 120389, 2020.

[9] Y. He, Z. Wang, H. Wang et al., "Metal-organic framework-derived nanomaterials in environment related fields: Fundamentals, properties and applications," *Coordination Chemistry Reviews*, vol. 429, Article ID 213618, 2021.

[10] P. J. Ramadhansyah, K. A. Masri, A. H. Norhidayah et al., "Nanoparticle in asphalt binder: A state-of-the-art review," *IOP Conference Series: Materials Science and Engineering*, vol. 712, no. 1, Article ID 012023, 2020.

[11] K. Snehal, B. B. Das, and M. Akanksha, "Early age , hydration , mechanical and microstructure properties of nano-silica blended cementitious composites," *Construction and Building Materials*, vol. 233, Article ID 117212, 2020.

[12] C. N. Fernandes, R. L. S. Ferreira, R. D. S. Bernardo, F. Avelino, and A. A. Bertini, "Using TiO2 nanoparticles as a SO2 catalyst in cement mortars," *Construction and Building Materials*, vol. 257, pp. 2–10, 2020.

[13] L. Zhang, Q. Lu, R. Shan, F. Zhang, Y. Muhammad, and K. Huang, "Photocatalytic degradation of vehicular exhaust by nitrogen-doped titanium dioxide modified pavement material," *Transportation Research Part D: Transport and Environment*, vol. 91, Article ID 102690, 2021.

[14] A. Ameli, A. H. Pakshir, R. Babagoli, N. Norouzi, D. Nasr, and S. Davoudinezhad, "Experimental investigation of the influence of Nano TiO2 on rheological properties of binders and performance of stone matrix asphalt mixtures containing steel slag aggregate," *Construction and Building Materials*, vol. 265, Article ID 120750, 2020.

[15] R. Babagoli, "Laboratory investigation of the performance of binders and asphalt mixtures modified by carbon nano tube, poly phosphoric acid, and styrene butadiene rubber," *Construction and Building Materials*, vol. 275, Article ID 122178, 2021.

[16] A. K. Arshad, J. Ahmad, and K. A. Masri, "Rutting resistance of nanosilica modified porous asphalt," *International Journal of Civil Engineering & Technology*, vol. 10, no. 1, pp. 2274–2284, 2019.

[17] P. Lin, C. Yan, W. Huang et al., "Rheological, chemical and aging characteristics of high content polymer modified asphalt," *Construction and Building Materials*, vol. 207, pp. 616–629, 2019.

[18] S. H. Razavi and A. Kavussi, "The role of nanomaterials in reducing moisture damage of asphalt mixes," *Construction and Building Materials*, vol. 239, Article ID 117827, 2020.

[19] A. K. Arshad, M. S. Samsudin, J. Ahmad, and K. A. Masri, "Microstructure of nanosilica modified binder by atomic force microscopy," *Jurnal Teknologi*, vol. 78, no. 7-3, 2016.

[20] J. M. L. Crucho, J. M. C. D. Neves, S. D. Capitão, and L. G. D. P. Santos, "Mechanical performance of asphalt concrete modified with nanoparticles: Nanosilica, zero-valent iron and nanoclay," *Construction and Building Materials*, vol. 181, pp. 309–318, 2018.

[21] N. A. N. M. Fauzi, K. A. Masri, P. J. Ramadhansyah et al., "Volumetric properties and resilient modulus of stone mastic asphalt incorporating cellulose fiber," *IOP Conference Series: Materials Science and Engineering*, vol. 712, Article ID 012028, 2020.

[22] P. J. Ramadhansyah, K. A. Masri, H. Awang et al., "Stability and stiffness of asphaltic concrete incorporating waste cooking oil," *International Journal of Recent Technology and Engineering*, vol. 7, no. 6, pp. 2277–3878, 2019.

[23] M. Ahmad, S. Beddu, S. Hussain, A. Manan, and Z. B. Itam, "Mechanical properties of hot-mix asphalt using waste crumber rubber and phenol formaldehyde polymer," *AIMS Materials Science*, vol. 6, no. 6, pp. 1164–1175, 2019.

Research Article

Investigating the Effect of Calcium Lignosulfonate on the Durability and Performance of Asphalt Mixtures

Saeed Fatemi [ID], Jafar Bolouri Bazaz [ID], and Seyed Ali Ziaee [ID]

Department of Civil Engineering Engineering Faculty, Ferdowsi University of Mashhad, Mashhad, Iran

Correspondence should be addressed to Seyed Ali Ziaee; sa-ziaee@um.ac.ir

Using bitumen modifiers to prolong the asphalt mixture's life has been considered a practical approach in constructing asphalt mixtures. Among various bitumen modifiers, biomass ones have been more noteworthy because of their abundance, cost-effectiveness, renewability, and sustainability. Calcium lignosulfonate (CLS), as a plant-based bitumen modifier, has been studied to enhance the rheological properties of bitumen. However, the feasibility of using CLS as a rutting retarder of asphalt mixtures is still unclear. This study focused on the durability of asphalt mixtures containing CLS powder as a bitumen modifier. Specifically, extensive laboratory tests were conducted to determine the performance of asphalt mixtures against traffic loadings. In this study, to begin, CLS-modified bitumen was manufactured using a high-shear mixer at various CLS dosages (5, 10, 15, and 20 wt.%). Afterward, the optimum bitumen content of asphalt mixtures was found using the Marshall mix design technique. Finally, a series of dynamic tests, including resilient modulus, dynamic creep, and wheel-tracking tests, were combined with Zhou's three-stage model and Tukey method to determine the influence of CLS on asphalt mixture's rutting potential. The Tukey method found that asphalt mixtures containing 15% CLS had the highest rutting performance among the samples tested under repetitive loadings. Meanwhile, the surface morphology and elemental analysis of CLS powder were investigated using a field emission scanning electron microscope (FESEM) and by energy-dispersive X-ray spectroscopy (EDX), respectively. The FESEM and EDX results showed that the CLS powder had a bumpy structure and its chemical structure contained metal oxide, carbon, magnesium, calcium, and silicon. The results indicated that the asphalt mixtures became stiff owing to the combination of CLS and bitumen, which significantly affected the rutting improvement of asphalt mixtures. Moreover, Zhou's three-stage model revealed that the incorporation of CLS into bitumen enhanced the rutting resistance capacity of asphalt mixtures against traffic loadings.

1. Introduction

Nowadays, asphalt mixtures are used as a significant material for road construction because of their good performance, comfort, and ease of maintenance [1, 2]. Asphalt mixtures consist of two major constituents, namely, stone skeleton and bitumen [3]. The pavements surface layer, constructed by the asphalt mixture, transfers compressive stress from the top to the bottom layer [4]. Moreover, the surface layer protects the pavement's body against environmental factors, including moisture damage, UV radiation, and oxygen [5]. When traffic loadings are conducted on asphalt mixtures, the serviceability of roads encounters degradation due to premature distress, including rutting, cracking, and fatigue failure [6, 7]. They can reduce the service life of pavements; therefore, the need for rehabilitation, which requires spending money and time, increases [8].

Rutting can be defined as the progressive accumulation of small deformations that occur by densification and shear deformations under applied traffic loadings [9]. Among the asphalt mixture's premature distress, rutting is more noticeable because it increases the risk of human life by disturbing pavements smooth and safe surface for vehicles to commute [10]. Therefore, rutting leads to endangering road safety and increases the burden on governments by increasing road maintenance costs [11, 12].

Various research studies have been conducted to determine how well asphalt mixtures resist rutting. Researchers showed that although bitumen formed a small

proportion of the total weight of asphalt mixtures, bitumen significantly affected the rutting potential of asphalt mixtures [13, 14]. Then, various bitumen modifiers have been studied to enhance the positive effects of bitumen on the rutting performance of asphalt mixtures. De Melo et al. [15] used carbon nanotubes for bitumen modification. The results revealed that carbon nanotubes increased the asphalt mixture's performance; moreover, they improved the rutting resistance of asphalt mixtures. Yoo et al. [16] conducted an experimental work on the combination of polypropylene and bitumen; their findings showed that polypropylene could enhance the rutting resistance of asphalt mixtures. In 2020, Ghanoon et al. [17] conducted experimental research and used styrene–butadiene–styrene (SBS) as a bitumen modifier. The findings indicated that the SBS-modified bitumen had a positive effect on the rutting behavior of asphalt mixtures.

Biomass materials have been more noteworthy for researchers among bitumen modifiers because of their abundance, cost-effectiveness, renewability, and sustainability [18]. Lignin, obtained from the biofuel and paper industries, is classified as a significant waste biomass material [19]. Lignin has the adequate capability to be used as a bitumen modifier because lignin's chemical structure contains reactive chemical compounds that can be employed to modify petroleum chemical substances [20]. Moreover, the chemical structure of lignin is comparable to petroleum bitumen's chemical structure [21]. Several investigations have examined the utilization of lignin as a bitumen modifier or extender. Batista et al. [22] studied the effect of lignin, sourced from the pulp industry, on the aging performance of bitumen. The results revealed that lignin could retard bitumen's aging process.

Similarly, Xu et al. [23] indicated that although lignin in bitumen could enhance bitumen's aging resistance, incorporating lignin into bitumen degraded the fatigue performance of modified bitumen. In 2020, apart from the role of lignin in bitumen modification, Zhang et al. [24] examined the influence of lignin fibers on the mechanical characteristics of asphalt mixtures. The results exhibited the positive effect of lignin fibers on the asphalt mixture's mechanical properties, including abrasion resistance, fatigue life, and moisture damage.

The rutting potential of asphalt mixtures can be assessed by two main laboratory methods: (1) static tests and (2) dynamic tests [25]. The former consists of static creep, indirect tensile, and Marshall tests; the latter contains dynamic creep, wheel tracking, and resilient modulus tests [26]. Researchers believe that dynamic tests are more accurate than static tests to appraise the asphalt mixture's rutting susceptibility [27]. Among dynamic tests, the dynamic creep test is considered one of the most effective techniques because laboratory outputs achieved by the dynamic creep test have a reasonable correlation with accumulated strains that occurred under repetitive loading on-field situations [28]. It is worth mentioning that the wheel-tracking test can determine the exact rut depth of asphalt mixtures [29].

Comprehensive research has been carried out regarding creation models to assess and predict the creep potential of asphalt mixtures. The outputs of the dynamic creep test have been proposed for application in creep models because the creep curve depicts the asphalt mixture's rutting performance based on the accumulation of permanent strain versus the load repetition [30]. Previous research studies revealed that creep models, including those by Barksdale, Monismith, Ohio State, and Superpave, could not precisely describe the creep curve of asphalt mixtures [31]. In 2004, Zhou [31] defined three stages for describing the rutting creep curve; moreover, he located two transition points between stages [32].

Different types of lignin can be categorized based on their chemical structure [33]. Organosolv lignin is obtained from wood processing using liquid organic solvents to treat wood chips [34]. Kraft lignin emanates from the pulping process, converting coniferous wood to pulp [35]. Klason lignin comes from the acid hydrolysis process of wood [36]. Applying the enzymatic hydrolysis method to produce bio-ethanol leads to the formation of enzymatic hydrolysis lignin [37]. Sulfonated lignin emanates from black liquor; moreover, sulfonated lignin is a nontoxic polymer [38]. Calcium lignosulfonate (CLS) emanates from the sulfite pulping process, leading to manufacturing of paper from softwood; moreover, CLS is a brownish powder and an amorphous polymer [39].

The annual production of CLS is estimated to be 50 million tons, but only one-half of them can be utilized. Therefore, the use of CLS for the construction of asphalt mixtures can reduce the consumption of natural materials and reduce the mass of CLS that ends up in landfills [40]. This study aims to investigate the rutting performance of asphalt mixtures containing CLS-modified bitumen because CLS contains chemical groups that tend to dissolve in petroleum-based materials; therefore, its solubility potential in bitumen is more than in lignin [41]. Moreover, the rutting performance of asphalt mixtures containing CLS-modified bitumen has barely been investigated.

2. Materials and Methods

2.1. Aggregate.
In this experimental research, the stone skeleton of the asphalt mixture consists of two principal objects—crushed aggregates and mineral filler—supplied from the limestone quarry. It has been used as the primary source for constructing asphalt mixtures in Mashhad, Iran's northeastern province [42]. X-ray fluorescence (XRF) analysis was used to assess the chemical composition of aggregates. An ARL PERFORM'X spectrometer was used to conduct the above-mentioned analysis [43]. The weight proportions of the major oxides are shown in Table 1 using the bulk chemical analysis approach. Moreover, the physical properties of the aggregates were obtained for comparison with the specification limits (Table 2).

Based on the No. 4 gradation of the Iran Road Pavement Code, an upper and a lower limit were given for the construction of asphalt mixtures (Figure 1) [44]. As seen in Figure 1, the selected gradation was within the top and lower bounds. It is worth mentioning that the selected gradation is the preferred aggregate gradation for the construction of asphalt mixtures among consultants and contractors in Iran [42].

TABLE 1: Chemical composition of aggregates.

Constituent	MgO	Al_2O_3	SiO_2	K_2O	CaO	Fe_eO_3	Loi (950°C)
Wt. (%)	17.6	0.03	0.29	0.06	35	0.22	46.8

TABLE 2: Physical characteristics of the coarse and fine aggregates.

Test properties Coarse aggregate	Unit	Value	Standard ASTM	Specification limit
Los Angeles abrasion value	%	21	C131	≤25
Fractured particles in one side	%	96	D5821	≥95
Fractured particles in two sides	%	92	D5821	≥90
Bulk specific gravity	Gr/ m^3	2.66	C127	–
Apparent specific gravity	Gr/ m^3	2.74	C127	–
Water absorption	%	0.84	C127	≤2.5
Fine aggregate				
Bulk specific gravity	Gr/ m^3	2.66	C128	–
Apparent specific gravity	Gr/ m^3	2.87	C128	–
Water absorption	%	3.3	C128	≤2.5
Sand equivalent	%	74	D2419	≥50
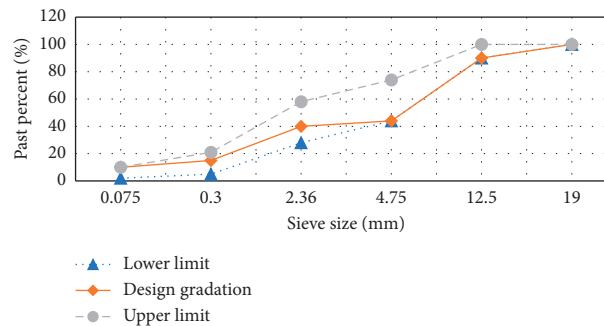
FIGURE 1: Upper, lower, and selected criteria for aggregate gradation.

2.2. Bitumen. This research employed the 60/70 penetration grade-paving bitumen supplied from the Shargh Oil Refinery (Mashhad, Iran). Table 3 shows its physical properties. The mentioned bitumen is compatible with Iran's climate conditions [45].

2.3. Calcium Lignosulfonate. Calcium lignosulfonate (CLS) is a recovered powder made from lignin, a residue of the wood and paper industries [46]. CLS provided for this study was light yellow–brown in color; in addition, its CAS number was 8061-52-7, and Ligno Tech South Africa Co. Ltd. provided this powder. In Table 4, there is some information about the essential characteristics of CLS. A field emission scanning electron microscope (FESEM) was employed to determine CLS powder's surface morphology [47]. According to Figure 2, the CLS surface had a bumpy structure. Simultaneously, the energy-dispersive X-ray spectroscopy (EDX) analysis was carried out to determine the elemental composition of CLS powder [48]. According to Table 5, the major constituents of CLS powder were metal oxide, carbon, magnesium, calcium, and silicon.

2.4. CLS-Modified Bitumen. At 160°C, a high-shear mixer with a rotational speed of 3000 rpm was employed for 30 minutes to incorporate CLS powder into virgin bitumen

[49]. Jedrzejczal and others [50] showed that the maximum amount of lignin powder mixed into bitumen could not exceed 20% because of the economic factors of the road construction process. Therefore, the incorporation of CLS into bitumen was limited to 20% during this study. In this experimental research, four percentages of CLS powder (5%, 10%, 15%, and 20%) were blended with virgin bitumen (by weight of bitumen). The key advantage of incorporating four levels of CLS into bitumen was to evaluate the effectiveness of CLS on the durability and performance of asphalt mixtures based on the comparative approach.

3. Research Approach

According to ASTM D1559, the control samples optimum bitumen content (OBC) was first determined using the Marshall mix design technique. For the determination of OBC, three Marshall samples of each bitumen content (4%, 4.5%, 5%, 5.5%, 6%, and 6.5%) were fabricated by 75 blows of the Marshall hammer on each side of the asphalt mixtures. The OBC of the control sample was then determined based on Marshall design parameters, including stability, flow, air void content, bulk density, and voids in mineral aggregates (VMA). After determining the OBC of the control sample, it was considered for fabricating the CLS-modified Marshall samples. At the next step, cylindrical samples were

TABLE 3: The virgin bitumen's physical characteristics.

Test properties	Standard ASTM	Unit	Test result
Penetration @ 25 °C	D5	0.1 mm	67
Softening point	C36	°C	51
Viscosity @ 135 °C		Pa.s	0.354
Specific gravity	D70	Gr/ cm^3	1.02
Ductility @ 25 °C	D113	Cm	+100
Flash point	D92	°C	280
PG		-	64–16

TABLE 4: Physical properties of the CLS powder.

Test	Unit	Results
Color	—	Light brown
Dry matter	% min	93.0
PH (10% solution)	—	7.5 ± 0.8
Insolubility (v/v)	% Max	0.5
Bulk density	kg/ m^3	500
Reducing sugars	%	3
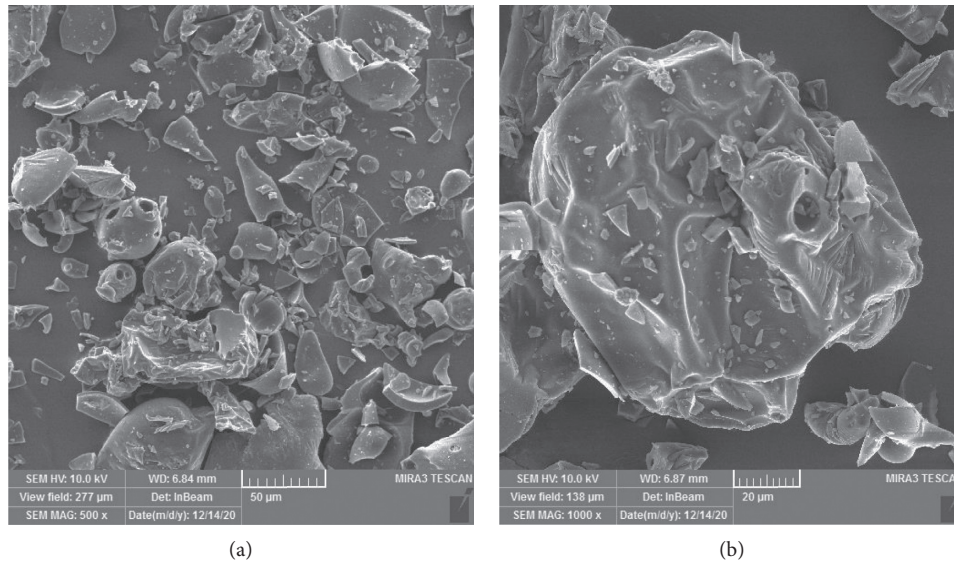
FIGURE 2: The FESEM images of CLS powder taken at (a) 500x zoom and (b) 1000x zoom.

TABLE 5: Elemental analysis of CLS powder by EDX.

Elt	Line	Int	Error	K	Kr	W%	A%	Zaf	Ox%	Pk/Bg
C	Ka	20.0	4.4546	0.2282	0.0929	23.70	31.61	0.3920	0.00	75.92
O	Ka	82.9	4.6018	0.4700	0.1914	59.57	59.65	0.3212	0.00	954.11
Mg	Ka	50.9	1.5427	0.1030	0.0419	7.26	4.78	0.5777	0.00	30.88
Al	Ka	2.3	1.5659	0.0045	0.0018	0.30	0.18	0.6229	0.00	3.36
Si	Ka	6.3	1.5891	0.0131	0.0053	0.73	0.41	0.7346	0.00	5.37
Ca	Ka	45.2	0.5246	0.1812	0.0738	8.45	3.38	0.8738	0.00	31.25
				1.0000	0.4073	100.00	100.00		0.00	

manufactured using a Superpave gyratory compactor (SGC) for resilient modulus and dynamic creep tests. Moreover, during the wheel-tracking test, a kneading compactor was employed to prepare slab specimens for rut depth calculation.

3.1. Marshall Stability Parameters. The determination of Marshall parameters for asphalt mixtures involved several steps. The Marshall hammer was used to first manufacture a total of 15 Marshall samples. Second, the manufactured samples were classified into five categories based on their CLS

content. It is worth mentioning that the compaction energy for sample preparation was equally simulated to heavy traffic loadings (i.e., 75 blows on each side of the asphalt mixtures) by the Marshall hammer [51]. After the compaction process, the Marshall stability, flow value, and Marshall quotient (MQ) were determined according to ASTM D1559 [52].

Marshall stability depends on the pressure loading applied on samples during the Marshall test. Therefore, Marshall stability can be defined as a specimens maximum bearing capacity under uniform vertical loading [53]. The samples deformation during vertical loading up to the maximum load denotes the flow value [54]. The Marshall quotient is calculated by dividing the Marshall stability by the flow value [55]. Higher MQ values indicate higher stiffness and better resistance against traffic loadings [56].

3.2. Resilient Modulus. The elastic stiffness of samples was determined by the resilient modulus test. The correlation between the applied load and the sample's deformation during repetitive loadings denotes the stiffness value [57]. Compared to the asphalt mixture's strength, the resilient modulus test is nondestructive because the load suffered by the sample is negligible [58].

The resilient modulus can calculate the optimum pavement thickness to design a new pavement [42]. In this research, the resilient modulus test was conducted at a temperature of 25°C with a haversine loading applied on samples using a universal testing machine (UTM) according to ASTM D4123 [59]. Figure 3 shows the resilient modulus test's loading pattern and testing machine. After 15 cycles of preloading, the computer software determined the average values at the last five cycles. Afterward, the resilient modulus was determined using the following equation [42]:

$$M_r = \frac{P(\nu + 0.27)}{t \Delta H}, \tag{1}$$

where M_r is the resilient modulus, P is the repetitive load (N), ν is Poisson's coefficient, ΔH is the average of reversible horizontal deformations (mm), and t is the specimen thickness (mm) [60]. It is worth mentioning that Poisson's coefficient was equal to 0.35 based on the test temperature [42]. Table 6 presents the setup parameters of the resilient modulus test.

3.3. Dynamic Creep Test. The dynamic creep test determines the tendency of asphalt mixtures to permanent deformations [61]. Cyclic loadings are applied to the specimens during the dynamic creep test to simulate actual traffic loads [62]. The significant outcome of the dynamic creep test is the vertical deformation against the loading cycles. While the dynamic creep test outputs do not correspond to the real rut depth, they can compare the rutting resistance of various asphalt mixtures [32].

As depicted in Figure 4, the creep curve obtained from the dynamic creep test can be divided into three zones. The creep strain rate increases sharply in the first phase due to the compaction process of the asphalt mixture [30]. The second phase involves an approximately constant strain rate.

The creep strain rate experiences an upward trend at the beginning of the tertiary phase, which denotes rutting failure [42]. The flow number (FN) can then be defined as the number of loading cycles at the beginning of the tertiary phase. Researchers determine the FN value as a benchmark to compare the rutting potential of asphalt mixtures [42, 63].

This study conducted the dynamic creep test on specimens of asphalt mixtures by UTM-14 at the Ferdowsi University of Mashhad following the AS-2891.12.1 standard (Figure 4) [64]. At the beginning of the dynamic creep test, samples were subjected to a static preloading stress of 10 kPa, which took 5 minutes to establish proper contact between the sample's surface and the loading's platen [42]. After the preloading stage, a cyclic stress level of 400 kPa with a frequency of 5 Hz was applied to the samples. The dynamic creep test was conducted at 50°C. Moreover, samples were treated at a temperature of 50°C for four hours before starting the test due to providing homogenous temperature within asphalt mixtures. Table 7 summarizes the required variables of the dynamic creep test.

3.4. Wheel Tracking Test. The Hamburg wheel-tracking (HWT) test has been used to measure the rut depth caused by the rolling wheel (Figure 5) [65]. The HWT outputs show the permanent deformations emanating from applying cyclic loadings on the surface of asphalt mixtures [57]. The HWT test was performed on $300 \times 300 \times 50$ mm compacted slabs with a 4% air void content at 50°C following the AASHTO T324 code (Figure 5) [66]. Moreover, the rubber wheel with an average contact stress of 50 psi was subjected to the slab samples with a 52 + 2 passes/minute loading rate [67]. A linear variable differential transformer (LVDT), placed at the side of the wheel, measured the rut depth data at each cycle. The HWT test was automatically terminated after 120 minutes. Figure 5 illustrates the HWT test apparatus and the compacted slab of the asphalt mixture.

The value of the wheel-tracking slope in the air (WTS$_{air}$), which denotes the grade of the deformation on the track for 1000 load cycles, was calculated using the following equation [68]:

$$\text{WTS}_{air} = \frac{(d_{6000} - d_{3000})}{3}, \tag{2}$$

where WTS$_{air}$ corresponds to the wheel-tracking slope (mm/10^3 load cycles) and d_{3000} and d_{6000} denote the rut depth values (mm) at 3000 and 6000 load cycles, respectively.

It is worth mentioning that the RD value, which indicates the total rut depth at the termination time (120 minutes), was determined [69]. To analyze the dynamic stability of asphalt mixtures, the DS parameter was obtained by the following equation [70]:

$$\text{DS} = \frac{N(t_2 - t_1)}{d_2 - d_1}, \tag{3}$$

where DS corresponds to the dynamic stability (cycle/min); d_1 and d_2 are the deformations of the asphalt mixture at rutting times t_1 and t_2, respectively (min); and N corresponds to the rolling rate (52 cycles/min).
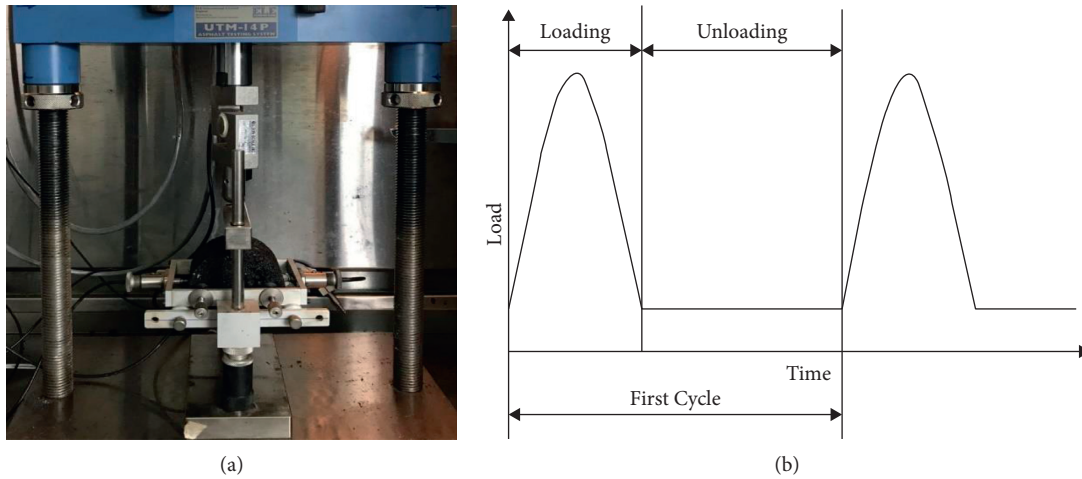
FIGURE 3: Resilient modulus test: (a) resilient modulus test apparatus and (b) loading shape.

TABLE 6: Setup parameters of the resilient modulus test.

Parameter	Unit	Value
Temperature	°C	25
Applied load	N	650
Poisson's ratio	—	0.35
Loading period	ms	100
Rest period	ms	900
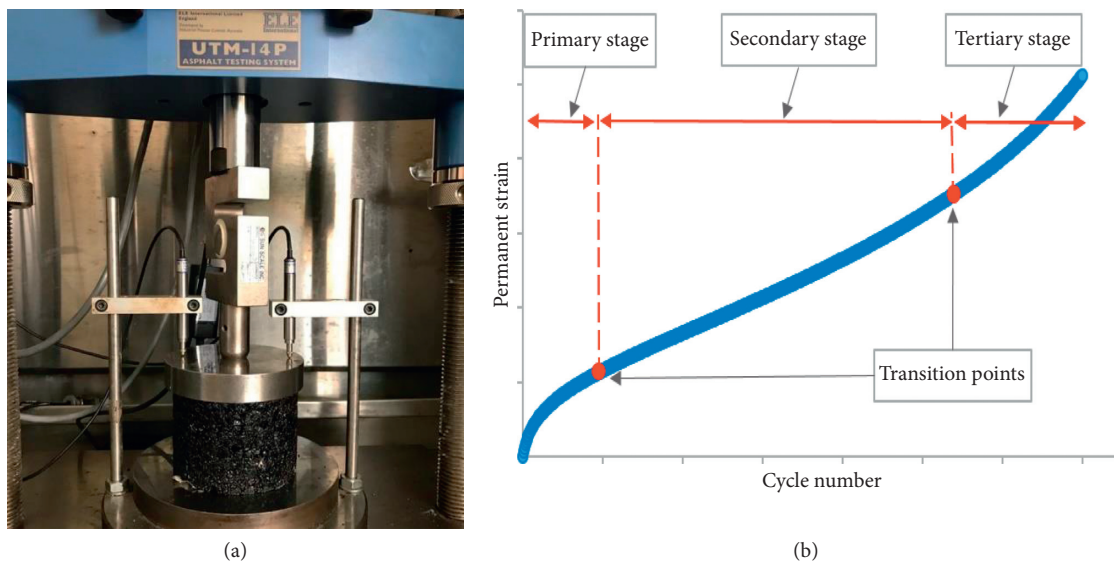
FIGURE 4: Dynamic creep test: (a) dynamic creep test apparatus and (b) permanent strain curve.

TABLE 7: Variables of the dynamic creep test.

Parameter	Unit	Value
Loading pattern	—	Rectangular
Rest period	ms	750
Loading period	ms	250
Contact stress	kPa	10
Applied repeated stress	kPa	400
Termination criteria	—	Until the tertiary stage appeared

(a)

(b)
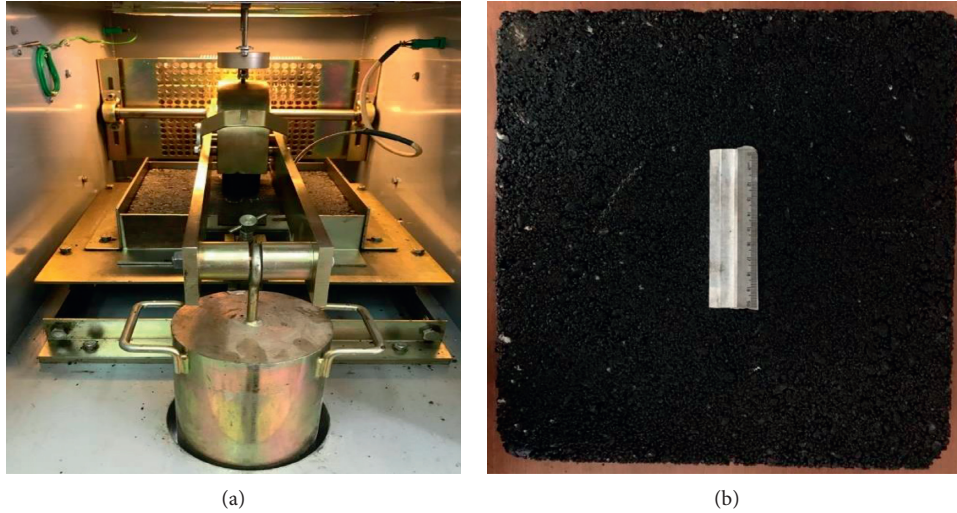
Figure 5: Wheel-tracking test: (a) wheel-tracking test apparatus and (b) manufactured slab of asphalt mixture.

3.5. Outline of Zhou Model and Tukey Method. Zhou considered three separate stages for creep behavior of asphalt mixtures based on the permanent deformation curve [27]. The power–law function was recommended to define the primary stage. The second stage was then described using a linear function. Finally, the exponential function was proposed to predict the tertiary stage [31]. The three-stage permanent deformation model proposed by Zhou can be calculated based on the following equations [27]:

$$N \leq N_{\text{PS}}, \quad \varepsilon_P = a N^b, \tag{4a}$$

$$
\begin{aligned}
& N_{\text{PS}} \leq N \leq N_{\text{ST}}, \\
& \varepsilon_{\text{PS}} = a N_{\text{PS}}^b, \\
& \varepsilon_P = \varepsilon_{\text{PS}} + C(N - N_{\text{PS}}),
\end{aligned} \tag{4b}
$$

$$
\begin{aligned}
& N \geq N_{\text{ST}}, \\
& \varepsilon_{\text{ST}} = \varepsilon_{\text{PS}} + C(N_{\text{ST}} - N_{\text{PS}}), \\
& \varepsilon_P = \varepsilon_{\text{ST}} + d\left(e^{f(N - N_{\text{ST}})} - 1\right),
\end{aligned} \tag{4c}
$$

where a, b, c, d, e, and f are the material constants; N_{PS} and N_{ST} denote to the number of load repetitions corresponding to the end of the primary and secondary stages, respectively; furthermore, ε_{PS} and ε_{ST} correspond to the permanent strain at the end of the primary and secondary stages, respectively.

This study calculated the permanent strain per cycle using UTM software for each sample during the dynamic creep test. In the next step, N_{PS}, N_{ST}, ε_{PS}, and ε_{ST} were determined according to Zhou's three-stage permanent deformation model. In addition, the one-way analysis of variance (ANOVA) was used to determine the effect of CLS on the creep behavior of the asphalt mixtures. The Tukey method with a 95% confidence level was also considered to rank the creep performance of asphalt mixtures [71].

4. Results and Discussion

In order to calculate the optimum bitumen content (OBC) of control asphalt mixtures, their Marshall design parameters are summarized in Table 8. According to the Iran Road Pavement Code, the OBC of control asphalt mixtures was the average of values achieved based on the following criteria:

(1) The OBC should provide 4% air voids within the compacted asphalt mixture.

(2) The OBC presents the maximum stability of the compacted asphalt mixture.

(3) The OBC brings the maximum specific gravity for compacted asphalt mixture.

After the determination of OBC, other Marshall design parameters, including voids in mineral aggregates (VMA), voids filled with bitumen (VFB), and flow values, were checked whether they satisfied the local code specification limits. The determined OBC for the control asphalt mixture was 4.9%. It is worth mentioning that the OBC of the control sample was selected to prepare CLS-modified samples.

4.1. Marshall Stability Parameters. When the OBC of the asphalt mixture was obtained, the Marshall stability parameters were determined for the five combinations categorized based on the CLS content. Figure 6(a) shows that the Marshall stability values experienced an upward trend versus an increment in the CLS content from 0% to 15%. Additional CLS within the bitumen from 15% to 20% decreased the Marshall stability value from 7.26 kN to 6.67 kN, respectively. Furthermore, the asphalt mixture containing 15% CLS shows a 31% increase in the Marshall stability value compared with the control asphalt mixtures. Figure 6(b) shows that the CLS-modified samples recorded lower flow values than the control sample; moreover, the asphalt sample

TABLE 8: Fitted equations of the Marshall design parameters.

Marshall parameter	Unit	Fitted equation	R-squared
Marshall stability	kN	$y = -5750x^2 + 542.04x - 7.38$	0.956
Flow	mm	$y = -1328.6x^2 + 182.87x - 2.08$	0.954
Unit weight	gr/m^3	$y = -292.86x^2 + 31.44x + 1.59$	0.977
Air voids	%	$y = 4821.4x^2 - 726.82x + 28.34$	0.968
VMA	%	$y = 10257x^2 - 1024.8x + 39.86$	0.983
VFB	%	$y = -19071x^2 + 3510.5x - 55.95$	0.961

(a)

(b)

(c)
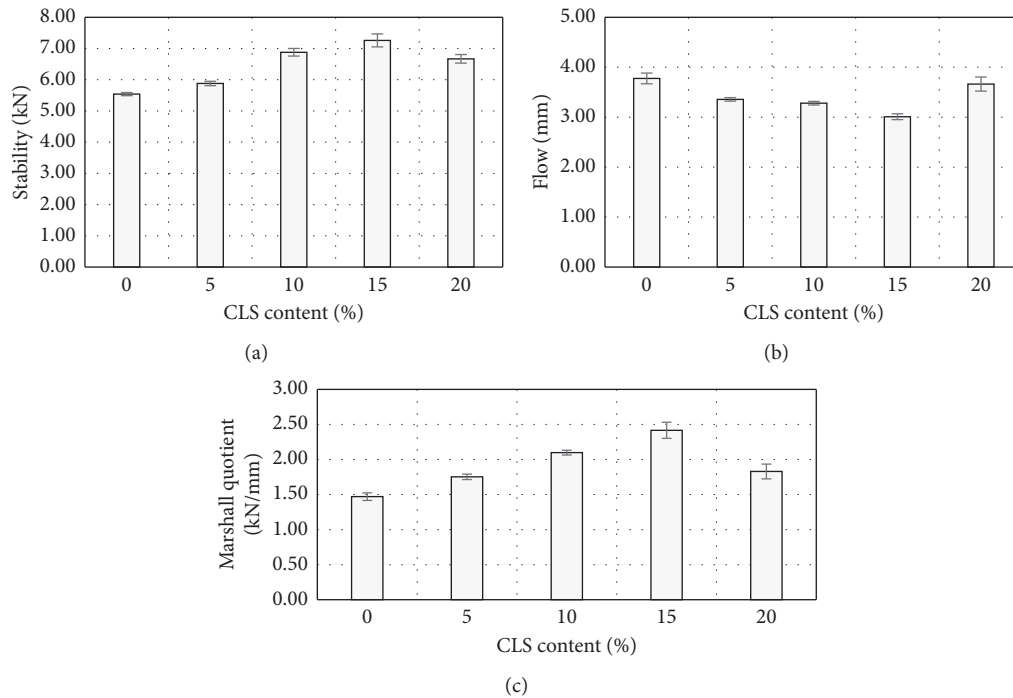
FIGURE 6: Marshall tests results: (a) Marshall stability outputs, (b) Marshall flow values, and (c) Marshall quotient results.

containing 15% CLS had the lowest flow value among all samples. The lowest flow value of asphalt mixtures was 3.01 mm, approximately 20% lower than the control sample's flow value.

The trend of Marshall stability and flow values depicted in Figure 6 is compatible with previous investigations on the effect of CLS on bitumen's stiffness potential [72, 73]. Figure 6(c) shows that when CLS content increased by more than 15% within the bitumen, the brittleness potential of asphalt mixtures soared. Then, the Marshall stability value decreased, and the flow value enlarged. The Marshall test results achieved are in accordance with our earlier observation, which showed that the combination of CLS and bitumen improved the consistency and stiffness of CLS-modified bitumen, leading to improvement in the asphalt mixture's Marshall parameters [33, 39].

Figure 6(c) reveals that the addition of CLS into the bitumen improved the performance of asphalt mixtures against rutting. The MQ values of CLS-modified asphalt mixtures were higher than those of the specimen fabricated by virgin bitumen. As depicted in Figure 6, the MQ values experienced a 64% increase when the CLS content increased from 0% to 15% and hit a peak containing a value of 2.42 kN/mm. Then,

asphalt mixtures containing 15% CLS showed the highest resistance to shear stress. The achieved Marshall quotient values were compatible with the findings of McCreedy and Williams [74]. They showed that lignin's presence in asphalt mixtures enhanced the asphalt mixture's rigidity.

4.2. Resilient Modulus. Figure 7 shows the resilient modulus values of asphalt mixtures. The resilient modulus test evaluated the response of asphalt mixtures under repeated loadings [75]. Moreover, that test was conducted at 25°C to simulate intermediate temperature conditions for asphalt mixtures [42]. As illustrated in Figure 7, the addition of CLS to the bitumen increased the resilient modulus of asphalt mixtures. The highest resilient modulus was about 17% higher than the resilient modulus of the control sample. More than 15% of CLS into the bitumen brought about a downward trend in resilient modulus values. Therefore, the stiffness of asphalt mixtures improved by adding CLS to the bitumen, which enhanced the asphalt mixture's durability against permanent deformations. On the other hand, an excessive increase in the resilient modulus values reduced the asphalt mixture's flexibility, which was responsible for
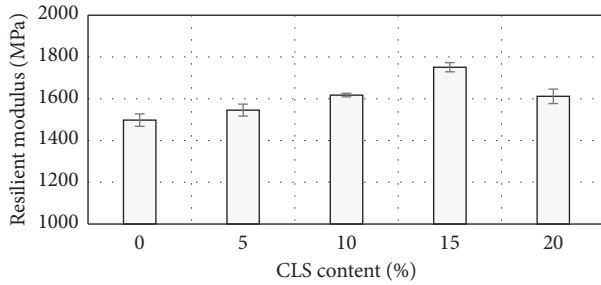
FIGURE 7: Resilient modulus of asphalt mixtures.

TABLE 9: Thickness reduction results based on resilient modulus values.

Mix type	Layer coefficient	Thickness reduction (%)
CLS-0%	0.311	0
CLS-5%	0.320	2.9
CLS-10%	0.334	7.4
CLS-15%	0.347	11.61
CLS-20%	0.338	8.6

the asphalt mixture's brittleness potential. In accordance with the resilient modulus results of the current study, Prez and others. [76] found that lignin could enhance the stiffness of asphalt mixtures, which led to a 10.48% increase in resilient modulus of asphalt mixtures containing 20% lignin compared with that of the control sample.

Based on the AASHTO flexible pavement design guide and Van Til and others' estimation method, the calculated thickness reduction for surface layers constructed by CLS-modified bitumen is presented in Table 9. It can be concluded that bitumen modification with CLS led to the surface layer's thickness reduction. As shown in Table 9, the thickness of the asphalt mixture containing 15% CLS was 11.61% lower than the thickness of the control sample during the road pavement's construction.

4.3. Dynamic Creep.

The dynamic creep test was conducted on unmodified and CLS-modified specimens to determine their creep behavior. It is worth mentioning that the dynamic creep test continued until samples reached the third phase of the cumulative strain curve. Three samples were fabricated with the same design procedure for each CLS content and tested using the UTM-14 machine under the same condition. Figure 8 shows that the asphalt mixture with 15% CLS had the lowest cumulative strain values. Moreover, all CLS-modified samples experienced higher rutting resistance than the control sample. The flow number (FN), determined at the end of the second phase of the dynamic creep curve, is reported in Figure 9. As shown in Figure 9, the presence of CLS can delay the plastic failure of the asphalt mixture due to traffic loads. For example, the FN value of the asphalt samples containing 15% CLS was recorded as 1013, which was about 1.8 times higher than the FN value of control samples. These findings are consistent with that of Xu et al. [23], who showed that incorporating lignin into bitumen could enhance the rutting performance of asphalt mixtures at high-temperature levels. Moreover, it is encouraging to compare the dynamic creep test results of the current study with the findings of Zhang et al. [24], who demonstrated that adding 2%, 4%, 6%, and 8% lignin into bitumen improved the resistance of asphalt mixtures against rutting.

4.4. Wheel Tracking.

Figure 10 demonstrates the curves of rut depth versus passing time derived from the HWT test. It can be observed that in contrast with the rut depth of CLS-modified samples, rut depth was more considerable for control specimens at 60°C. Moreover, the mixture containing 15% CLS had the lowest rut depth, and the control sample had the highest value after 120 minutes. At the end of the HWT experiment, when the CLS content increased from 0% to 15%, a decrease of about 45% in the rut depth was observed. Therefore, CLS had a beneficial impact on the rutting resistance of asphalt mixtures. The HWT test results are compatible with previous research performed by Xie et al. [77], who found that lignin could strengthen the high-temperature performance of asphalt mixtures.

Table 10 presents the final rut depth, dynamic stability, and wheel-tracking slope values of the HWT test. It can be found that the rutting parameters (i.e., RD, WTS, and DS) had lower values for CLS-modified samples than for the control specimen. Meanwhile, the samples containing 15% CLS exhibited the highest performance during the HWT test. Then, modification of bitumen by the CLS could effectively improve the rutting performance of asphalt mixtures.

4.5. Zhou Model and Tukey Method.

Table 11 presents the cycle's repetition number and permanent deformation at transition points of asphalt mixtures based on Zhou's three-stage model. According to Table 11, when the CLS content increased from 0% to 15%, the loading repetition number of primary and secondary stages increased. It can be observed that the stiffness of CLS-modified samples improved their rutting performance. Although 20% CLS decreased the rutting performance of asphalt mixtures compared to those containing 15% CLS, control samples had the highest susceptibility to rutting.

Table 12 explains the findings of the one-way ANOVA conducted by Minitab software. The statistical analysis was performed based on the null hypothesis in which all means were assumed equal. The p value was less than 0.05, indicating that the null hypothesis was unacceptable at the transition points. Then, the p value indicates that the presence of CLS had a significant influence on the rutting performance of asphalt mixtures.

As shown in Table 13, the Tukey method is used to rank the performance of asphalt mixtures in terms of creep behavior. It can be concluded that while the asphalt mixtures containing 15% CLS had the highest rutting performance, control specimens had the lowest rutting performance against traffic loadings. As can be seen from Table 13, the Tukey method did not show any significant differences in second transition point values between samples containing 10% CLS and 20% CLS.
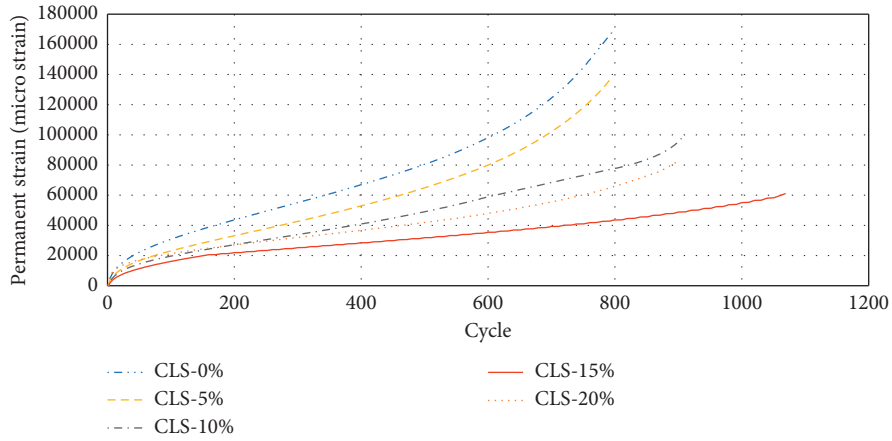
Figure 8: Creep curve for asphalt mixtures.
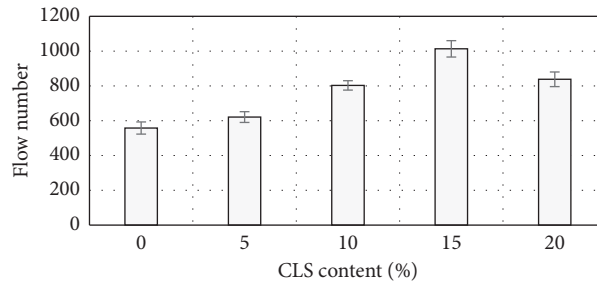
Figure 9: Flow number of asphalt mixtures.
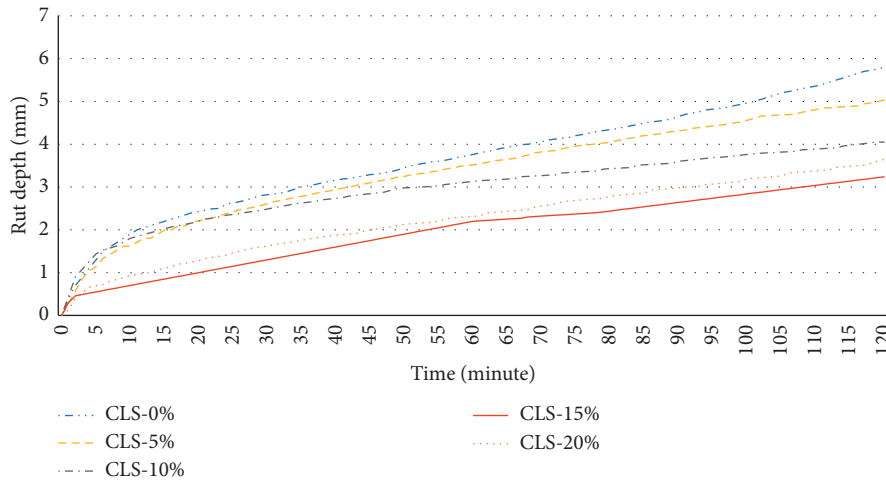
Figure 10: Measurements of the rut depth at 60°C.

Table 10: Final rut depth, wheel-tracking slope, and dynamic stability values of mixtures emanated from the wheel-tracking test.

Mix type	RD_{air} (mm)	WTS_{air} (mm per 10^3 cycles)	DS (cycle/min)
CLS-0%	5.81	0.64	1554
CLS-5%	5.04	0.48	2094
CLS-10%	4.05	0.34	2928
CLS-15%	3.24	0.31	3351
CLS-20%	3.65	0.41	2492

TABLE 11: Creep curve models derived from Zhou's transition points.

Sample code	First transition point		Second transition point	
	First stage model	End of the first stage	Second stage model	End of the second stage
CLS-0%	$\varepsilon_P = 3043.7691N^{0.5044}$	107	$\varepsilon_P = 32142.0423 + 121.9299(N{-}107)$	558
CLS-5%	$\varepsilon_P = 1466.2776N^{0.5279}$	135	$\varepsilon_P = 19536.2273 + 103.2894(N{-}135)$	621
CLS-10%	$\varepsilon_P = 2330.5186N^{0.4641}$	146	$\varepsilon_P = 23546.6286 + 78.4503(N{-}146)$	803
CLS-15%	$\varepsilon_P = 1400.5292N^{0.5302}$	160	$\varepsilon_P = 20655.0756 + 36.3122(N{-}160)$	1013
CLS-20%	$\varepsilon_P = 4630.2121N^{0.3316}$	151	$\varepsilon_P = 24442.7261 + 56.5546(N{-}151)$	828

TABLE 12: One-way ANOVA: transition point values versus CLS content.

Source	Df	Adj SS	Adj MS	F-value	P value
First transition point					
CLS content	4	5012.4	1253.1	55.94	<0.001
Error	10	224	22.4		
Total	14	5236.4			
Second transition point					
CLS content	4	391504	97875.9	352.83	<0.001
Error	10	2774	277.4		
Total	14	394278			

TABLE 13: Classification of transition points using the Tukey procedure with a confidence level of 95%.

CLS content (%)	N	Mean	Grouping			
First transition point						
15	3	160	A			
20	3	151	A	B		
10	3	146		B	C	
5	3	135			C	
0	3	107				D
Second transition point						
15	3	1013	A			
20	3	828		B		
10	3	803		B		
5	3	621			C	
0	3	558				D

5. Conclusions

The following results can be obtained with regard to the effects of adding CLS as a bitumen modifier in hot mix asphalt mixtures:

(i) The bumpy surface structure of CLS particles was detected through the FESEM test. Moreover, metal oxides, carbon, magnesium, calcium, and silicon were the significant elements of CLS, according to the EDX analysis.

(ii) Although the Marshall stability of CLS-modified asphalt mixtures recorded higher values than control samples, the flow outputs of asphalt mixtures containing the CLS powder had lower values than the control specimen. As a result, the presence of CLS increased the stiffness of asphalt mixtures. According to the Marshall quotient values, the highest stiffness was achieved for the asphalt mixture containing 15% CLS.

(iii) The incorporation of CLS into bitumen improved the response of the asphalt mixture to cyclic loadings because CLS-modified asphalt mixtures had a higher resilient modulus than control specimens. Moreover, CLS could decrease the thickness of the surface layer, leading to cost-benefit features during the road construction process.

(iv) The addition of CLS into bitumen enhanced the rutting performance of asphalt mixtures against cyclic loadings. Among the four kinds of asphalt mixtures made by 5%, 10%, 15%, and 20% CLS, the asphalt mixture with 15% CLS demonstrated the highest resistance to cyclic loadings during the dynamic creep test.

(v) Increasing the CLS content up to 15% achieved the lowest value of rut depth during the wheel-tracking test. The rutting susceptibility of asphalt mixtures experienced an upward trend when the CLS content increased more than 15%.

(vi) In future investigations, it will be interesting to evaluate the rutting performance of asphalt mixtures containing CLS powder based on different loading shapes during the dynamic creep test. Moreover, further research can investigate the temperature and loading's frequency interactive

effects on the rutting potential of CLS-modified asphalt mixtures based on the response surface methodology.

Data Availability

Based on the logical request of the responsible author, all data supporting the conclusion of this research will be available.

Conflicts of Interest

The authors state that there are no conflicts of interest associated with the publication of this study.

References

[1] X. Yang, A. Shen, Y. Jiang, Y. Meng, and H. Wu, "Properties and mechanism of flame retardance and smoke suppression in asphalt binder containing organic montmorillonite," *Construction and Building Materials*, vol. 302, Article ID 124148, 2021.

[2] Z. Zhang, A. Sha, X. Liu et al., "State-of-the-art of porous asphalt pavement: experience and considerations of mixture design," *Construction and Building Materials*, vol. 262, Article ID 119998, 2020.

[3] G. H. Hamedi, M. R. Esmaeeli, V. Najafi Moghaddam Gilani, and S. M. Hosseinian, "The effect of aggregate-forming minerals on thermodynamic parameters using surface free energy concept and its relationship with the moisture susceptibility of asphalt mixtures," *Advances in Civil Engineering*, vol. 2021, 2021.

[4] X. Wang and Y. Zhong, "Reflective crack in semi-rigid base asphalt pavement under temperature-traffic coupled dynamics using XFEM," *Construction and Building Materials*, vol. 214, pp. 280–289, 2019.

[5] M. Zheng, Y. Tian, and L. He, "Analysis on environmental thermal effect of functionally graded nanocomposite heat reflective coatings for asphalt pavement," *Coatings*, vol. 9, no. 3, p. 178, 2019.

[6] M. Irfan, Y. Ali, S. Ahmed, S. Iqbal, and H. Wang, "Rutting and fatigue properties of cellulose fiber-added stone mastic asphalt concrete mixtures," *Advances in Materials Science and Engineering*, vol. 2019, Article ID 5604197, 8 pages, 2019.

[7] T. Ahmed, E. Y. Hajj, A. Warrag, and M. Piratheepan, "Postmortem evaluation of accelerated rate of raveling of in-service asphalt pavements in arid climatic conditions-case of Kuwait," *Case Studies in Construction Materials*, vol. 14, Article ID e00533, 2021.

[8] H.-P. Wang, Y.-X. Guo, M.-Y. Wu, K. Xiang, and S.-R. Sun, "Review on structural damage rehabilitation and performance assessment of asphalt pavements," *Reviews on Advanced Materials Science*, vol. 60, no. 1, pp. 438–449, 2021.

[9] J. Zhang, H. Li, P. Liu et al., "Experimental exploration of influence of recycled polymer components on rutting resistance and fatigue behavior of asphalt mixtures," *Journal of Materials in Civil Engineering*, vol. 32, no. 6, Article ID 04020129, 2020.

[10] Y. Xu and L. Sun, "Study on permanent deformation of asphalt mixtures by single penetration repeated shear test," *Procedia - Social and Behavioral Sciences*, vol. 96, pp. 886–893, 2013.

[11] H. Majidifard, B. Jahangiri, P. Rath, L. Urra Contreras, W. G. Buttlar, and A. H. Alavi, "Developing a prediction model for rutting depth of asphalt mixtures using gene expression programming," *Construction and Building Materials*, vol. 267, Article ID 120543, 2021.

[12] W. Rafiq, M. A. Musarat, M. Altaf et al., "Life cycle cost analysis comparison of hot mix asphalt and reclaimed asphalt pavement: a case study," *Sustainable Times*, vol. 13, 2021.

[13] S. Kocak and M. Emin Kutay, "Combined effect of SBS and devulcanized rubber (DVR) modification on performance grade and fatigue cracking resistance of asphalt binders," *RILEM Bookseries*, vol. 13, pp. 269–274, 2016.

[14] H. Singh, T. Chopra, S. Jain, A. Kaur, and S. Kamotra, "Effect of aggregate type and polymer modification on the performance of bituminous concrete mixes," *Int. J. Appl. Sci. Eng.*vol. 16, pp. 1–13, 2019.

[15] J. V. S. de Melo, G. Trichês, and L. T. de Rosso, "Experimental evaluation of the influence of reinforcement with Multi-Walled Carbon Nanotubes (MWCNTs) on the properties and fatigue life of hot mix asphalt," *Construction and Building Materials*, vol. 162, pp. 369–382, 2018.

[16] P. J. Yoo and T. W. Kim, "Strengthening of hot-mix asphalt mixtures reinforced by polypropylene-impregnated multifilament glass fibres and scraps," *Construction and Building Materials*, vol. 75, pp. 415–420, 2015.

[17] S. A. Ghanoon, J. Tanzadeh, and M. Mirsepahi, "Laboratory evaluation of the composition of nano-clay, nano-lime and SBS modifiers on rutting resistance of asphalt binder," *Construction and Building Materials*, vol. 238, Article ID 117592, 2020.

[18] J. Yu, M. Vaidya, G. Su, S. Adhikari, E. Korolev, and S. Shekhovtsova, "Experimental study of soda lignin powder as an asphalt modifier for a sustainable pavement material," *Construction and Building Materials*, vol. 298, Article ID 123884, 2021.

[19] S. Ren, X. Liu, Y. Zhang et al., "Multi-scale characterization of lignin modified bitumen using experimental and molecular dynamics simulation methods," *Construction and Building Materials*, vol. 287, Article ID 123058, 2021.

[20] A. Grossman and W. Vermerris, "Lignin-based polymers and nanomaterials," *Current Opinion in Biotechnology*, vol. 56, pp. 112–120, 2019.

[21] J. Wu, Q. Liu, C. Wang, W. Wu, and W. Han, "Investigation of lignin as an alternative extender of bitumen for asphalt pavements," *Journal of Cleaner Production*, vol. 283, Article ID 124663, 2021.

[22] K. B. Batista, R. P. L. Padilha, T. O. Castro et al., "High-temperature, low-temperature and weathering aging performance of lignin modified asphalt binders," *Industrial Crops and Products*, vol. 111, pp. 107–116, 2018.

[23] G. Xu, H. Wang, and H. Zhu, "Rheological properties and anti-aging performance of asphalt binder modified with wood lignin," *Construction and Building Materials*, vol. 151, pp. 801–808, 2017.

[24] Y. Zhang, X. Wang, G. Ji et al., "Mechanical performance characterization of lignin-modified asphalt mixture," *Applied Sciences*, vol. 10, no. 9, p. 3324, 2020.

[25] B. Javilla, H. Fang, L. Mo, B. Shu, and S. Wu, "Test evaluation of rutting performance indicators of asphalt mixtures," *Construction and Building Materials*, vol. 155, pp. 1215–1223, 2017.

[26] M. Irfan, Y. Ali, S. Iqbal, S. Ahmed, and I. Hafeez, "Rutting evaluation of asphalt mixtures using static, dynamic, and repeated creep load tests," *Arabian Journal for Science and Engineering*, vol. 43, no. 10, pp. 5143–5155, 2017.

[27] A. Khodaii and A. Mehrara, "Evaluation of permanent deformation of unmodified and SBS modified asphalt mixtures using dynamic creep test," *Construction and Building Materials*, vol. 23, no. 7, pp. 2586–2592, 2009.

[28] H. Ziari, M. Nakhaei, A. Akbari Nasrekani, and A. Moniri, "Characterization of rutting resistance of EBS-modified asphalt mixtures," *Petroleum Science and Technology*, vol. 34, no. 13, pp. 1107–1112, 2016.

[29] L. N. Mohammad, M. Elseifi, W. Cao, A. Raghavendra, and M. Ye, "Evaluation of various hamburg wheel-Tracking devices and AASHTO T 324 specification for rutting testing of asphalt mixtures," *Asph. Paving Technol. Assoc. Asph. Paving Technol. Tech. Sess.* vol. 86, pp. 165–185, 2017.

[30] H. Y. Katman, M. R. Ibrahim, M. R. Karim, N. Salim Mashaan, and S. Koting, "Evaluation of permanent deformation of unmodified and rubber-reinforced SMA asphalt mixtures using dynamic creep test," *Advances in Materials Science and Engineering*, vol. 2015, 2015.

[31] F. Zhou, T. Scullion, and L. Sun, "Verification and modeling of three-stage permanent deformation behavior of asphalt mixes," *Journal of Transportation Engineering*, vol. 130, no. 4, pp. 486–494, 2004.

[32] T. Baghaee Moghaddam, M. Soltani, and M. R. Karim, "Evaluation of permanent deformation characteristics of unmodified and Polyethylene Terephthalate modified asphalt mixtures using dynamic creep test," *Materials & Design*, vol. 53, pp. 317–324, 2014.

[33] S. Fatemi, J. Bolouri Bazaz, and S. A. Ziaee, "Evaluation of rutting and fatigue behaviors of asphalt binders modified with calcium lignosulfonate," *Advances in Civil Engineering*, vol. 2021, 2021.

[34] R. El Hage, N. Brosse, L. Chrusciel, C. Sanchez, P. Sannigrahi, and A. Ragauskas, "Characterization of milled wood lignin and ethanol organosolv lignin from miscanthus," *Polymer Degradation and Stability*, vol. 94, no. 10, pp. 1632–1638, 2009.

[35] J. Hu, Q. Zhang, and D.-J. Lee, "Kraft lignin biorefinery: a perspective," *Bioresource Technology*, vol. 247, pp. 1181–1183, 2018.

[36] P. J. Van Soest, J. B. Robertson, M. B. Hall, and M. C. Barry, "Klason lignin is a nutritionally heterogeneous fraction unsuitable for the prediction of forage neutral-detergent fibre digestibility in ruminants," *British Journal of Nutrition*, vol. 124, no. 7, pp. 693–700, 2020.

[37] X. Lu, X. Zhu, H. Guo et al., "Investigation on the thermal degradation behavior of enzymatic hydrolysis lignin with or without steam explosion treatment characterized by TG-FTIR and Py-GC/MS," *Biomass Convers. Biorefinery*, vol. 342, pp. 1–10, 2020.

[38] T. Aro and P. Fatehi, "Production and application of lignosulfonates and sulfonated lignin," *ChemSusChem*, vol. 10, no. 9, pp. 1861–1877, 2017.

[39] S. Fatemi, J. B. Bazaz, and S. A. Ziaee, "The pros and cons of using calcium lignosulfonate as a recycled anti-aging additive on engineering properties of bituminous mastics," *Case Studies in Construction Materials*, vol. 15, Article ID e00739, 2021.

[40] C. Xu and F. Ferdosian, "Structure and properties of lignin," *Conversion of Lignin into Bio-Based Chemicals and Materials. Green Chemistry and Sustainable Technology*, Springer, Berlin, Heidelberg, pp. 1–12, 2017.

[41] K. S. Khitrin, S. L. Fuks, S. V. Khitrin, S. A. Kazienkov, and D. S. Meteleva, "Lignin utilization options and methods," *Russian Journal of General Chemistry*, vol. 82, no. 5, pp. 977–984, 2012.

[42] S. Fatemi and R. Imaninasab, "Performance evaluation of recycled asphalt mixtures by construction and demolition waste materials," *Construction and Building Materials*, vol. 120, pp. 450–456, 2016.

[43] A. Gobetti, G. Cornacchia, and G. Ramorino, "Innovative reuse of electric arc furnace slag as filler for different polymer matrixes," *Minerals*, vol. 11, no. 8, p. 832, 2021.

[44] H. Ziari, M. Naghavi, and R. Imaninasab, "Performance evaluation of rubberised asphalt mixes containing WMA additives," *International Journal of Pavement Engineering*, vol. 19, no. 7, pp. 623–629, 2018.

[45] S. Aflaki and N. Tabatabaee, "Proposals for modification of Iranian bitumen to meet the climatic requirements of Iran," *Construction and Building Materials*, vol. 23, no. 6, pp. 2141–2150, 2009.

[46] X. Ouyang, X. Qiu, and P. Chen, "Physicochemical characterization of calcium lignosulfonate-A potentially useful water reducer," *Colloids Surfaces A Physicochem. Eng. Asp.* vol. 282–283, pp. 489–497, 2006.

[47] K. K. Khichar, S. B. Dangi, V. Dhayal et al., "Structural, optical, and surface morphological studies of ethyl cellulose/ graphene oxide nanocomposites," *Polymer Composites*, vol. 41, no. 7, pp. 2792–2802, 2020.

[48] J. O. Akinyele, R. W. Salim, and W. K. Kupolati, "The impact of rubber crumb on the mechanical and chemical properties of concrete," *Engineering Structures and Technologies*, vol. 7, no. 4, pp. 197–204, 2016.

[49] Y. Zhang, X. Liu, P. Apostolidis et al., "Chemical and rheological evaluation of aged lignin-modified bitumen," *Materials*, vol. 12, no. 24, p. 4176, 2019.

[50] P. Jędrzejczak, M. N. Collins, T. Jesionowski, and Ł. Klapiszewski, "The role of lignin and lignin-based materials in sustainable construction – a comprehensive review," *International Journal of Biological Macromolecules*, vol. 187, pp. 624–650, 2021.

[51] M. A. Kadhim, S. Al-Busaltan, and R. R. Almuhanna, "An evaluation of the effect of crushed waste glass on the performance of cold bituminous emulsion mixtures," *International Journal of Pavement Research and Technology*, vol. 12, no. 4, pp. 396–406, 2019.

[52] A. I. Al-Hadidy, "Performance of SBS-hma mixes made with sasobit and zeolite," *Journal of Materials in Civil Engineering*, vol. 32, no. 10, Article ID 06020017, 2020.

[53] N. M. Asmael and M. Q. Waheed, "Investigation of using polymers to improve asphalt pavement performance," *Am. Sci. Res. J. Eng. Technol. Sci.* vol. 39, pp. 38–48, 2018, http://asrjetsjournal.org/index.php/American_Scientific_Journal/article/download/3768/1364 accessed.

[54] H. Chen, Q. Xu, S. Chen, and Z. Zhang, "Evaluation and design of fiber-reinforced asphalt mixtures," *Materials & Design*, vol. 30, no. 7, pp. 2595–2603, 2009.

[55] R. Mistry and T. Kumar Roy, "Predicting Marshall stability and flow of bituminous mix containing waste fillers by fuzzy logic," *Revista de la construcción*, vol. 19, no. 2, pp. 209–219, 2020.

[56] M. Ameri, S. Hesami, and H. Goli, "Laboratory evaluation of warm mix asphalt mixtures containing electric arc furnace (EAF) steel slag," *Construction and Building Materials*, vol. 49, pp. 611–617, 2013.

[57] H. Ziari, A. Moniri, R. Imaninasab, and M. Nakhaei, "Effect of copper slag on performance of warm mix asphalt," *International Journal of Pavement Engineering*, vol. 20, no. 7, pp. 775–781, 2019.

[58] R. H. Ariyapijati, S. P. Hadiwardoyo, and R. J. Sumabrata, "Contributions crumb rubber in hot mix asphalt to the

resilient modulus," *AIP Conference Proceedings*, vol. 1855, Article ID 030005, 2017.

[59] M. K. Idham, H. Mohd Rosli, H. Yaacob, M. N. M. Warid, and M. E. Abdullah, "Effect of aging on resilient modulus of hot mix asphalt mixtures," *Advanced Materials Research*, vol. 723, pp. 291–297, 2013.

[60] G. Shafabakhsh and A. Tanakizadeh, "Investigation of loading features effects on resilient modulus of asphalt mixtures using Adaptive Neuro-Fuzzy Inference System," *Construction and Building Materials*, vol. 76, pp. 256–263, 2015.

[61] A. Azarhoosh, M. Koohmishi, and G. H. Hamedi, "Rutting resistance of hot mix asphalt containing coarse recycled concrete aggregates coated with waste plastic bottles," *Advances in Civil Engineering*, vol. 2021, pp. 1–11, Article ID 9558241, 2021.

[62] N. Li, H. Zhan, X. Yu, W. Tang, H. Yu, and F. Dong, "Research on the high temperature performance of asphalt pavement based on field cores with different rutting development levels," *Mater. Struct. Constr.*vol. 54, 2021.

[63] E. Y. Hajj, A. Ulloa, R. Siddharthan, and P. E. Sebaaly, "Characteristics of the loading pulse for the flow number performance test," *Asph. Paving Technol. Assoc. Asph. Paving Technol. Tech. Sess.*vol. 79, pp. 253–285, 2010, https://trid.trb.org/view/1087096 accessed.

[64] T. A. Sangita, S. Khan, D. K. Sabina, and D. K. Sharma, "Effect of waste polymer modifier on the properties of bituminous concrete mixes," *Construction and Building Materials*, vol. 25, no. 10, pp. 3841–3848, 2011.

[65] P. Zieliński, "Indirect tensile test as a simple method for rut resistance evaluation of asphalt mixtures–Polish experience," *Road Materials and Pavement Design*, vol. 23, no. 1, pp. 112–128, 2020.

[66] Y. Zhao, Y. Gao, K. Zhang, Y. Zhang, and M. Yu, "Establishment of rutting model of wheel-tracking test for real-time prediction of rut depth of asphalt layers," *Advances in Civil Engineering*, vol. 2021, pp. 1–16, 2021.

[67] P. Chaturabong and H. U. Bahia, "Mechanisms of asphalt mixture rutting in the dry Hamburg Wheel Tracking test and the potential to be alternative test in measuring rutting resistance," *Construction and Building Materials*, vol. 146, pp. 175–182, 2017.

[68] D. Movilla-Quesada, A. C. Raposeiras, L. T. Silva-Klein, P. Lastra-González, and D. Castro-Fresno, "Use of plastic scrap in asphalt mixtures added by dry method as a partial substitute for bitumen," *Waste Management*, vol. 87, pp. 751–760, 2019.

[69] Q. Lv, W. Huang, M. Zheng, H. Sadek, Y. Zhang, and C. Yan, "Influence of gradation on asphalt mix rutting resistance measured by Hamburg Wheel Tracking test," *Construction and Building Materials*, vol. 238, p. 117674, 2020.

[70] X. Yan, R. Ying, J. Jin, and Y. Zhang, "Study on cracking resistance of basalt fiber-reinforced microbond asphalt macadam," *Advances in Civil Engineering*, vol. 2021, 2021.

[71] H. Ziari, A. T. Barakoohi, and A. Moniri, "Laboratory investigation of the effect of temperature on frictional properties of concrete pavements containing crushed glass," *International Journal of Pavement Research and Technology*, vol. 10, no. 4, pp. 297–303, 2017.

[72] M. Zarei, A. Abdi Kordani, and M. Zahedi, "Pure mode I and pure mode II fracture resistance of modified hot mix asphalt at low and intermediate temperatures," *Fatigue and Fracture of Engineering Materials and Structures*, vol. 44, no. 8, pp. 2222–2243, 2021.

[73] M. Zarei, A. Abdi Kordani, Z. ghamarimajd, m. khajehzadeh, M. Khanjari, and M. Zahedi, "Evaluation of fracture resistance of asphalt concrete involving Calcium Lignosulfonate and Polyester fiber under freeze-thaw damage," *Theoretical and Applied Fracture Mechanics*, vol. 117, Article ID 103168, 2022.

[74] N. S. McCready and R. C. Williams, "Utilization of biofuel coproducts as performance enhancers in asphalt binder," *Transportation Research Record: Journal of the Transportation Research Board*, vol. 2051, no. 1, pp. 8–14, 2008.

[75] M. Karami, H. Nikraz, S. Sebayang, and L. Irianti, "Laboratory experiment on resilient modulus of BRA modified asphalt mixtures," *International Journal of Pavement Research and Technology*, vol. 11, no. 1, pp. 38–46, 2018.

[76] I. P. Pérez, A. M. Rodríguez Pasandín, J. C. Pais, and P. A. Alves Pereira, "Use of lignin biopolymer from industrial waste as bitumen extender for asphalt mixtures," *Journal of Cleaner Production*, vol. 220, pp. 87–98, 2019.

[77] S. Xie, Q. Li, P. Karki, F. Zhou, and J. S. Yuan, "Lignin as renewable and superior asphalt binder modifier," *ACS Sustainable Chemistry & Engineering*, vol. 5, no. 4, pp. 2817–2823, 2017.

Research Article

The Effects of Using Waste Engine Oil Bottom on Physical, Rheological Properties and Composite Modification Mechanism of SBS-Modified Asphalt

Yanbo Wang (ID), **Ailian Liu, Weixiang Ding, Fangping Rao, Jun Yuan, Zhihua Zhang, Zhen Xu, and Chuanzhou Dong**

The Third Construction Engineering Co. Ltd. of China Construction Third Engineering Bureau,
No. 2 Guannanyuan Road Hongshan District, Wuhan 430000, Hubei, China

Correspondence should be addressed to Yanbo Wang; pissaa@163.com

This research explores the effects of using waste engine oil bottom on physical, rheological properties and composite modification mechanism of SBS-modified asphalt. The SBS asphalt binder was modified by WEOB with different concentrations (2, 4, and 6 wt %). The GC-MS and FTIR spectrometry were conducted to evaluate the chemical compositions of WEOB- and WEOB-modified asphalt. RV, DSR, and BBR were tested to evaluate high- and low-temperature pavement performance. Fluorescence microscope (FM) test, bar thin layer chromatograph (BTLC) test, and AFM test were performed to evaluate the micromorphologies and modification mechanism. The test results showed that a new characteristic peak appeared in the infrared spectrum of the WEOB-modified SBS asphalt, indicating a chemical reaction in the modification process. Incorporation of WEOB improves both the high-temperature and low-temperature properties of the SBS asphalt binder. It was confirmed that with the increase of WEOB concentration, the content of colloid gradually increases, which promotes the swelling and compaction of SBS polymer network structure. Furthermore, WEOB promotes the polarity of SBS and forms graft product MAH-g-SBS with asphalt, thus inhibiting the thermal movement of asphalt molecules. On the contrary, light components have a good correlation with the surface roughness of modified asphalt; the results show that the modified asphalt has good rutting resistance.

1. Introduction

The large-scale construction of highway pavement is accompanied by a large consumption of asphalt, which is a nonrenewable material [1]. Therefore, modifying or regenerating asphalt to improve the quality of binder or reducing the consumption of new asphalt is an important means to save fossil fuel. Through the simple processing of waste oil materials, it can become an effective additive to modify asphalt. On the basis of improving the property of asphalt, it can also play a significant effect in environmental protection [2–4].

With the development of transportation industry and the continuous growth of car ownership, the production of waste engine oil (WEO) after vehicle maintenance is also

ever-growing. WEO is classified as a hazardous waste because it poses a certain threat to the environment and human production and life [5]. The WEO is usually treated by combustion, which inevitably leads to soil and air pollution to a certain extent [6]. At present, WEO is generally recycled by ecological methods such as sedimentation and distillation, and the residue after process becomes waste engine oil bottom (WEOB) [1, 4, 7]. This method can maximize the use of resources and become the mainstream WEO disposal method.

A new survey shows that America can generate millions of gallons of WEOB annually [6]. The engine oil and asphalt belong to different products in the process of petroleum refining and have homology, which has been confirmed in previous studies [8]. In the process of production and use,

the engine oil will inevitably change after passing through an environment of high temperature and high pressure [9, 10]. In addition, certain physical and chemical changes will also occur in the process of refining and purifying waste engine oil. Therefore, the research on the properties of WEOB and asphalt blend has been a hot topic. Hesp's research team has been carrying out research on the properties after mixing between WEOB and asphalt in the recent 10 years [11].

The research team detected the existence of WEOB in asphalt by microscopic methods and verified the hypothesis that the early failure of asphalt pavement is related to the existence of WEOB [12]. After that, some researcher studied the influence of WEOB from different sources on the property of asphalt binder and found that WEOB had a negative impact on the high- and low-temperature performance of asphalt [13, 14].

However, different researchers hold diametrically opposite views on the promotion effect of WEOB on the property of asphalt binder [4, 14–16]. For instance, Qurashi et al. [7] evaluated the properties of WEOB-modified bitumens and found that WEOB increases the grade span and reduces the cracking performance of bitumen. Some research reported that the asphalt added with WEOB has good stress relaxation ability under short-term aging conditions [15]. Moreover, as it contains light components, WEO can act as a rejuvenator to recover some properties of asphalt [7, 17].

However, little research results have been reported at this point concerning the influence of the fusion of WEOB and SBS polymers on the properties of modified asphalt. In fact, modified asphalt is more used as binder in road construction. Therefore, it is particularly important to carry out the research between SBS-modified asphalt and WEOB modifier.

In this paper, four kinds of WEOB concentration were selected to prepare four types of WEOB-modified SBS asphalt. The effects of organic reagents on the properties of modified asphalt were studied in the microstructure level. Thus, the objectives of this study will be as follows:

(1) To evaluate the synergistic effect of WEOB and SBS polymer on physical and rheological properties of asphalt binder and then recommend an optimum WEOB content

(2) To explore the modification mechanisms of WEOB/ SBS-modified asphalt

For convenience, the flowchart of this work is summarized and illustrated in Figure 1.

2. Materials and Methods

2.1. Materials. Tests were performed on representative samples of SBS-modified binder (the dosage of SBS was 4.3 wt%), and its properties are listed in Table 1. WEOB used was purchased from local Motor Madness. It was a byproduct of refining waste engine oil through vacuum distillation, centrifugal separation, and other processes.

Figure 2 shows the processing technology of WEOB. Elemental compositions of WEOB are listed in Table 2.

2.2. Preparation of WEOB-Modified Binders. As engine oil and bitumen are products of crude oil refining, they are homologous, which makes direct mixing possible [18]. WEOB-modified SBS asphalt was prepared by heating blending method, the details of which are presented in Figure 3. The WEOB contents were selected based on the conclusions of previous research, as shown in Table 3. Four WEOB contents were designed as 0%, 2%, 4%, and 6% of asphalt binder mass, respectively.

2.3. Experimental Methods. The Brookfield viscosity test was introduced to evaluate the viscosity of different kinds of asphalt binders, which was done at test temperature ranges from 110°C to 180°C at intervals of 10° according to the AASHTO method.

The multiple stress creep recovery (MSCR) was conducted at repeat loading of 0.1 kPa and 3.2 kPa to evaluate the deformation resistance, which was characterized by the parameter of the average recovery rate (R) and unrecoverable flexibility (Jnr).

The bending beam rheometer (BBR) was obtained to characterize the cracking resistance of WEOB-modified asphalt. Tests were performed at −12°C and −18°C.

The gas chromatograph (GC-MS) was conducted to evaluate the chemical component of WEOB. The potential chemical reaction of WEOB- and SBS-modified asphalt was obtained by FTIR (NICOLET 6700 TM).

In view of the different fluorescence effects of asphalt and SBS polymer, the swelling property of the WEOB-modified asphalt were evaluated by FM (MIKON, USA) images.

The AFM equipment (Bruker Corporation, Innova, USA) was proposed to observe the micromorphology characteristics of the binders. The test method adopts tapping mode and the resonance frequency of 260 KHz.

The content of four components (asphaltene, resin, aromatic hydrocarbon, and saturated hydrocarbons) of asphalt will change during the modification process. Therefore, the layered adsorption of different components can be quantitatively analyzed by bar thin layer chromatograph (BTLC) equipment, which is shown in Figure 4.

3. Results and Discussion

3.1. Chemical Components of WEOB. Figure 5 shows the GC-MS chromatogram of WEOB, from which we can see the peaks formed by different compounds. The name and molecular structure of the compound can be found by analyzing the corresponding peak positions. The results are shown in Table 4. It can be seen that WEOB is mainly composed of cycloalkanes, linear alkanes, various anhydrides, and their derivatives. The molar mass of each compound is small, belonging to olefin oil and aromatic solvents, while anhydride is mainly the anhydride product formed by synthetic engine oil compound through high-temperature and high-pressure engine degreasing and other reactions.
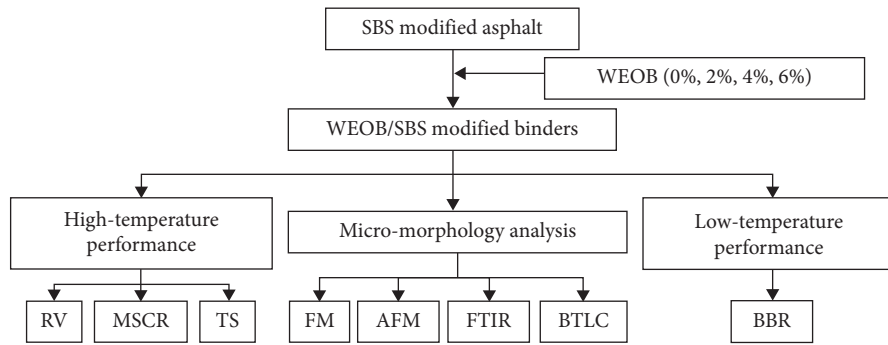
Figure 1: Flowchart of experimental procedure.

Table 1: Properties of SBS-modified binder.

Test properties	Unit	Test result
Penetration (25°C, 100 g, 5 s)	0.1 mm	50.7
Ductility (5°C, 5 cm/min)	cm	40.5
Softening point (TR&B)	°C	71.6

3.2. Viscosity. Figure 6 shows the influence trend of WEOB on the viscosity of SBS-modified asphalt. It can be seen from the figure that the rotational viscosity of modified asphalt has a significant correlation with the test temperature and WEOB content. Specifically, the increase of temperature and the decrease of WEOB content will weaken the viscosity of modified asphalt. The increase of ambient temperature weakens the thermal movement limit of asphalt molecules, while the addition of WEOB improves the expansion of SBS polymer network structure, makes the three-dimensional structure more uniform and denser, and limits the flow capacity of asphalt molecules to a certain extent. In order to facilitate construction, the specification has strict requirements on rotational viscosity, that is, at 135°C, the rotational viscosity shall not exceed 3.0 Pa·s. It can be seen from the figure that the limit rotational viscosity value of WEOB-modified asphalt does not exceed the threshold under this temperature condition. Therefore, under certain dosage conditions, the addition of WEOB can meet the construction requirements.

3.3. High-Temperature Property. The cumulative strain results of modified asphalt with different WEOB content under 64°C and 3.2 kPa stress are shown in Figure 7. Obviously, compared with SBS-modified asphalt without WEOB, the cumulative strain of asphalt decreases sharply after adding, and the downward trend is more obvious with the increase of content, which shows that WEOB has a positive effect on improving the high-temperature deformation resistance of SBS-modified asphalt. The result is the same as the conclusion of rotational viscosity.

To quantitatively evaluate the influence of WEOB on the cumulative strain of modified asphalt at high temperature, the R and Jnr are calculated based on the data (Figure 7) and equations (1) and (2), and the results are shown in Figure 8. Regardless of the stress level and test temperature, the concentration dependency of R and J are remarkable in that the R increase and J reduces as WEOB content rises, which indicates that the existence of WEOB improves the high-temperature recovery ability of WEOB-modified asphalt more, and the larger WEOB content corresponds to the better high-temperature property. This result can be explained by the fact that the light component contained in WEOB reacts with SBS polymer to form a network structure, and the more the content is, the denser the structure is, and the stronger the high-temperature deformation resistance is.

To distinctly compare the high-temperature creep and recovery behaviors of SBS-modified binders with various WEOB contents, the data at the fifth loading stage from Figure 7 are extracted and plotted in Figure 9. The creep behavior (Figure 9(a)) is first discussed. It is obvious that a decrease of accumulated strain is observed with the introduction of WEOB into asphalt, meaning that the existence of WEOB causes a reduction in the creep behavior of the SBS-modified binder. Figure 9(a) also demonstrates that among these WEOB/SBS-modified binders, the binder containing 6 wt% of WEOB exhibits larger creep behavior than the counterparts with 2 wt% and 4 wt% WEOB which have little difference in creep behavior. Furthermore, the strain of all binder samples increases exponentially with time. Based on this curve feature and the previous work by You et al. [21], Burgers model (see Equations (1) and (2)) is applied to fit the creep behavior of these binders, and the fitting results are shown in Table 5. It can be seen that the correlation coefficients exceed 0.999, suggesting the excellent applicability of Burgers model in fitting the creep behavior of SBS/WEOB-modified binders. Importantly, the elastic and viscous deformations are further divided into instantaneous and delayed parts, respectively, which provides the possibility to better understand the deformation process of the binder.

To facilitate evaluation of the WEOB content influence on the high-temperature recovery behavior of the binder, the strain in the recovery stage is normalized and then plotted in Figure 9(b). The normalized value is referred to as residual deformation [22]. As it can be seen, the residual
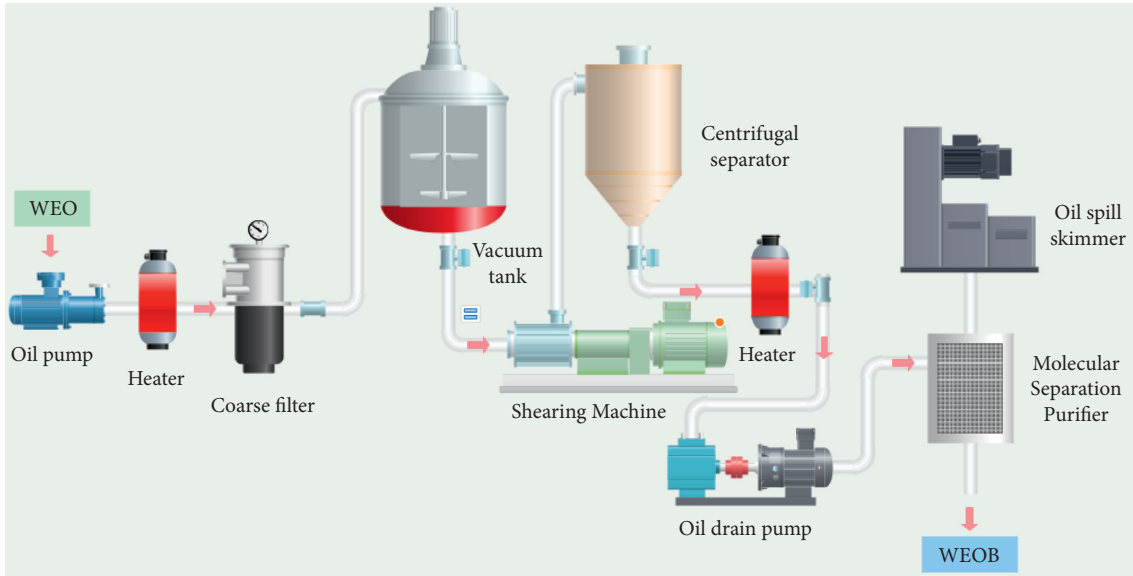
FIGURE 2: Processing technology of WEOB.

TABLE 2: Elemental composition and technical properties of WEOB.

Phosphorus (%)	Sulfur (%)	Calcium (%)	Iron (%)	Copper (%)	Zinc (%)	Molybdenum (%)	Dynamic viscosity (Pa·s)	pH
1.39	1.68	0.91	0.15	0.4	0.59	0.04	18.2 @60°C	3.4
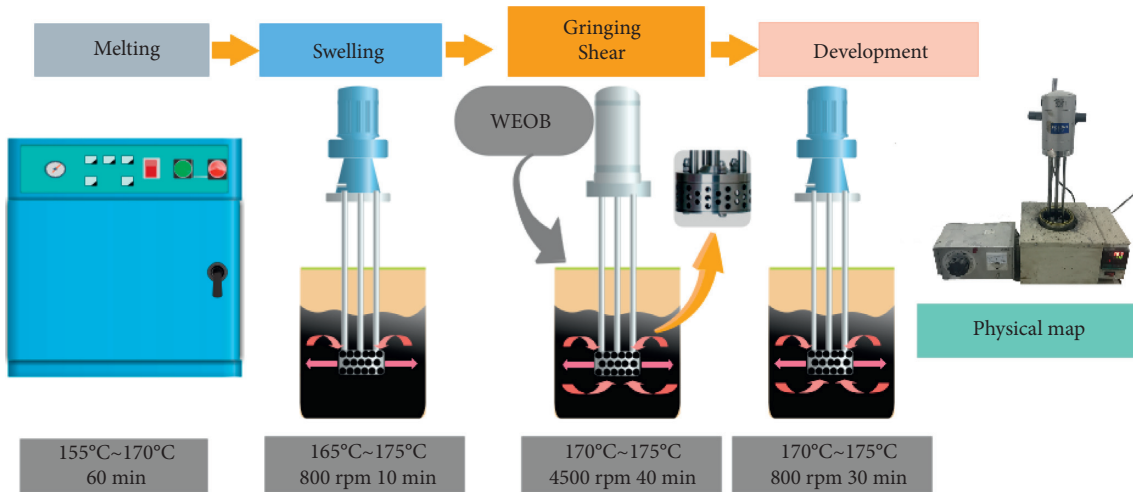
FIGURE 3: Preparation process of WEOB/SBS-modified binder.

TABLE 3: WEOB or WEO content in existing studies and practices.

Content	Asphalt type	Literature
0%, 2%, 4%, 6%, 8%	VG-30	Qurashi and Swamy [7]
6%, 8%	Polymer-modified binders	Paliukaiteet al. [19]
0%, 4%, 8%	60/80 pen-grade base asphalt and SBS-modified asphalt	Liu et al. [20]

deformations from large to small are 0.64, 0.60, 0.52, and 0.29 corresponding to SBS-modified binders with the WEOB content of 2%, 4%, 0%, and 6%, respectively. Considering the residual deformation is a consequence of viscous flow, the creep deformation of the binder with 6 wt% of WEOB is primarily caused by elasticity. However, other binders that have the residual deformation larger than 0.5 show more viscous deformation than elastic deformation. In view of the
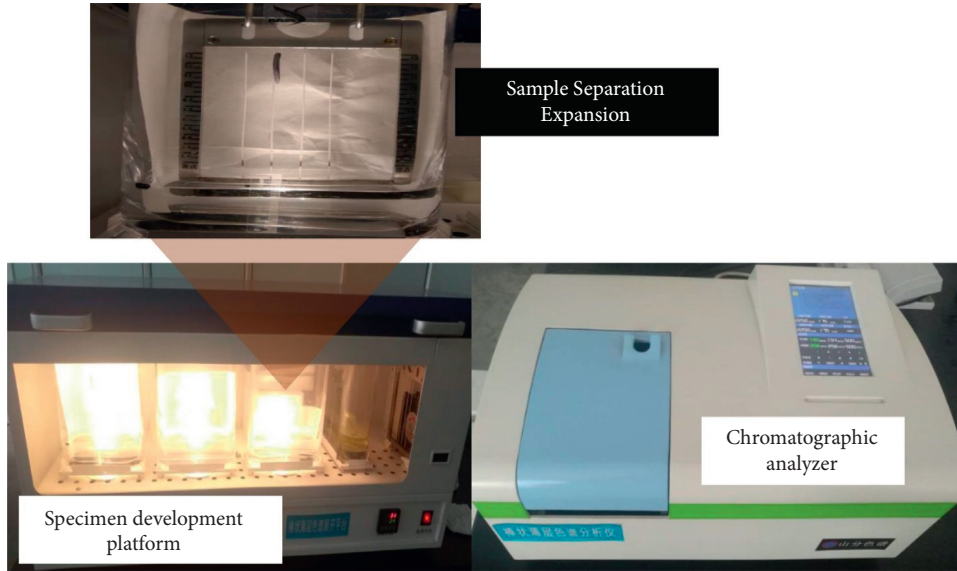
FIGURE 4: Setup for bar thin layer chromatography analyzer.
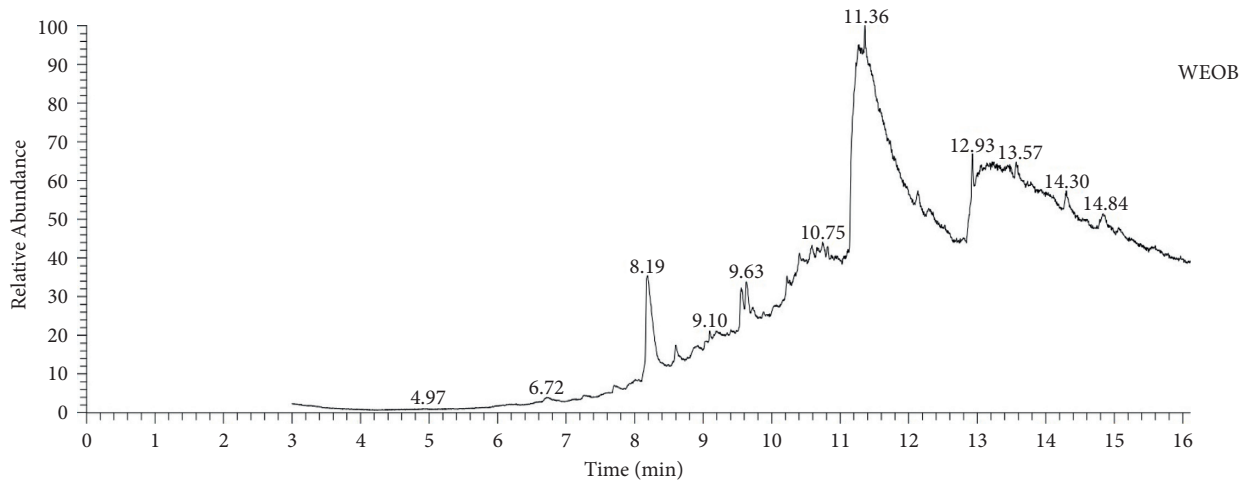
FIGURE 5: GC-MS chromatogram of WEOB.

similar curve feature in Figure 9(a), the curves in Figure 9(b) can be fitted by Burgers model as well. According to the result in Table 6, it is obtained that Burgers model is capable of perfectly fitting the recovery behavior of SBS/WEOB-modified binders owing to the R^2 exceeding 0.99.

$$\varepsilon(t) = \frac{\sigma_0}{E_1} + \frac{\sigma_0}{\eta_1} + \frac{\sigma_0}{E_2}\left(1 - e^{-E_2 t/\eta_2}\right). \quad (1)$$

$$\varepsilon(t) = \frac{E_1 \eta_1 E_2}{\eta_1 E_2 + E_1 E_2 t + E_1 \eta_1 \left(1 - e^{-E_2 t/\eta_2}\right)}, \quad (2)$$

where σ_0 is the initial stress (Pa), Young's modulus (Pa) is recorded as E, and η is the viscosity (Pa·s).

3.4. Low-Temperature Property.

The creep stiffness modulus (S) and creep slope (m) of modified asphalt with various WEOB content under different low-temperature environments are shown in Figure 10. Generally, a larger S represents more tensile stress, and a larger m value means more stress relaxation. Apparently, the small S value and large m value at low temperature are preferred for asphalt binder. It can be seen from Figure 10 that at the temperatures of $-12°C$ and $-18°C$, with the increase of WEOB content, S value decreases and m value increases, which significantly improves the low-temperature deformation resistance of surface asphalt with the addition of WEOB. The possible reason for this phenomenon is that the addition of light components, which increases the maltenes concentration of asphalt. Moreover, the SBS polymer expands effectively in the surplus light component environment and forms a network structure with resistance to low-temperature cracking and deformation. In addition, under the action of MAH, WEOB and SBS form graft products, which play a positive role in improving the relaxation and deformation ability.

TABLE 4: The chemical composition of WEOB.

Retention time (min)	Formula	Structure	Retention time (min)	Formula	Structure
6.72	$C_4H_2O_3$		11.36	$C_{16}H_{32}O_2$	
8.19	$C_{15}H_{24}O$		12.93	$C_{17}H_{32}O_2$	
9.10	$C_{16}H_{26}O_3$		13.57	$C_{19}H_{40}$	
9.63	$C_{20}H_{42}$		14.30	$C_{28}H_{48}O$	
10.75	$C_{15}H_{24}O_2$		14.87	$C_{20}H_{38}O_2$	
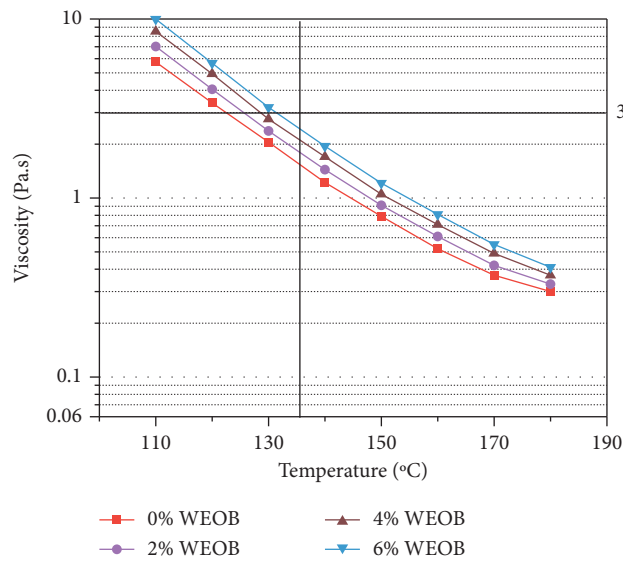
FIGURE 6: Viscosity results of the WEOB/SBS-modified binders.

3.5. Mechanical Analysis

3.5.1. SARA Fractions. SARA fraction contents play an important role in explaining the property changes of asphalt binder. Figure 11 records the quantitative analysis results of four components of asphalt. As WEOB contains a certain number of light components, with the increase of the WEOB contents, the number of aromatic hydrocarbons and saturated hydrocarbons in the four components gradually

increases, which plays a good role in improving the low-temperature property of asphalt. On the contrary, the content of asphaltene shows a downward trend because it is dissolved by the light components in WEOB. However, the resin content has increased to a certain extent. It is speculated that the possible reason is that a large number of aromatic hydrocarbons in WEOB are compatible with SBS and penetrate into the branch chain to produce substances
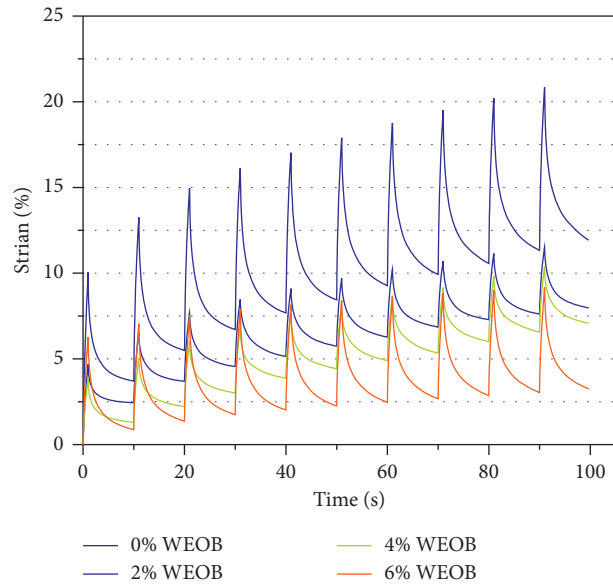
FIGURE 7: Strain response in MSCR test (10 cycles) for binders at 64°C and 3200 Pa.
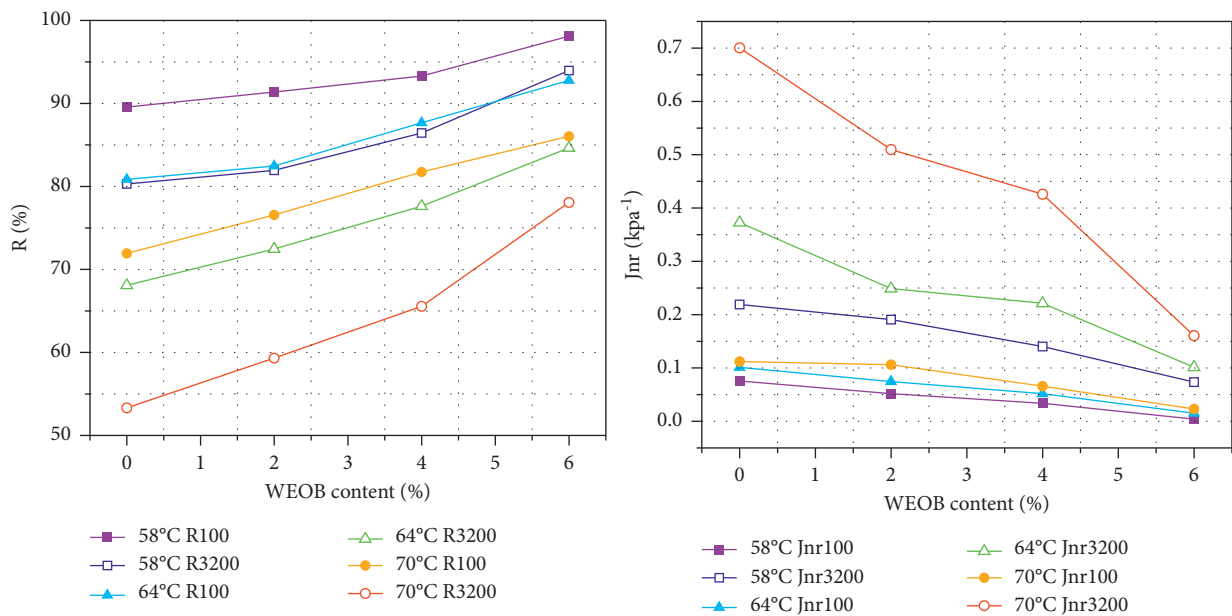
FIGURE 8: R (a) and J (b) for WEOB/SBS-modified binders at various temperatures.

similar to resins, which increases the stability of SBS network structure. This is also proved by the improvement of high-temperature performance of asphalt.

3.5.2. Fluorescence Microscopy. The fusion degree of different contents of WEOB- and SBS-modified asphalt can be seen from the fluorescence microscopic image in Figure 12. In Figure 12(a), it can be seen that in the modified asphalt without WEOB, SBS presents uniform monomer particle dispersion, and there is little fusion between SBS polymers. After adding WEOB, SBS polymer shows a network structure after expansion and fusion, and with the increase of content, the structure gradually develops from two-dimensional plane

network structure to three-dimensional network structure, as shown in Figures 12(b)–12(d), and the thermal movement of asphalt molecules is limited to a certain extent. When the content of WEOB increased to 6%, the expanded network structure was denser and uniform. In addition, the maleic anhydride in WEOB reacted with SBS. Under the dual action of swelling and grafting, the high-temperature performance of WEOB-modified asphalt was significantly improved [23, 24].

3.5.3. FTIR. The FTIR spectra of the SBS-modified asphalts with various WEOB contents are given in Figure 13. A peak at 724 cm^{-1} was awarded to the bending vibration of −CH$_2$, while that at 1,713 cm^{-1} was credited to tensile vibration of

(a)

(b)
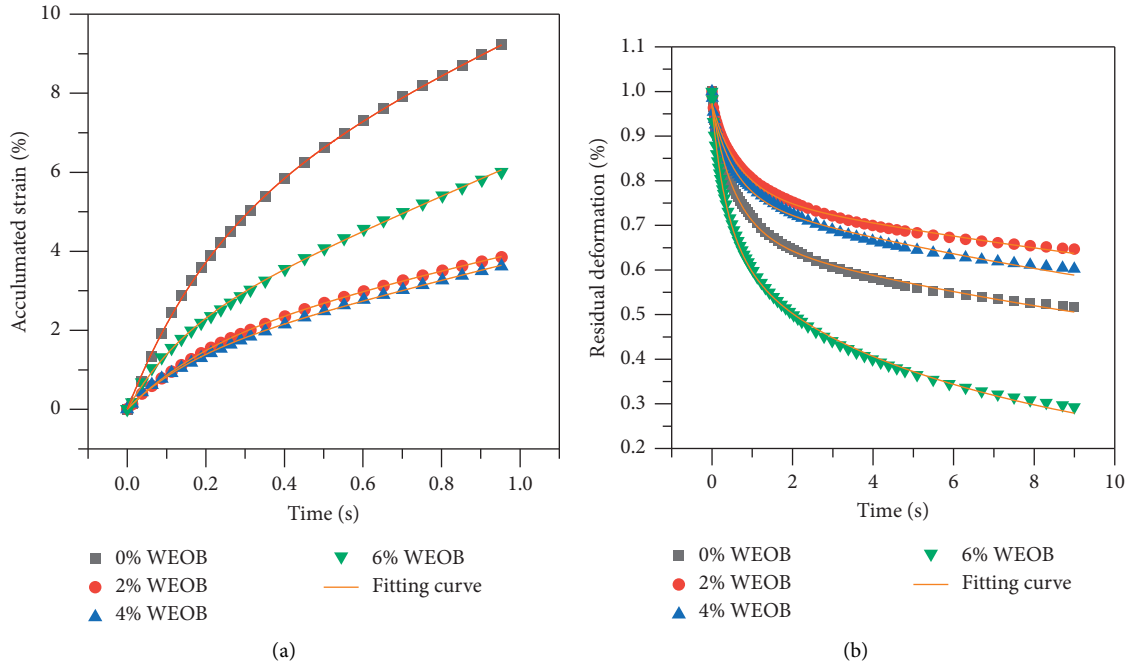
FIGURE 9: Comparison of measured and predicted values of SBS asphalt with different WEOB content in Burgers Model.

TABLE 5: Regression analysis of creep for SBS modifier asphalt with different WEOB content in Burgers model.

Ratio	Regression equation and parameters of Burgers model	
	Equation	R^2
0	$\varepsilon(t) = \frac{\sigma_0}{500.16} + \frac{\sigma_0}{9347.2} + \frac{\sigma_0}{1126.08}\left(1 - e^{-1126.08t/901.44}\right)$	0.9995
2	$\varepsilon(t) = \frac{\sigma_0}{285.664} + \frac{\sigma_0}{9760} + \frac{\sigma_0}{1077.76}\left(1 - e^{-1077.76t/875.2}\right)$	0.9999
4	$\varepsilon(t) = \frac{\sigma_0}{345.28} + \frac{\sigma_0}{8377.6} + \frac{\sigma_0}{1264.32}\left(1 - e^{-1264.32t/896.64}\right)$	0.9995
6	$\varepsilon(t) = \frac{\sigma_0}{1091.2} + \frac{\sigma_0}{5001.6} + \frac{\sigma_0}{2109.44}\left(1 - e^{-2109.44t/1332.48}\right)$	0.9994

TABLE 6: Regression analysis of relaxation for SBS modifier asphalt with different WEOB content in Burgers model.

Ratio	Regression and equation parameters of Burgers model	
	Equation	R^2
0	$\varepsilon(t) = \frac{5.6^*10^5}{4.1 + 376t + 312\left(1 - e^{-657.28t/154.976}\right)}$	0.9955
2	$\varepsilon(t) = \frac{4.6^*10^5}{3.2 + 320t + 241\left(1 - e^{-1845.44t/418.88}\right)}$	0.9957
4	$\varepsilon(t) = \frac{1.8^*10^5}{2.6 + 134t + 74.8\left(1 - e^{-2414.08t/476.16}\right)}$	0.9936
6	$\varepsilon(t) = \frac{8.34^*10^4}{1.23 + 111t + 51\left(1 - e^{-1652.16t/260.48}\right)}$	0.9981

C=O, indicating the presence of ketones or carboxylic acids in the asphalt. The two strong absorptions at $1,376\,\mathrm{cm}^{-1}$ and $1,456\,\mathrm{cm}^{-1}$ were the flexural vibration peak of saturated C–H bond. The stretching peak of methyl C=C bond appeared at $1,608\,\mathrm{cm}^{-1}$, suggesting the existence of olefins. This result is consistent with a previous study. At $1,780\,\mathrm{cm}^{-1}$, the symmetrical tensile vibration peak is –OH, which is the characteristic peak of maleic anhydride (MAH), proving the existence of SBS-g-MAH. The several peaks in the

2852–$2923\,\mathrm{cm}^{-1}$ wavenumber range are attributed to the stretching of the alkane –CH bond.

3.5.4. Atomic Force Microscope.

A typical "bee-like" structure AFM image of asphalt is shown in Figure 14. Studies have shown that the volume and distribution of black-and-white "bee-like" structure are related to asphaltene in asphalt. It can be seen from the Figures 14(a)–14(d) that the size and shape of "bee-like" structure are various under different WEOB content, but they all show a state of uniform distribution. With the increase of WEOB content, the bee-like structure gradually becomes smaller, and the length decreases from $3.21\,\mu\mathrm{m}$ to $1.27\,\mu\mathrm{m}$. It is speculated that the reason is that more light components in WEOB dissolve parts of asphaltene, and the movement resistance between asphaltenes is reduced and the compatibility is improved, so that the bee-like structure is dispersed more evenly.

Quantitative microstructures can be identified with surface roughness using the Nanoscope Analysis 1.5 software. Theoretically, surface roughness can be used to evaluate the adhesion and self-healing performance of asphalt materials. The higher the surface roughness of the asphalt binders, the better the adhesion and self-healing properties of the asphalt binders. The statistical results for surface roughness of four asphalt types are presented in Table 7. It can be seen that the surface roughness of asphalt binder increases with the increasing contents of WEOB.

Figure 15 shows that the variation trend of lightweight components and surface roughness with WEOB content. It is obvious to see that the lightweight components and surface roughness of SBS-modified asphalt specimens are in
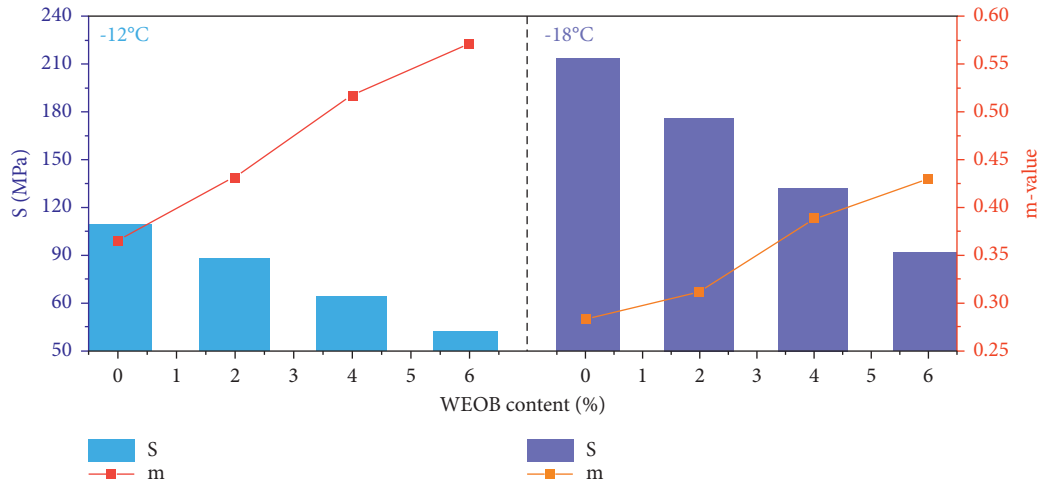
FIGURE 10: BBR test results of WEOB/SBS-modified binders at −12°C and −18°C.
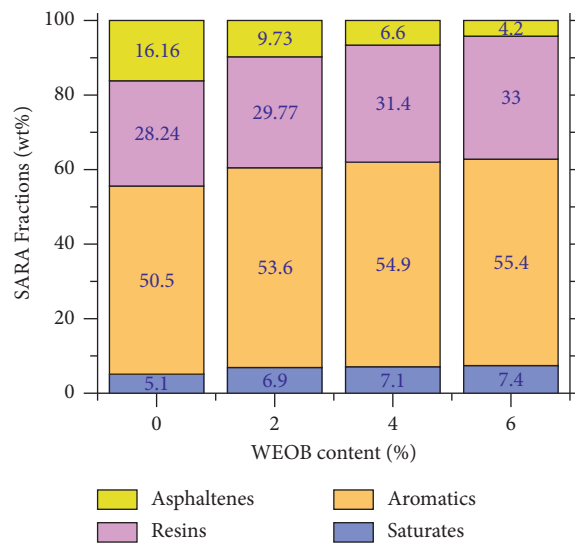
FIGURE 11: SARA fraction contents of WEOB/SBS-modified binders.
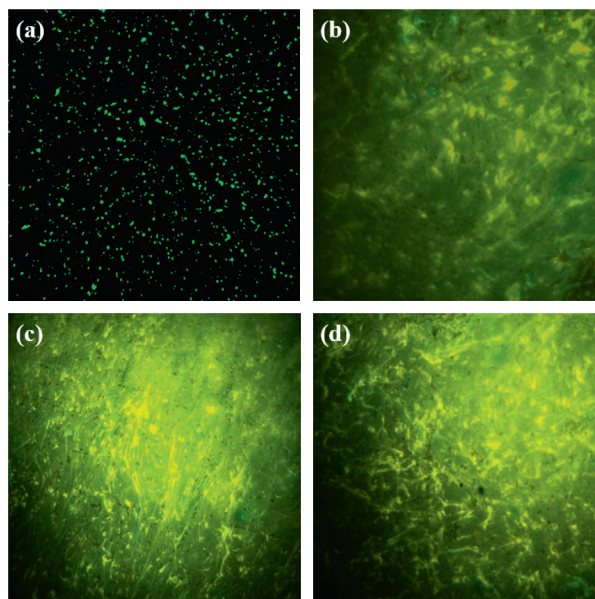
FIGURE 12: Fluorescence Microscopy for WEOB/SBS-modified binders with various WEOB content (a) 0%, (b) 2%, (c) 4%, and (d) 6%.
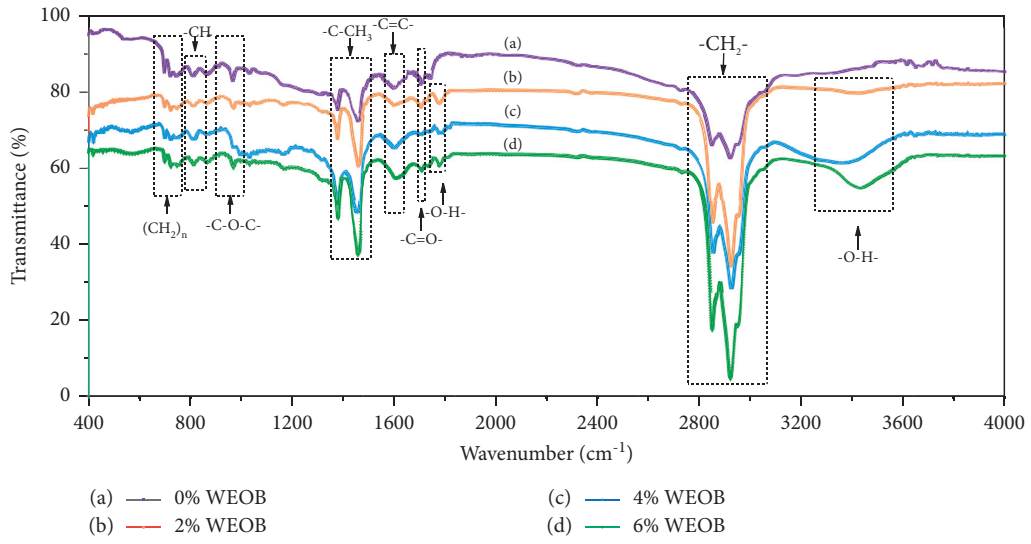
Figure 13: FTIR of WEOB-modified asphalt.

(a)

(b)

(c)

(d)
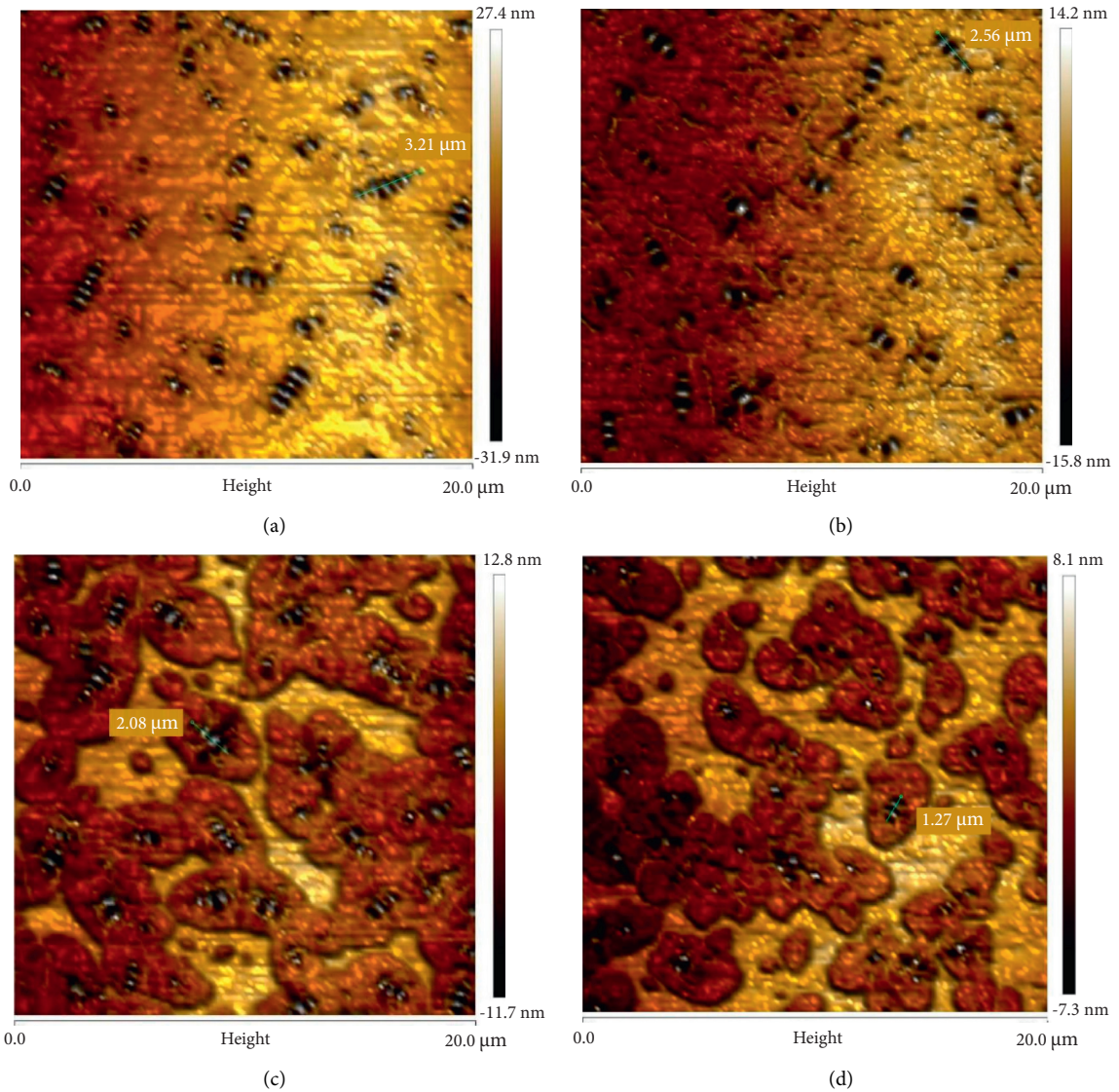
Figure 14: Phase images of WEOB-modified SBS asphalt, (a) 0%, (b) 2%, (c) 4%, and (d) 6%.

TABLE 7: Statistical results of surface roughness.

Asphalt type	Average surface roughness (R_a)	RMS value of roughness (R_q)
0% WEOB	2.38	4.00
2% WEOB	2.75	4.62
4% WEOB	3.22	5.09
6% WEOB	3.54	5.42
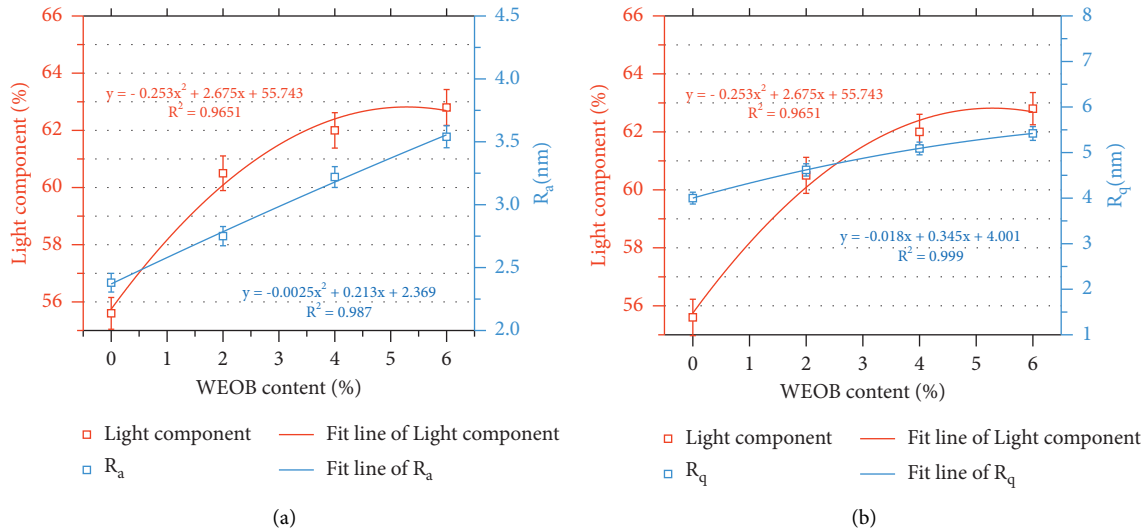
FIGURE 15: (a) R_a and (b) R_q of the specimens with different WEOB contents.

good correlation with their WEOB contents. Meantime, the R_a and R_q of modified asphalt binder advance as the lightweight components increase, which indicates that the adhesion property has improved.

4. Conclusion

In this paper, the influence of WEOB as an additive on SBS-modified asphalt has been studied, including chemical compounds, low- and high-temperature property, and rheology. The mechanism for the influences was analyzed. Based on the above results and discussion, the following conclusions can be drawn:

(1) WEOB is mainly composed of small molecular compounds similar to the asphalt composition, such as cycloalkanes, linear alkanes, various anhydrides, and their derivatives, which favored their physical miscibility between WEOB and asphalt.

(2) Adding WEOB can improve the high-temperature resistance against rutting performance and low-temperature fatigue cracking resistance of SBS-modified asphalt.

(3) With the increase of WEOB concentration, the contents of colloid gradually increases, which promotes the swelling and compaction of SBS polymer network structure. Furthermore, WEOB promotes the polarity of SBS and forms graft product MAH-g-SBS with asphalt, thus inhibiting the thermal movement of asphalt molecules. On the contrary, light components have a good correlation with the surface roughness of modified asphalt, the results show that the modified asphalt has good rutting resistance.

(4) As a preliminary study, the data in this paper were limited because only one WEOB source was included in evaluating the properties of SBS-modified asphalt. Therefore, a follow-up study should focus on increasing the number of different samples, in addition, it is necessary to investigate the aging resistance of the modified asphalt binders, to verify and evaluate the overall performance of WEOB-modified SBS asphalt.

Data Availability

All data, models, and code generated or used during the study appear in the submitted article.

Conflicts of Interest

The authors declare no conflicts of interest.

Acknowledgments

References

[1] V. Pelitli, Ö. Doğan, and H. J. Köroğlu, "Waste oil management: analyses of waste oils from vehicle crankcases and gearboxes," *Global Journal of Environmental Science and Management*, vol. 3, no. 1, pp. 11–20, 2017.

[2] J. Rincón, P. Cañizares, and M. T. García, "Regeneration of used lubricant oil by ethane extraction," *The Journal of Supercritical Fluids*, vol. 39, no. 3, pp. 315–322, 2007.

[3] T. You, Y. Shi, L. N. Mohammad, and S. B. Cooper, "Laboratory performance of asphalt mixtures containing Re-refined engine oil bottoms modified asphalt binders," *Transportation Research Record: Journal of the Transportation Research Board*, vol. 2672, no. 28, pp. 88–95, 2018.

[4] S. B. Cooper, L. N. Mohammad, and M. A. Elseifi, "Laboratory performance of asphalt mixtures containing recycled asphalt shingles and Re-refined engine oil bottoms," *Journal of Materials in Civil Engineering*, vol. 29, no. 9, Article ID 04017106, 2017.

[5] A. I. Essawy, A. M. M. Saleh, M. T. Zaky, R. K. Farag, and A. A. Ragab, "Environmentally friendly road construction," *Egyptian Journal of Petroleum*, vol. 22, no. 1, pp. 189–198, 2013.

[6] R. C. Barborak, C. E. Coward, and R. E. Lee, "Detection and estimation of Re-refined engine oil bottoms in asphalt binders: Texas department of transportation's approach with wavelength dispersive X-ray fluorescence spectroscopy," *Transportation Research Record: Journal of the Transportation Research Board*, vol. 2574, no. 1, pp. 48–56, 2016.

[7] I. A. Qurashi and A. K. Swamy, "Viscoelastic properties of recycled asphalt binder containing waste engine oil," *Journal of Cleaner Production*, vol. 182, pp. 992–1000, 2018.

[8] S. Liu, A. Peng, J. Wu, and S. B. Zhou, "Waste engine oil influences on chemical and rheological properties of different asphalt binders," *Construction and Building Materials*, vol. 191, pp. 1210–1220, 2018.

[9] S. Aleer, E. M. Adetutu, T. H. Makadia, S. Patil, and A. S. Ball, "Harnessing the hydrocarbon-degrading potential of contaminated soils for the bioremediation of waste engine oil," *Water, Air, and Soil Pollution*, vol. 218, no. 1-4, pp. 121–130, 2010.

[10] W. Wang, M. Jia, W. Jiang et al., "High temperature property and modification mechanism of asphalt containing waste engine oil bottom," *Construction and Building Materials*, vol. 261, 2020.

[11] A. Soleimani, S. Walsh, and S. A. M. Hesp, "Asphalt cement loss tangent as surrogate performance indicator for control of thermal cracking," *Transportation Research Record: Journal of the Transportation Research Board*, vol. 2126, no. 1, pp. 39–46, 2009.

[12] S. A. M. Hesp and H. F. Shurvell, "X-ray fluorescence detection of waste engine oil residue in asphalt and its effect on cracking in service," *International Journal of Pavement Engineering*, vol. 11, no. 6, pp. 541–553, 2010.

[13] J. D'Angelo, K. Grzybowski, and S. Lewis, "Canadian technical asphalt, A," in *Asphalt Binder Modification with Re-refined Heavy Vacuum Distillation Oil*, pp. 257–275, RHVDO, British Columbia, Canada, 2012.

[14] M. Yu, J. Li, X. Cui, D. Guo, and X. Li, "Antiageing performance evaluation of recycled engine oil bottom used in asphalt rejuvenation," *Advances in Materials Science and Engineering*, vol. 2019, Article ID 2947170, 8 pages, 2019.

[15] D. J. Mensching, A. Andriescu, C. DeCarlo, X. Li, and J. S. Youtcheff, "Effect of extended aging on asphalt materials containing re-refined engine oil bottoms," *Transportation Research Record: Journal of the Transportation Research Board*, vol. 2632, no. 1, pp. 60–69, 2017.

[16] X. Li, N. Gibson, A. Andriescu, and T. Arnold, "Performance evaluation of REOB-modified asphalt binders and mixtures," *Road Materials and Pavement Design*, vol. 18, no. 1, pp. 128–153, 2017.

[17] D. J. Mensching, A. Andriescu, C. DeCarlo, X. Li, and J. S. Youtcheff, "Effect of extended aging on asphalt materials containing Re-refined engine oil bottoms," *Transportation Research Record: Journal of the Transportation Research Board*, vol. 2632, no. 1, pp. 60–69, 2017.

[18] X. Yang, J. Mills-Beale, and Z. You, "Chemical characterization and oxidative aging of bio-asphalt and its compatibility with petroleum asphalt," *Journal of Cleaner Production*, vol. 142, pp. 1837–1847, 2017.

[19] M. Paliukaite, M. Assuras, and S. A. M. Hesp, "Effect of recycled engine oil bottoms on the ductile failure properties of straight and polymer-modified asphalt cements," *Construction and Building Materials*, vol. 126, pp. 190–196, 2016.

[20] S. Liu, S. B. Zhou, and Y. Xu, "Evaluation of cracking properties of SBS-modified binders containing organic montmorillonite," *Construction and Building Materials*, vol. 175, pp. 196–205, 2018.

[21] 316-13, A. T., *Standard Method of Test for Viscosity Determination of Asphalt Binder Using Rotational Viscometer*, American Association of State and Highway Transportation Official, Washington, DC, USA, 2013.

[22] R. Zhang, H. Wang, Z. You, X. Jiang, and X. Yang, "Optimization of bio-asphalt using bio-oil and distilled water," *Journal of Cleaner Production*, vol. 165, pp. 281–289, 2017.

[23] H. Shi, D. Shi, C. Li, S. Luan, J. Yin, and R. K. Y. Li, "Preparation of functionalized graphene/SEBS-g-MAH nanocomposites and improvement of its electrical, mechanical properties," *Materials Letters*, vol. 133, pp. 200–203, 2014.

[24] A. Zhang Aimin and L. Chao, "Chemical initiation mechanism of maleic anhydride grafted onto styrene-butadiene-styrene block copolymer," *European Polymer Journal*, vol. 39, no. 6, pp. 1291–1295, 2003.

Review Article

A Review of Asphaltic Crack Healing Approaches and Its Mechanism

Mohd Fahmi Haikal Mohd Ghazali,[1] **Mohd Rosli Mohd Hasan** ![ORCID],[1] **Anasyida Abu Seman** ![ORCID],[2] **Dillon Dipagk Dorett,**[1] **Najib Mukhtar,**[1,3] **and Ramadhansyah Putra Jaya** ![ORCID][4]

[1]*School of Civil Engineering, Universiti Sains Malaysia, Pulau Pinang 14300, Malaysia*
[2]*School of Materials and Mineral Resources Engineering, Universiti Sains Malaysia, Pulau Pinang 14300, Malaysia*
[3]*Department of Civil Engineering, Bayero University Kano, Kano 700241, Nigeria*
[4]*Department of Civil Engineering, College of Engineering, Universiti Malaysia Pahang, Gambang, Kuantan 26300, Pahang, Malaysia*

Correspondence should be addressed to Mohd Rosli Mohd Hasan; cerosli@usm.my

The concept of self-healing has an excellent potential to extend the life of asphalt pavement. This technology can be considered a sustainable technology due to its ability to reduce the utilization of asphalt mixture production materials used for road maintenance, polluting the environment. It is a complex physicochemical process wherein the molecular diffusion healing mechanisms in asphalt materials are inspired by self-healing polymeric systems, which describe the self-recovery behaviors based on polymer chain dynamics. Several methods have been adopted to improve the self-healing of asphalt, one of which is induction healing. It is the process of heating the asphalt pavement incorporated with an electrically conductive material such as steel fibers, wherein asphalt healing is undertaken via electric field induction. Induction healing via induction heating occurs with eddy current where the electric current flows within the conductive fibers when magnetically susceptible under the magnetic field. Microwave heating is another self-healing method similar to induction in which magnetic radiation is employed to treat asphalt mixtures instead of the electric field-induced induction healing processes. The conductive fibers can absorb the electromagnetic (EM) waves to convert them into heat energy through doublet polarization, interface polarization, and electrical conduction dissipation when placed in the microwave field. These two types of heating systems, which are induction heating and microwave heating, are compared and discussed thoroughly in this study. Finally, some recommendations for the future development of self-healing asphalt are proposed.

1. Introduction

1.1. Asphalt Concrete in Civil Engineering. Asphalt concrete (AC) consists of a mixture of bitumen and aggregate produced as a composite of viscoelastic and nonviscoelastic materials used primarily on civil engineering structures such as airports and highways [1, 2]. It is a material that deforms at high temperatures and can become brittle at low temperatures [3]. Asphalt concrete is utilized to build flexible pavements and road networks that connect one city to another. According to the Asia Trade Hub website,

Malaysia's road network covers 144,403 kilometers, where 116,169 kilometers are paved and 1,821 kilometers are expressways [4]. However, after several years in service, the flexibility and relaxation capacity of these asphalt concrete roads gradually decrease due to the repeated daily traffic loads and environment interchange (mainly temperature and moisture) [5]. The asphalt binder becomes brittle, lowering its adhesion capabilities, thereby causing the separation of aggregates and the binder [2]. Therefore, from time to time, such paved asphalt concrete needs to be maintained to ensure the estimated lifespan of the road is

achieved while preventing traffic accidents from occurring due to the asphalt pavement distress [6]. One of the primary indications of asphalt pavement distress is cracks. The cracking mechanism related to bituminous materials is complicated and depends on traffic loading conditions and atmospheric temperatures. Atmospheric conditions that can cause oxidation are one of the main reasons for the degradation of asphalt mixtures. This event is also known as aging, where the asphalt binders and their viscoelastic properties become stiffer compared to their original states. As time goes by, the materials will reach a certain level of stiffness that causes them to become brittle, hence unable to resist and recover during loading/unloading conditions, which eventually leads to cracking at microscopic and macroscopic levels. Many researchers have conducted studies to solve the damage caused by cracking failure via promoting crack closure at an early stage. Although the capability of asphalt as a self-healing material has been proven, its ability to heal is obviously limited due to nonstop traffic loading and is not enough to accommodate the asphalt degradation that keeps happening due to atmospheric conditions. Therefore, the induction of self-healing technology into asphalt mixtures was investigated and introduced to overcome these problems [7].

1.2. Asphalt as Self-Healing Materials. Asphalt concrete is a self-healing material that has the capability of restoring some of its functionality. This usually occurs due to the potential of bitumen to behave like a Newtonian fluid at temperatures ranging from 30 to 70°C, depending on the type of bitumen [8]. Dai et al. [3] reported the healing behavior of asphalt as the self-recovery capability of asphalt materials under specific loading and/or environmental conditions, especially during rest time. Xu et al. [9] also mentioned that the fundamental of self-healing in asphalt pavement depends on the initiation of a "mobile phase" during the rest period that gradually results in crack closure. The self-healing material will regain a certain rate of its functionality where the bitumen can flow and diffuse to close its microcracks when it is not exposed to loads [10, 11]. This process mainly occurs due to the viscosity and gravitational force acting on the bitumen [12]. However, it would not be possible to halt traffic on the roads and allow enough self-healing and recovery at ambient temperatures [13]. Hence, the healing of asphalt mixtures becomes somewhat influenced by external conditions, wherein further propagation of micro-to macrocracks results from consistent loading, loading level, number of load repetitions, aging, and moisture conditions [14].

The primary goal of self-healing technology is to ensure that the material heals after being subjected to fatigue damage. It is a technology that plays a role mainly during maintenance in areas where pavement distresses occur. Even without a self-healing technology, a fatigued pavement can be restored but it will consume a lot of time and energy to recover its initial performance. Thus, this technology aims to overcome the local or global level of damage, extend, and renew the damaged part, system, or component [15]. Fatigue damage occurs when shear forces

are exerted on the stones within the road surface. This causes strain within the adhesive bridges between the stones. With recurring forces (repeated traffic load), "fatigue taxation" will occur. Fatigue in these adhesive bridges leads to the first stage of the three-stage damage mechanism: crack initiation. The second stage is crack growth, which is followed by the third stage: a complete breakage of a singular adhesive bridge [16].

According to Tabaković and Schlangen [17], the self-healing or self-repairing property of a material is referred to as "its ability to substantially return to an original, proper operating state or condition before exposure to a dynamic and susceptible environment by making the necessary adjustments to restore to normality and/or its ability to resist the formation of irregularities and/or defects." The repair is, in principle, an automatic initiated response to damage or failure. In order to repair the damage, the self-healing system must be able to identify and perform the restoration mechanism. Fischer [15] states that repair is classified into two categories:

(1) Attributive repair: Attempting to restore the attributes of the system to their initial state.

(2) Functional repair: To restore the functionality of the system. If the functionality cannot be fully reinstated, the residual resources are utilized to supplement the existing functionality.

Moreover, self-healing is also known as a very complex physicochemical process. The molecular diffusion healing mechanisms in asphalt materials are derived based on self-healing polymeric systems, which describe its self-recovery behavior based on polymer chain dynamics [18]. Wool and O'Connor [19] divided the theory of crack healing into five stages based on molecular interdiffusion. These five stages are as follows:

(1) The surface rearrangement stage that affects the diffusion initiation function and topological features of the interface

(2) Approach stage that affects the healing mode

(3) The wetting stage that controls the wetting distribution of the two faces of microcrack

(4) Diffusion stage that develops the mechanical properties during healing

(5) Randomization stage that involves complete loss of memory of the crack interface

According to Tabaković and Schlangen [17], wetting, diffusion, and randomization are the only primary stages in an autonomous asphalt self-healing process. Meanwhile, Qiu et al. [14] mentioned that self-healing is influenced by the hydrogen bond and van Waals forces between molecules.

Moreover, Sun et al. [2] observed an ongoing event between healing and fatigue in pavement during its service life. This process was noticed to be dependent upon variations in the pavement temperature. Figure 1 shows the schematic diagram of its mechanism. Moreover, asphalt type and properties also influence the wetting capacity of
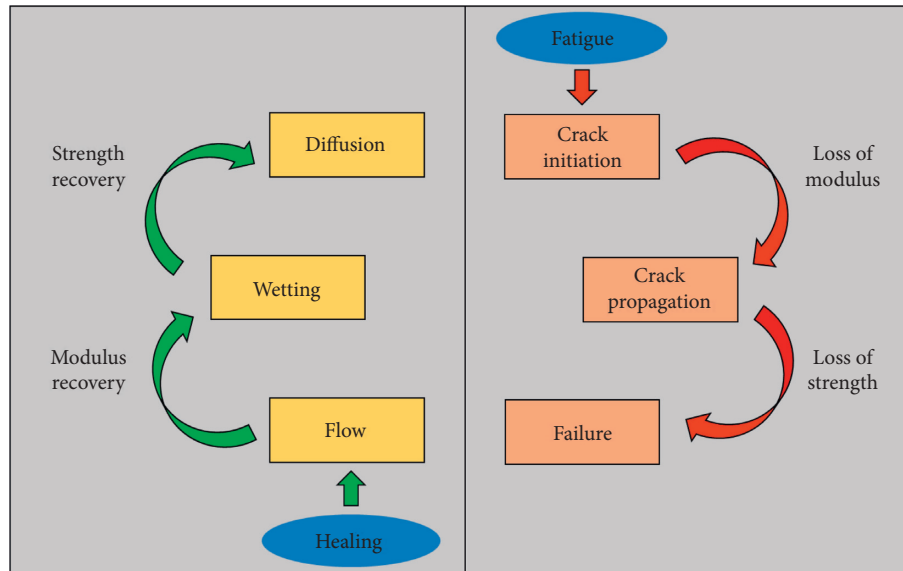
Figure 1: Three-step healing mechanism in asphalt [2].

aggregate phases during healing. The wetting rate is directly proportional to the asphalt surface energy. Hence, the diffusion ability can be said to correspond to the portability of the asphalt molecules. Nonetheless, some researchers have discovered that the asphalt consisting of more molecules with fewer and longer branched chains has higher molecule mobility than smaller chains and larger branches [2].

Several methods of inducing self-healing in asphalt pavement design have been presented and critically analyzed concerning their functionality, design, and performance to prolong its service life [20]. Some of the methods of self-healing, as proposed by Tabaković and Schlangen [17], are as follows:

(1) Incorporation of nanoparticles
(2) Induction healing
(3) Rejuvenation

This paper will focus on the mechanisms of induction healing using different approaches based on different studies reported in the literature.

2. Induction Healing Technology

The practice of heating asphalt surface layer "in situ" has been in use for a long time. Despite the poor heat conductivity of asphalt due to mineral aggregates, the road surfaces were heated up using infrared heaters. The desired level of heating to the asphalt layers especially at its lowest layer was obtained by overheating the asphalt for a long period of time by using "additive heat radiation." One of the disadvantages of this method was accompanied by great waste of energy and constant burning of the bitumen in the asphalt surface layer [16]. The poor heat conductivity of the mineral aggregates in the asphalt mixture and too much loss in heat energy were addressed by using electrically conductive asphalt.

The first induction heating technology was invented by Minsk [21]. His invention was based on preventing ice and snow accumulation on flexible pavements by adding graphite particles in an asphaltic concrete to make it electrically conductive. García et al. [22] and Liu et al. [13] defined a conductive asphalt concrete as the portion of asphaltic concrete that contains the bitumen, aggregates, and conductive particles such as carbon fibers. Hence, an induction heating device can effectively achieve localized heating of the particles through heat diffusion, thereby heating the binder and healing the cracks [23]. Asphalt-containing conductive particles are exposed to a high frequency alternating electromagnetic field during induction heating by inducing eddy currents in electrically and magnetically susceptible materials. The induced eddy currents heat the metallic fibers while the heat energy diffuses into the bitumen to increase its temperature. Such induction mechanism is conducive in aiding asphalt mixtures heal quickly because bitumen mostly behaves as a Newtonian fluid when its temperature is above its softening point [24]. Hassan et al. [55] observed that a very small volume of fibers of more than 0% served to increase binder temperatures via induction heating. Meanwhile, García et al. [22] found that there is an optimum volume of fibers for each mixture below which the conductivity of the material suddenly drops to that of a nonconductive material. However, above such volume of fiber, they experienced difficulties in mixing while the increase in the conductivity was also very low [22]. Furthermore, García et al. [25] reported that the resistivity of the mastic sample would keep reducing with the volume of conductive additive. Until a certain level of conductive volume content, the increasing of conductive volume will not reduce the resistivity of the mastic sample any further. This can be seen in Table 1 based on a study by García et al. [25] where the conductive additive reaches its peak for steel wool, with a 5.83% steel wool + graphite and 6.54% steel wool + graphite at approximately 2, 1, and 1 Ωm,

TABLE 1: Conductive particles-bitumen ratio for asphalt mortar systems at different conductive additive content [25].

Conductive additives content (vol %)	Log resistivity (Ωm)			
	Graphite	Steel wool	5.83% steel wool + graphite	6.54% steel wool + graphite
5.5	11	9.5	9	N/A
7	10.5	2	8.5	1
10.5	9.8	N/A	8.3	1
13	9.5	N/A	3	1
15.5	8.8	N/A	1.5	1
17	8.5	N/A	1	1
20.5	8	N/A	1	1

respectively. Further increment of steel wool content can cause the mixing to become harder and form a cluster ball. Thus, it is limited to approximately 6% steel wool content in his study. Next, the test was conducted on the asphalt mastic sample prepared with graphite (without steel wool), the resistivity keeps reducing due to the filler particle size of graphite where the connection between one particle and another particle to induce current are weaker compared to steel wool. This condition can be illustrated as in Figure 2 where the steel wool fibers form a connection between one and another to form a conductive asphalt mastic.

Furthermore, García et al. [22] and Dai et al. [3] utilized the gel permeation chromatography technique to test inducted healed specimens and noninducted specimens, which demonstrated the chemical properties of the asphalt, such as its averaged molecular weight not to be influenced by induction healing. Similarly, the effect of chemical composition was also observed to exhibit a strong influence on the induction healing properties of asphalt by which asphalt with higher small molecule content/large molecular content ratio combined with higher aromatics content had greater self-healing abilities than those with smaller molecular and lower aromatic contents [26].

2.1. Induced Healing via Induction Heating.

Asphalt concrete mixtures are generally added with conductive fibers in order to improve their electrical conductivity so as to facilitate effective induction heating. The process of adding the steel fibers to the mixture is direct during mixing, without affecting the gradation of the mixture. Liu et al. [13] reported that the addition of long steel wool was more effective in making asphalt concrete electrically conductive for 9.5 mm steels long enough to conduct electric currents. Moreover, the performance of long fibers with small diameters was found by Sun et al. [27] to be better than short fibers with bigger diameters. This finding was also supported by Gao et al. [28] due to several benefits such as improving the flexural strength and particle loss resistance of the asphaltic concrete. However, asphalt mixtures with long fibers tended to form cluster balls and increase the air void content of the mixtures, which was associated with a reduction in the mechanical properties of the mixtures as reported by Norambuena et al. [29] and González et al. [30].

Based on such observations, Xu et al. [24] recommended the use of short and thick steel wool fibers with a diameter of 70–130 μm and length 4.2 mm because it is quite easier to
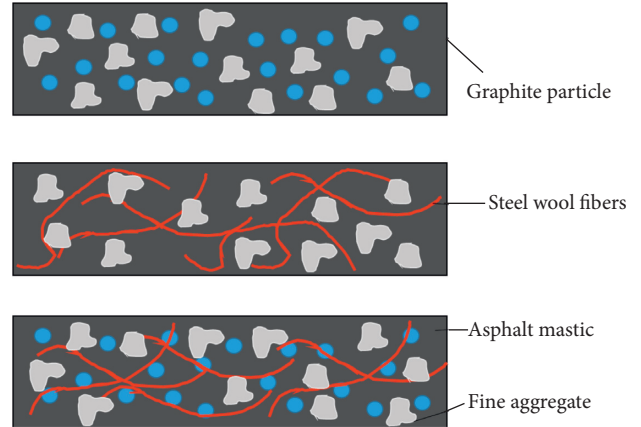
FIGURE 2: Illustration of asphalt mastic composition with and without steel wool and graphite.

mix using the standard mixing procedure at an optimal steel wool content of 6% by the volume of bitumen. Nonetheless, some studies such as those conducted by Ameri et al. [31] and Sun et al. [18] replaced a portion of the aggregate from the asphalt mixture with steel slags as conductive materials by which they attested to the fact that the steel slag-asphalt mixture showed a better performance in healing when the temperature distribution was more uniform. Furthermore, laboratory test results also evidently indicated the use of coarse steel slag aggregates in warm mix asphalt (WMA) mixture in the enhancement of the tensile strength, resilient modulus, Marshall stability, resistance to moisture damage, and resistance to permanent deformation of the mixture [31]. Similar reports on the mechanical performance of asphalt mixture were mentioned by Dai et al. [3] while investigating the induction healing effects of electrically conductive asphalt mastic and asphalt concrete beams through fracture-healing tests as asphalt mixture samples were observed to still maintain at least half of their original fracture strengths, after six fracture-healing cycles [32].

2.2. Induced Healing via Microwave Heating.

The second technique used to increase the temperature of asphalt mixtures for the improvement of asphalt road maintenance was microwave radiation heating [33–35]. The preliminary analysis for production and cost was conducted by Bevacqua et al. [36]. The results show that the performance of microwave healing in terms of cost-saving for a lifespan of 100 years is improved compared to a traditional method, such as

reconstructing the asphaltic layer that requires transportation and additional resource [37]. Microwave heating is usually considered a potential technique for stimulating the self-healing of composite materials, very much similar to induction heating. Asphalt mixtures here are mostly exposed to alternating electromagnetic fields under high frequencies (in the order of megahertz) by using an electromagnetic radiation device like a microwave, which is environmentally friendly due to the reduction of carbon dioxide emission [37, 38]. This heating effect has been established to affect the properties of both water and bitumen in asphalt mixtures [35], wherein it induced a change in the orientation of their polar molecules as a result of alternating magnetic fields. As a result, the molecule's mobility becomes disrupted and impeded while their temperature increases. Generally, asphalt mixtures are not susceptible to heating with induction heating energy; however, the incorporation of metallic particles known as microwave absorbers in asphalt mixtures may help reflect the microwave radiation, thereby boosting its temperature susceptibility [39]. Hence, the incorporation of metallic and ferrous particles susceptible to electromagnetic radiation such as steel slag can help increase the heating rates of asphalt mixtures by absorbing and conducting more thermal energy to other components of the mixtures, that is, aggregates and bitumen [40]. The recommended sizes for the metallic particles of steel fiber as a microwave reflecting admixture by Deng et al. [41] are 0.4–0.8 mm and 0.5 mm length to width, respectively. Recent findings have established microwave heating to be more advantageous than induction heating in terms of its high heating efficiency (rapid heating), no direct contact with liquids, no air emissions, fast thermal response, precise temperature control, and selective energy absorption [18, 42, 43]. The rapid increase of total energy means that the sample can absorb more energy to increase the temperature [44]. Microwave heating proved to be more economical and effective than electromagnetic induction in promoting self-healing of asphalt mixture with steel wool and graphite [45]. A study by Xu et al. [46] also shows that microwave heating can alter the structure of air voids compared to induction heating. Lastly, the amount of power consumption and the optimal steel wool dosages on employing microwave heating have also been 10 times lower than required for electromagnetic induction heating [47, 48].

3. Conductive Particles Used for Induction Healing

The induction healing technology has ventured into the field of materials engineering in the last few years. The utilization of this technology has resulted in a revolution in the field of material sciences and engineering. Some of the applications of induction healing technology in engineering materials and its recovery performance are presented in Tables 2 and 3, respectively.

Mostly steel fibers and steel wools are the prevalent materials utilized for both electromagnetic heating and induction heating of asphalt mixtures. As shown in Table 2, Liu et al. [11, 13, 50, 51] and Garcia et al. [23, 52] utilized steel

fiber and steel wool for asphalt mixture induction and microwave radiation heating processes, while steel shavings, carbon fibers, and utensil steel wool have also been employed for crack healing procedures via both induction and microwave radiation heating mechanism [53–56]. Similarly, steel by-products such as slags, wools, and fibers have also been widely used in road pavements, due to their excellent mechanical properties, in terms of roughness, shape, angularity, hardness, polishing, and wear resistance [56, 57]. Table 3 also proved that the healing performance of asphalt mixtures by several researchers was able to improve the healing by 50–100% depending on the type of conductive material used. Therefore, both induction and microwave heating systems are successful innovations that are able to increase the lifespan of the asphalt pavement and lower the maintenance cost.

Wu et al. [58] reported that the mechanical characteristics of carbon fiber-reinforced asphalt matrix had improved due to the nature of the insulating conductive polymer composites. The incorporated high-aspect-ratio carbon fibers were helpful to improve the conductivity of the insulating polymer matrix even at relatively low concentrations. Therefore, the utilization of steel in the pavement can be inferred to be quite suitable for both mechanical and healing performances [59, 60].

4. Mechanism of Induction Heating

The induction heating system comprises alternating power generators, induction coils, and electrically conductive steel fibers incorporated and dispersed between the mixture's interstices, as shown in Figure 3. The coil normally produces the magnetic field for a uniform amount of frequency under an alternating electric power supply. As shown in Figure 3, each conductive steel fibers within asphalt mixtures were induced. Based on Faraday's law, the presence of a magnetically susceptible and electrical material within a magnetic field leads to an electric current (eddy current) being induced upon it at the same frequency as the magnetic field. At the same time, the intensity of the current is proportional to the intensity of each coil circulation [61]. Induction heating in asphalt mixtures is usually generated through the dominant joule effect, dielectric hysteresis, and contact resistance between heated fibers. Joule heating (also known as resistive or ohmic heating) generates heat from electric energy due to the resistance imposed to current flow. In a solid or liquid with finite conductivity, electric energy is converted to heat through resistive losses in the material. This causes heat to be generated by the conductor via electron energy transfer to its atoms through electron-electron collisions, which spreads across all its atoms. The phenomena observed in the binder-conductor interfaces result in heat transfer between conductor and asphalt binder atoms; hence, uniform heating between both interfaces is achieved. The transfer of energy from the applied electric field results in unrecoverable heat loss between both atomic interfaces refers to its dielectric loss, hysteresis, or dissipation. The amount of energy transfer is also mainly dependent on the properties of both the conductor and binder used,

TABLE 2: List of research studies on the different types of material used for induction healing.

Healing Type	References	Materials Used	Diameter (μm)	Length (mm)	Temperature Heating (°C)	Duration of Heating (s)	Relevant Conclusion
Induction Heating	Liu et al. [23]	Steel fibre type 1	29.6–191.1	<1	—	180	(i) The porous asphalt concrete with the best performance, i.e., higher resistance to particle loss and water damage, was 8% by volume of bitumen of steel wool (type 00) of the length of 9.5 mm (ii) Optimum content for the steel fibre type 1, 00, and 000 are 20%, 12%, and 10%, respectively, while the maximum temperatures reached by each types of steel fibre are 207°C, 169°C, and 137°C, respectively.
		Steel wool type 00	8.89–12.7	3.2/6.4/9.5			
		Steel wool type 000	6.38–8.89	6			
Induction Heating	García et al. [24]	Steel wool type 000	6.35–8.89	3–22, 30	—	60, 120, 180	(i) At an optimal volume of fibre addition, the graphite can increase and stabilize the conductivity of the mastic. (ii) The maximum temperature for the 6% volume of fibre after 60 s, 120 s, 180 s are approximately 100°C, 150°C, and 200°C, respectively. (iii) Increasing the volume of steel fibre by more than 6% does not increase the maximum temperature further. The resistivity graph proves that the increase of steel fibre content by more than 6% will improve conductivity by approximately 10%.
		Graphite filler	<20	—			
Induction Heating	García et al. [51]	Steel wool type 00	8.89–12.7	1–15	—	180	(i) Based on the Marshall tests, the mechanical resistance of the asphalt concrete remains unaffected with any change in the volume of fibers and the mixing time. The response remained constant even though the parameters were changed. (ii) At the initial period of mixing, the mixing time had a negative effect on the length of the fibres. (iii) The temperature increased linearly for the increase in the volume of fibres. (iv) The maximum temperature reached was lower when the fibre was added in the first place to the mixer than the fibre added in the last place after aggregate and bitumen. This is due to the length reduction of the fibre when it is mixed with the aggregate.

TABLE 2: Continued.

Healing Type	References	Materials Used	Diameter (μm)	Length (mm)	Temperature Heating (°C)	Duration of Heating (s)	Relevant Conclusion
Induction Heating	Liu et al. [52]	Steel wool type 00	8.89–12.7	10	30, 50, 70, 85, 100	—	(i) The mortar of porous asphalt concrete exhibits a higher nanoindentation modulus when strengthened with steel wool. (ii) Heating of the beam fracture at 20°C does not result in any healing. The fracture recovery increased from 14.9 to 78.8% when the heating time is from 30 to 85°C.
Induction Heating	Liu et al. [53]	Steel wool type 00	8.89–12.7	10	70, 85, 100	180	(i) The best outcome of healing effects is obtained for an optimal heating temperature of 85°C. Overheating may result in problems like swelling and binder drainage, inhibiting healing. (ii) Performing induction heating multiple times can extend the fatigue life of porous asphalt concrete. (iii) The fatigue life extension ratio (healing rate) of the fatigue damaged beams can be improved by induction heating, wherein the rate of healing is dependent on the higher level of microstrain developed.
Induction Heating	García et al. [54]	Steel wool type 3 Steel wool type 1 Steel wool type 00 Steel wool type 0000	154.98 83.89 36.42 28.55	Length for each steel type. Short fibres: 2.5, Long fibres: 7	—	60	(i) Steel wool fibers might negatively impact the abrasion loss performance of the asphalt concrete mixture when they are not homogeneously distributed, characterized by the appearance of fibre clusters. (ii) The mechanical resistance of the test samples could be recovered up to 60% when the material was damaged. This happened at around 100°C.
Induction Heating	Liu et al. [11]	Steel fibres Steel slag	70–130 Replace partially of coarse aggregate	4.2 —	80	—	(i) The induction heating rate of the asphalt mixture can be increased with the suitable composition of steel fibres and steel slag. The order of heating rate for different asphalt mixtures is SF + SS > SF > SS. The selection of the right composition can facilitate homogenous heating and the efficiency of induction healing. (ii) Incorporating steel slag or steel fibres may also improve the water stability, Marshall stability, and residual Marshall stability ratio.

TABLE 2: Continued.

Healing Type	References	Materials Used	Diameter (μm)	Length (mm)	Temperature Heating (°C)	Duration of Heating (s)	Relevant Conclusion
Microwave Heating	Tabaković et al. [55]	Grade 3 coarse-grained Trollull Steel Wool	90	10	—	180 (at 300 W)	(i) Busy airports that face problems of runway closure can benefit from the microwave healing process using steel fibres. The addition of steel fibres with 3 min of microwave healing initiates a rapid healing process. (ii) Optimum steel fibre content for the Porous Friction Course (PFC) mix is 5% with 300 W heating power.
Microwave Heating	Wang et al. [56]	IM8 Carbon fibres	5.2	6.35	—	120 (at 1100 W)	(i) The electrical resistivity of the mastic can be decreased with an optimal addition of carbon fibres. It can even absorb more microwave energy for healing. Thus, less energy is required to heal cracks on using carbon fibres. (ii) 3% of AS4 and 2% of IM8 carbon fibres by bitumen weight have the best healing performance. (iii) The microwave energy was absorbed by the carbon fibre and heal the crack when the surface temperature went up to around 100°C.
		AS4 Carbon fibres	7.1	6.35			
Microwave Heating	Hassan et al. [57]	Kitchen wash steel wool	97.54	3–7	—	60, 90 (at 700 W)	(i) Steel wool content of 3 and 5% by volume of bitumen have an excellent bonding between the fractured surfaces 24 hours after heating. (ii) Modified asphalt with steel wool causes the bulk density to reduce while the air void percentage increases. Thus, to overcome this problem, higher compaction energy is required.
Microwave Heating	González et al. [58]	Steel shavings	1.310	3–21	—	40 (at 700 W)	(i) After microwave radiation, the average surface temperature of the asphalt reached 71.7°C. (ii) The number of air voids in the mixture increased with the addition of shavings which was observed in SEM analysis. The air voids are due to the complex geometry and rough surface of the shavings.

while the contact resistance depends on the resistance to current flow due to the surface conditions of both materials used. The heated binder usually exhibits Newtonian flow when its temperature reached 50°C depending on the source and composition of the asphalt binder as established by García [62], which helps fill the asphalt mixture cracks in a sort of capillary flow. The capillary pressure drives the binder to flow over crack space. However, such flow depends on the bituminous flow threshold as different types of bitumen exhibit different threshold temperatures for flow, depending on their rheological properties, usually ranging from 30°C to 70°C. Menozzi et al. [63] claimed in their study that the flow behavior index, n where it is near-Newtonian, occurs when the flow behavior index is within $0.9 \leq n < 1$. It is the temperature where the Newtonian behavior occurs almost starting from 30°C and above. Hence, the microcracks heal and fill the binder while ensuring its bonding and adhesive strength have been restored [3]. Additionally, the flow

TABLE 3: Comparison of recovery performance between the microwave and induction heating system.

Healing type	References	Optimum heating temperature or duration of heating	Recovery performance of optimum steel fibre content in term of strength at optimum heating			Healing index
			Initial	Pre-healing	Post-healing	
Induction heating	Liu et al. [23]	120 seconds	N/A	N/A	N/A	Post-healing: 100%
Induction heating	García et al. [24]	100°C	N/A	N/A	N/A	Post-healing: 60%
Induction heating	Liu et al. [52]	85°C	2.5 kN	Cycle 1: 2.1 kN Cycle 2: 2 kN Cycle 3: 2 kN Cycle 4: 2 kN	Cycle 5: 2 kN	Pre-healing: 84% Post-healing: 80%
Induction heating	Liu et al. [53]	85°C	2200 MPa	Cycle 1: 2000 MPa Cycle 2: 2100 MPa Cycle 3: 1900 MPa	Cycle 4: 2000 MPa	Pre-healing: 86–95% Post-healing: 91%
Induction heating	García et al. [54]	100°C	N/A	N/A	N/A	Post-healing: 60%
Induction heating	Liu et al. [11]	90°C	N/A	N/A	N/A	Post-healing: 52–70%
Microwave heating	Tabaković et al. [55]	180 seconds (at 300 W)	2200 MPa	Cycle 1: 1900 MPa	Cycle 2: 2000 MPa	Pre-healing: 86% Post-healing: 91%
Microwave heating	Wang et al. [56]	120 seconds (at 1100 W)	3.8 kN	Cycle 1: 3.6 kN Cycle 2: 3.4 kN Cycle 3: 3.2 kN Cycle 4: 2.9 kN	Cycle 5: 2.9 kN	Pre-healing: 76–94% Post-healing: 76%
Microwave heating	González et al. [58]	40 seconds (at 700 W)	N/A	N/A	N/A	Post-healing: 50-60%
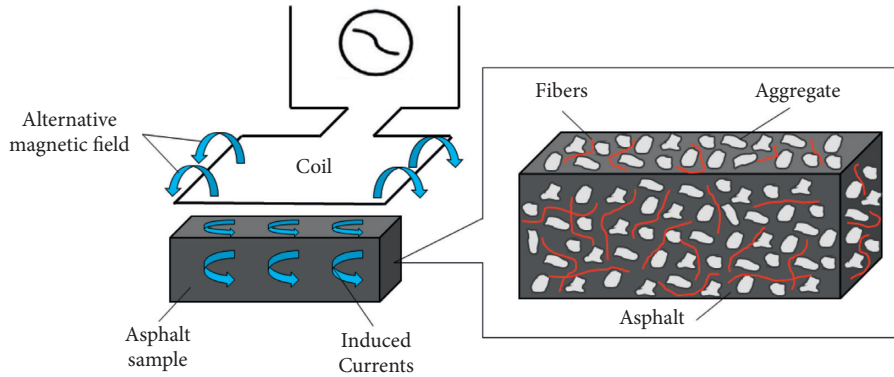
FIGURE 3: Schematic demonstration of induction healing mechanism for thermoplastic asphalt materials [3].

behavior index of the bitumen has also been found to be essential in characterizing the threshold for the initial self-healing temperature of bitumen [64, 65]. In the case of microcrack, molecular interdiffusion models can predict crack occurrences between binder and aggregate interfaces, while capillary flow healing models best describe the macrocracking self-healing phenomenon [66].

According to the simple model derived by García et al. [49] as in the following equation:

$$\dot{q}'_{in\ du\ ction} = \frac{\pi r^4 L_{eq}}{16\rho}\mu_m B_r \omega^2, \tag{1}$$

where $\dot{q}'_{in\ du\ ction}$ = power dissipated by time unit, r = radius of each individual fiber, L_{eq} = equivalent length or total length of fibers being heated, μ_m = magnetic permeability of the mastic, B_r = resultant magnetic field, and (ω) = frequency of the alternating magnetic field.

Based on the formula, the power dissipated per unit time is related to the total equivalent fibers length. The power exhibits a linearly increasing trend with an increase in the volume of fibers, wherein the relationship is valid until the percolation threshold is reached. Beyond that threshold point, the effective length will be the same for all sample widths wherein no more fibers can fit into the sample.

The process of induction heating, as mentioned earlier, is based on electromagnetic induction and Joule's heating, which can be expressed using electromagnetic induction Faraday's law. The electromotive force (ε, in volts) and magnetic flux (ϕ_B, in Webers) are related based on the following equation [2]:

$$\varepsilon = -\frac{d\phi_B}{dt}. \tag{2}$$

Apart from that, Faraday's law emphasized that the strength of these currents and the magnetic field are linear to the magnitude of the current flowing through the coil. Electrically nonconductive bitumen requires particles that are conductive to be added to its mixture, such as steel fibers, to build closed loops of eddy currents and facilitate the transfer of electron energy between the bituminous and steel phases. Moreover, the induced electromotive force of steel fibers modified asphalt mixtures can be expressed as follows [2]:

$$\varepsilon = \omega.A.B = 2\pi.f.A.H.\mu_m, \tag{3}$$

where ω is the frequency of the alternating magnetic field, A is the enclosed loop area of the conductive fiber, B is the magnetic flux, f is the magnetic field frequency, H is the magnetic field intensity, and μ_m is the magnetic permeability.

Based on Joule's effect, the eddy current heating the material is expressed as follows [2]:

$$P = t.I^2.R, \tag{4}$$

where P is the heat generated per unit time, t is the time of exposure to the magnetic field, I is the constant current, and R is the material resistance.

The following equation shows the relationship between the power generated and the source in the sample [2]:

$$P = \frac{(2\pi.f.A.H.\mu)^2}{R}. \tag{5}$$

Equation (5) shows that the time required to heat a composite to a specific temperature decreases quadratically as the frequency increases. A phenomenon called the "skin effect" is observed during higher frequencies, wherein the penetration depth of the electromagnetic field might be limited, even though more power can be dissipated. Rudnev et al. [65] stated that the phenomenon depends on the occurrence of electromagnetic fields by induced currents, which have opposite field directions than the generating field (Figure 4). The penetration depth d is expressed using Maxwell's formulations in the following equation [66]:
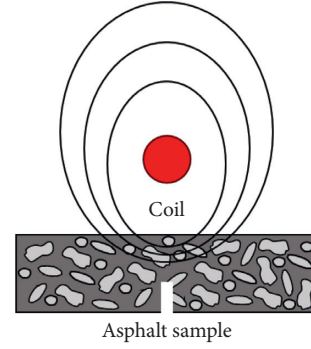
FIGURE 4: Schematic diagram of "skin effect" phenomenon [66].

$$\delta = \sqrt{\frac{\rho}{\mu.\pi.f}}. \tag{6}$$

From equation (6), an inverse relationship between frequency and heating depth can be inferred, that is, higher frequency leads to a lower heating depth. Thus, it is essential to take into consideration the contributing factors in the self-healing process, such as frequency and so on.

5. Mechanism of Microwave Heating

Another technology related to the self-healing of asphalt pavement is microwave radiation. Microwaves are electromagnetic (EM) waves is similar in nature to radar, ultraviolet (UV), and infrared (IR). Both the waves are differentiated from each other based on their wavelength (known as frequency). For example, ultraviolet has a wavelength between 4.3×10^{-7} m and 3×10^{-9} m, while the wavelength of microwave ranges between 3 mm and 3 m, corresponding to frequencies between 100 MHz and 100 GHz [42, 67]. A microwave oven typically functions at 2.45 GHz, which usually corresponds to an approximate wavelength of 120 mm [45, 68, 69].

Microwaves are nonionizing electromagnetic radiation that causes heating of the matter by oscillation, rotation, or vibrations of molecules [70]. Conventional processing methods involve heating the surface of materials while transferring the heat into the material via conduction, convection, and radiation modes. In contrast, in microwave heating, atomic level heating occurs, which gives rise to volumetric heating in the processed component [71]. The electromagnetic energy is converted into heat within the material during microwave heating. The heat generated in the core moves in the outward direction. The electromagnetic waves only increase the energy stored thermally by an object when they are absorbed. This phenomenon can be inferred that the more thermally stored energy within a material, the more the occurrence of vibration and oscillation of its molecules under electromagnetic radiation. Such an increase in vibration and oscillation of molecules in form of kinetic energy leads to the dissipation of heat energy within the material that can cause the increment of temperature [5]. However, the energy of electromagnetic radiation and its absorbance depends on the photon wavelength, that is, color that varies over a wide range. This
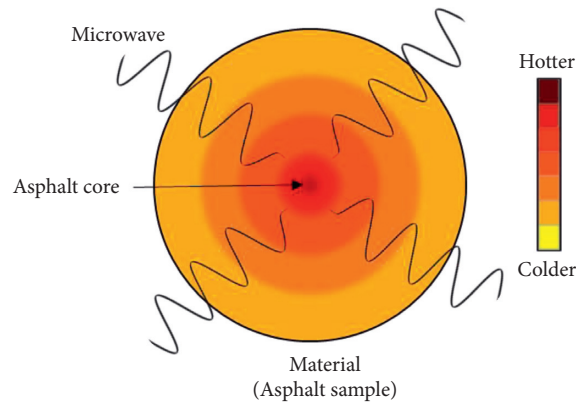
FIGURE 5: Phenomenon of heat generation in microwave heating [72].
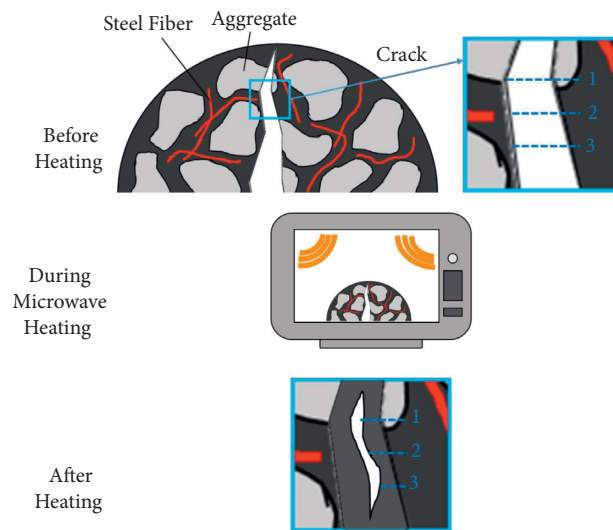
FIGURE 6: Schematic diagram of crack closure via microwave heating [38].

determines its rate of heat transfer, wherein, for instance, photon wavelengths of black surfaces have higher heat transfer rates than transparent surfaces, which makes the utilization of asphalt black surfaces incorporated with conductive materials very efficient in terms of heat transfer between the bitumen and conductor molecular interfaces. This phenomenon helps ensure uniform heat dissipation from the bituminous phase to the conductor phase, which leads to effective capillary flow in both phases. The heating mechanisms of asphalt in a microwave system are shown in Figure 5. An example of microwave heating towards the asphalt sample that can increase the temperature of the binder and close the crack is shown in Figure 6.

The EM waves can be absorbed by the steel fibers when they are placed in the microwave field. The steel fibers can absorb the microwaves and convert them to heat through a combination of different phenomena, such as double polarization, interface polarization, and electrical conduction dissipation [73]. The converted heat is passed on to the asphalt and aggregates. The effect of temperature on the asphalt at the time of microwave heating results in a Newtonian flow of the asphalt, enabling it to fill the cracks in the mixture. On a microscale, the process of crack healing in a microscale can be considered to be characterized by a combination of capillary flow induced by the surface tension force, the gravity of liquid asphalt, and friction between aggregate particles and flowing asphalt. The recovery of adhesion strength occurs when the molecular diffusion and rebinding process occurs, while the binder flows into the microcrack space. The recovered strength was ascribed to two major aspects: the molecular diffusion in asphalt and the rebinding of asphalt and aggregates [54]. The healing mechanism of asphalt mixture via microwave heating is shown in Figure 7.

The efficiency materials in absorbing energy from microwave radiations, which ultimately induce increments in its temperature via the penetration of such wave into its molecular structure, can be expressed by its dielectric properties. Three related parameters in this field are as follows:

(1) The dielectric constant of the material (ε')
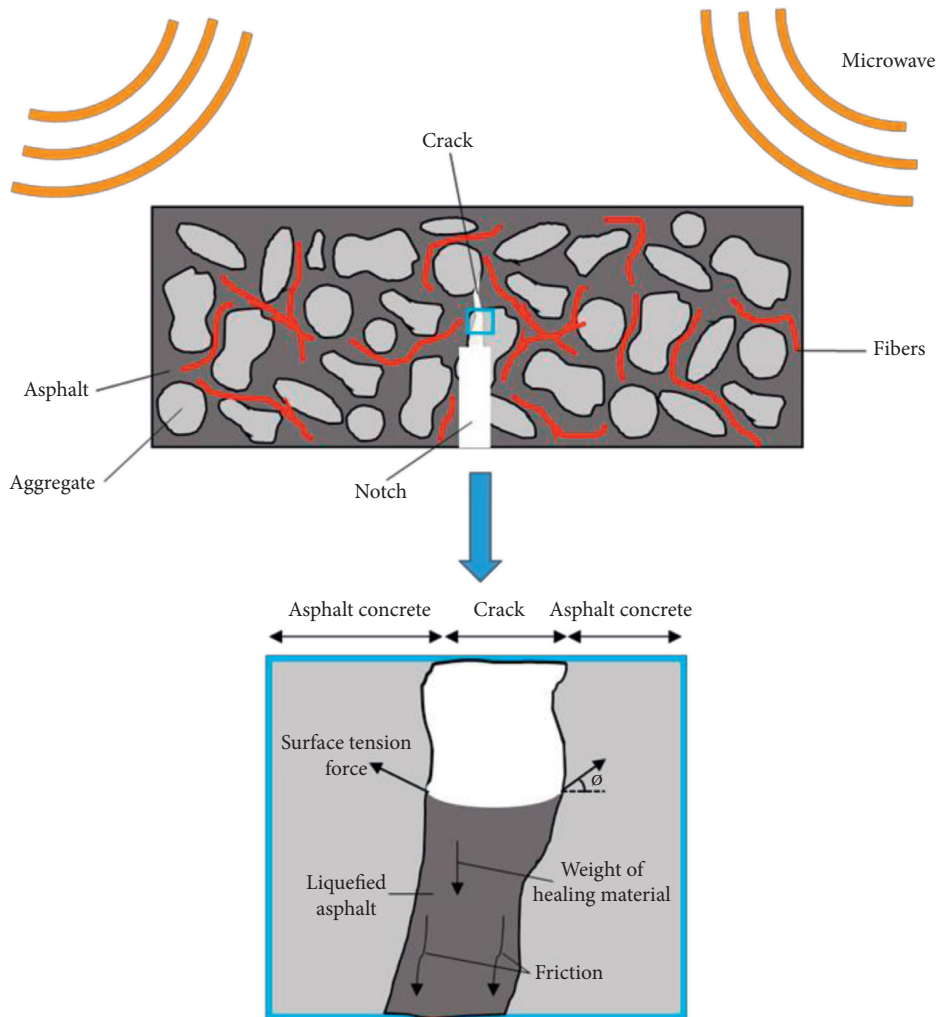
FIGURE 7: Schematic demonstration of microwave healing mechanism [54].

(2) The dielectric loss factor (ε")

(3) The dissipation factor or loss tangent of the material (tan δ)

The dielectric constant (ε') affect the electrical field energy that is stored within the material. The dielectric loss factor (ε") determines the value of that energy is dissipated in the form of heat, while the loss tangent, which equals ε"ε', is the parameter that quantifies the inherent dissipation of electromagnetic energy [74]. By discovering these factors, several researchers such as Wan et al. [75] and Zhang et al. [76] are making an improvement to the ability of asphalt mixtures toward the microwave absorption via increment of the dielectric constant of asphalt mixtures.

6. Conclusions and Way Forward

An extensive review of the research works carried out on the advancement of self-healing has revealed that the method is a competent technology for road maintenance with a great potential to prolong the service life of asphalt pavements. The innovation of self-healing by using induction/microwave heating can help enhance the temperature absorption

of the binder, which can help improve its fatigue resistance under repeated traffic loading. Such loads also inhibit the performance of pavements under various adverse weather and stress loading conditions. Asphalt self-healing processes mainly entail the wetting of nanocrack surfaces, diffusion of binder molecules between binder-aggregate interfaces, and the randomization of these diffused molecules, which help achieve the strength of cracked interfaces relatively similar to that of the original materials. Thus, self-healing is an effective method of enhancing the ability of asphalt pavement to heal, especially on microcracks healing.

Incorporating self-healing technologies into asphalt pavements leads to more durable roads and addresses environmental and economic challenges by lowering costs and emissions during maintenance and manufacturing processes. Such incorporation between sustainable materials can aid in developing asphalt pavements with self-healing technologies and construction of asphalt pavements as a whole. Moreover, these technologies can help reduce the consumption of natural resources, saving the cost of aggregates and bitumen that would otherwise be used in reconstruction or repair/maintenance actions of road networks while mitigating the effect of related costs and CO_2

emissions, as well as minimizing the traffic disruptions during road construction cycles. Additionally, the utilization of renewable and sustainable materials on asphalt pavement construction has led to the quest for material efficiency, suitability, and productivity in both the fields of material and transportation engineering. Contrastingly, different materials may or may not be compatible with asphalt mixtures based on their nature and composition; materials such as steel and its by-product have been established to be suitable in improving asphalt mixture mechanical and healing strengths as a result of its efficient physical and conductive properties. Hence this review recommends further exploration concerning the effect of steel slags, wools, and fibers in terms of the impact of bituminous and steel free energy phases on healing while also taking into consideration the influence of chemical compositions on steel rusting and deterioration for a thorough understanding between steel and bitumen as a singular system.

Data Availability

The data used to support the findings of this study are included within the article.

Conflicts of Interest

The authors declare that they have no conflicts of interest.

Acknowledgments

References

[1] S. M. Abtahi, M. Sheikhzadeh, and S. M. Hejazi, "Fiber-reinforced asphalt-concrete - a review," *Construction and Building Materials*, vol. 24, no. 6, pp. 871–877, 2010.

[2] D. Sun, G. Sun, X. Zhu et al., "A comprehensive review on self-healing of asphalt materials: mechanism, model, characterization and enhancement," *Advances in Colloid and Interface Science*, vol. 256, pp. 65–93, 2018.

[3] Q. Dai, Z. Wang, and M. R. Mohd Hasan, "Investigation of induction healing effects on electrically conductive asphalt mastic and asphalt concrete beams through fracture-healing tests," *Construction and Building Materials*, vol. 49, pp. 729–737, 2013.

[4] "Asia trade Hub," Available from: <https://malaysia.asiatradehub.com/Infrastructure/1476/Roads>. [10 May 2020]..

[5] B. Lou, A. Sha, D. M. Barbieri, Z. Liu, and F. Zhang, "Microwave heating properties of steel slag asphalt mixture using a coupled electromagnetic and heat transfer model," *Construction and Building Materials*, vol. 291, pp. 123248–123312, 2021.

[6] Y. Song, Z. Wang, Y. Zhou, and R. Hu, "Research on microwave heating performance of modified steel slag asphalt mixture," *Advances in Mechanical Engineering*, vol. 13, no. 4, pp. 168781402199047–7, 2021.

[7] R. Abejón, "Self-healing asphalt: a systematic b analysis for identification of hot research topics during the 2003-2018 period," *Materials*, vol. 14, no. 3, pp. 565–618, 2021.

[8] A. García, J. Norambuena-Contreras, and M. N. Partl, "Experimental evaluation of dense asphalt concrete properties for induction heating purposes," *Construction and Building Materials*, vol. 46, pp. 48–54, 2013.

[9] S. Xu, X. Liu, A. Tabaković, and E. Schlangen, "The prospect of microwave heating: towards a faster and deeper crack healing in asphalt pavement," *Processes*, vol. 9, no. 3, p. 507, 2021b.

[10] Ö. E. Yamaç, M. Yilmaz, E. Yalçın, B. V. Kök, J. Norambuena-Contreras, and A. Garcia, "Self-healing of asphalt mastic using capsules containing waste oils," *Construction and Building Materials*, vol. 270, p. 121417, 2021.

[11] Q. Liu, B. Li, E. Schlangen, Y. Sun, and S. Wu, "Research on the mechanical, thermal, induction heating and healing properties of steel slag/steel fibers composite asphalt mixture," *Applied Sciences*, vol. 7, no. 10, p. 1088, 2017.

[12] N. Ruiz-riancho, T. Saadoon, A. Garcia, D. Grossegger, and R. Hudson-griffiths, "Optimisation of self-healing properties for asphalts containing encapsulated oil to mitigate reflective cracking and maximize skid and rutting resistance % Passing Sieve Size (mm)," *Construction and Building Materials*, vol. 300, Article ID 123879, 2021.

[13] Q. Liu, E. Schlangen, M. van de Ven, and Á. García, "Healing of porous asphalt concrete via induction heating," *Road Materials and Pavement Design*, vol. 11, no. sup1, pp. 527–542, 2010.

[14] J. Qui, M. F. C. Van De Ven, S. Wu, J. Yu, and A. A. A. Molenaar, "Investigating the self healing capability of bituminous binders," *Road Materials and Pavement Design*, vol. 10, no. SI, pp. 81–94, 2009.

[15] H. Fischer, "Self-repairing material systems—a dream or a reality?" *Natural Science*, vol. 2, no. 8, pp. 873–901, 2010.

[16] G. van Bochove, "Self Healing Asphalt-extending the service life by induction heating of asphalt," in *Proceedings of the 6th Eurasphalt & Eurobitume Congress*, June 2017.

[17] A. Tabaković and E. Schlangen, "Self-healing technology for asphalt pavements," *Self-healing Materials*, vol. 273, pp. 285–306, 2015.

[18] Y. Sun, S. Wu, Q. Liu, J. Hu, Y. Yuan, and Q. Ye, "Snow and ice melting properties of self-healing asphalt mixtures with induction heating and microwave heating," *Applied Thermal Engineering*, vol. 129, pp. 871–883, 2018.

[19] R. P. Wool and K. M. O'Connor, "A theory crack healing in polymers," *Journal of Applied Physics*, vol. 52, no. 10, pp. 5953–5963, 1981.

[20] B. Shu, M. Zhou, T. Yang et al., "The properties of different healing agents considering the micro-self-healing process of asphalt with encapsulations," *Materials*, vol. 14, no. 1, pp. 16–18, 2021.

[21] L. Minsk, "Electrically conductive asphaltic concrete," *U.S. Patent*, vol. 3, p. 573, 1969.

[22] Á. García, E. Schlangen, M. Van De Ven, and D. Van Vliet, "Induction heating of mastic containing conductive fibers and fillers," *Materials and Structures*, vol. 44, no. 2, pp. 499–508, 2011.

[23] A. García, M. Bueno, J. Norambuena-Contreras, and M. N. Partl, "Induction healing of dense asphalt concrete," *Construction and Building Materials*, vol. 49, pp. 1–7, 2013.

[24] S. Xu, A. García, J. Su, Q. Liu, A. Tabaković, and E. Schlangen, "Self-healing asphalt review: from idea to practice," *Advanced Materials Interfaces*, vol. 5, no. 17, pp. 1800536–1800621, 2018.

[25] Á. García, E. Schlangen, M. van de Ven, and Q. Liu, "Electrical conductivity of asphalt mortar containing conductive fibers and fillers," *Construction and Building Materials*, vol. 23, no. 10, pp. 3175–3181, 2009.

[26] D. Sun, F. Yu, L. Li, T. Lin, and X. Y. Zhu, "Effect of chemical composition and structure of asphalt binders on self-healing," *Construction and Building Materials*, vol. 133, pp. 495–501, 2017.

[27] Y. Sun, S. Wu, Q. Liu et al., "Self-healing performance of asphalt mixtures through heating fibers or aggregate," *Construction and Building Materials*, vol. 150, pp. 673–680, 2017.

[28] J. Gao, H. Guo, X. Wang et al., "Microwave deicing for asphalt mixture containing steel wool fibers," *Journal of Cleaner Production*, vol. 206, pp. 1110–1122, 2019.

[29] J. Norambuena-Contreras, R. Serpell, G. Valdés Vidal, A. González, and E. Schlangen, "Effect of fibres addition on the physical and mechanical properties of asphalt mixtures with crack-healing purposes by microwave radiation," *Construction and Building Materials*, vol. 127, pp. 369–382, 2016.

[30] A. González, J. Valderrama, and J. Norambuena-Contreras, "Microwave crack healing on conventional and modified asphalt mixtures with different additives: an experimental approach," *Road Materials and Pavement Design*, vol. 20, no. sup1, pp. S149–S162, 2019.

[31] M. Ameri, S. Hesami, and H. Goli, "Laboratory evaluation of warm mix asphalt mixtures containing electric arc furnace (EAF) steel slag," *Construction and Building Materials*, vol. 49, pp. 611–617, 2013.

[32] Q. Liu, W. Yu, E. Schlangen, and G. Van Bochove, "Unravelling porous asphalt concrete with induction heating," *Construction and Building Materials*, vol. 71, pp. 152–157, 2014.

[33] B. Lou, A. Sha, D. M. Barbieri, Z. Liu, F. Zhang, and W. Jiang, "Improved microwave heating uniformity and self-healing properties of steel slag asphalt containing ferrite filler," *Materials and Structures*, vol. 54, no. 1, pp. 1–14, 2021.

[34] B. Shu, L. Guo, B. Qiu et al., "Effect of encapsulation combined with microwave heating on self-healing performance of asphalt mixture," *Journal of Renewable Materials*, vol. 9, no. 10, pp. 1781–1794, 2021.

[35] J. Norambuena-Contreras and A. Garcia, "Self-healing of asphalt mixture by microwave and induction heating," *Materials & Design*, vol. 106, pp. 404–414, 2016.

[36] M. T. Bevacqua, T. Isernia, F. G. Praticò, and S. Zumbo, "A method for bottom-up cracks healing via selective and deep microwave heating," *Automation in Construction*, vol. 121, p. 103426, Article ID 103426, 2021.

[37] B. Liang, F. Lan, K. Shi, G. Qian, Z. Liu, and J. Zheng, "Review on the self-healing of asphalt materials: mechanism, affecting factors, assessments and improvements," *Construction and Building Materials*, vol. 266, p. 120453, Article ID 120453, 2021.

[38] J. Norambuena-Contreras and I. Gonzalez-Torre, "Influence of the microwave heating time on the self-healing properties of asphalt mixtures," *Applied Sciences*, vol. 7, no. 10, p. 1076, 2017.

[39] M. Atakan and K. Yildiz, "Farklı a metal ai?pabmiki?p," *Journal of Polytechnic*, vol. 1, no. 1, 2020.

[40] J. Liu, Z. Wang, H. Guo, and F. Yan, "Thermal transfer characteristics of asphalt mixtures containing hot poured steel slag through microwave heating," *Journal of Cleaner Production*, vol. 308, p. 127225, 2021.

[41] Y. Deng, J. Ma, T. Lu, and D. Sun, "Enhanced heating-healing performance of asphalt concrete modified with heterogenous microwave sensitive admixtures," *Construction and Building Materials*, vol. 299, p. 123949, 2021.

[42] A. Dulaimi, S. Al-busaltan, and M. Sadique, "The development of a novel, microwave assisted, half-warm mixed asphalt," *Construction and Building Materials*, vol. 301, p. 124043, Article ID 124043, 2021.

[43] F. Gulisano and J. Gallego, "Microwave heating of asphalt paving materials: principles, current status and next steps," *Construction and Building Materials*, vol. 278, p. 121993, Article ID 121993, 2021.

[44] Z. Wang, N. Dai, X. Wang, J. Zhang, and H. Guo, "Laboratory investigation on effects of microwave heating on early strength of cement bitumen emulsion mixture," *Construction and Building Materials*, vol. 236, p. 117439, 2020.

[45] J. Gallego, M. A. Del Val, V. Contreras, and A. Páez, "Heating asphalt mixtures with microwaves to promote self-healing," *Construction and Building Materials*, vol. 42, pp. 1–4, 2013.

[46] S. Xu, X. Liu, A. Tabaković, and E. Schlangen, "Experimental investigation of the performance of a hybrid self-healing system in porous asphalt under fatigue loadings," *Materials*, vol. 14, no. 12, p. 3415, 2021a.

[47] S. Fan, H. Zhu, H. Yuan, and C. Chen, "Fracture -healing properties of asphalt mixtures and microwave heating thermo-sensitivity analysis of their constituent materials," *Journal of Cleaner Production*, vol. 312, p. 127763, 2021.

[48] W. Zhang, D. Wang, and B. Han, "Self-healing concrete-based composites," *Self-Healing Composite Materials*, pp. 259–284, 2020.

[49] Á. García, E. Schlangen, M. Van De Ven, and Q. Liu, "A simple model to define induction heating in asphalt mastic," *Construction and Building Materials*, vol. 31, pp. 38–46, 2012.

[50] Q. Liu, E. Schlangen, and M. Van De Ven, "Induction healing of porous asphalt concrete beams on an elastic foundation," *Journal of Materials in Civil Engineering*, vol. 25, no. 7, pp. 880–885, 2013.

[51] Q. Liu, E. Schlangen, M. Van De Ven, G. Van Bochove, and J. Van Montfort, "Evaluation of the induction healing effect of porous asphalt concrete through four point bending fatigue test," *Construction and Building Materials*, vol. 29, pp. 403–409, 2012.

[52] A. García, J. Norambuena-Contreras, M. Bueno, and M. N. Partl, "Influence of steel wool fibers on the mechanical, termal, and healing properties of dense asphalt concrete," *Journal of Testing and Evaluation*, vol. 42, no. 5, p. 20130197, 2014.

[53] A. Tabaković, D. O'Prey, D. McKenna, and D. Woodward, "Microwave self-healing technology as airfield porous asphalt friction course repair and maintenance system," *Case Studies in Construction Materials*, vol. 10, p. e00233, 2019.

[54] Z. Wang, Q. Dai, D. Porter, and Z. You, "Investigation of microwave healing performance of electrically conductive carbon fiber modified asphalt mixture beams," *Construction and Building Materials*, vol. 126, pp. 1012–1019, 2016.

[55] S. Jendia, N. Hassan, K. Ramlawi, and H. Abu-aisha, "Study of the mechanical and physical properties of self-healing asphalt," *Journal of Engineering Research and Technology*, vol. 3, no. 4, p. 7, 2016.

[56] A. González, J. Norambuena-Contreras, L. Storey, and E. Schlangen, "Self-healing properties of recycled asphalt mixtures containing metal waste: an approach through

microwave radiation heating," *Journal of Environmental Management*, vol. 214, pp. 242–251, 2018.

[57] M. Skaf, J. M. Manso, Á. Aragón, J. A. Fuente-Alonso, and V. Ortega-López, "EAF slag in asphalt mixes: a brief review of its possible re-use," *Resources, Conservation and Recycling*, vol. 120, pp. 176–185, 2017.

[58] S. Wu, L. Mo, Z. Shui, and Z. Chen, "Investigation of the conductivity of asphalt concrete containing conductive fillers," *Carbon*, vol. 43, no. 7, pp. 1358–1363, 2005.

[59] Á. García, E. Schlangen, M. v. d. Ven, and G. v. Bochove, "Optimization of composition and mixing process of a self-healing porous asphalt," *Construction and Building Materials*, vol. 30, pp. 59–65, 2012.

[60] Á. García, "Self-healing of open cracks in asphalt mastic," *Fuel*, vol. 93, pp. 264–272, 2012.

[61] A. Menozzi, A. Garcia, M. N. Partl, G. Tebaldi, and P. Schuetz, "Induction healing of fatigue damage in asphalt test samples," *Construction and Building Materials*, vol. 74, pp. 162–168, 2015.

[62] Q. Liu, W. Yu, S. Wu, E. Schlangen, and P. Pan, "A comparative study of the induction healing behaviors of hot and warm mix asphalt," *Construction and Building Materials*, vol. 144, pp. 663–670, 2017.

[63] H. Xiang, Z. He, L. Chen, H. Zhu, and Z. Wang, "Key factors and optimal conditions for self-healing of bituminous binder," *Journal of Materials in Civil Engineering*, vol. 31, no. 9, Article ID 04019172, 2019.

[64] J. Gallego, F. Gulisano, V. Contreras, and A. Páez, "The crucial effect of re-compaction energy on the healing response of hot asphalt mortars heated by microwaves," *Construction and Building Materials*, vol. 285, p. 122861, 2021.

[65] V. Rudnev, D. Loveless, R. L. Cook, and M. Black, "Handbook of induction heating," *Handbook of Induction Heating*, vol. 2, Article ID 28904, 2002.

[66] T. Bayerl, M. Duhovic, P. Mitschang, and D. Bhattacharyya, "The heating of polymer composites by electromagnetic induction - a review," *Composites Part A: Applied Science and Manufacturing*, vol. 57, pp. 27–40, 2014.

[67] J. Tang, "Unlocking potentials of microwaves for food safety and quality," *Journal of Food Science*, vol. 80, no. 8, pp. E1776–E1793, 2015.

[68] C. Li, G. Zeng, M. Zhou et al., "Performance evolution of Fe3O4 used in the production of sustainable self-healing asphalt materials," *Journal of Cleaner Production*, vol. 314, p. 127960, 2021.

[69] E. Yalcin, "Effects of microwave and induction heating on the mechanical and self-healing characteristics of the asphalt mixtures containing waste metal," *Construction and Building Materials*, vol. 286, p. 122965, 2021.

[70] L. Trigos, J. Gallego, and J. I. Escavy, "Heating potential of aggregates in asphalt mixtures exposed to microwaves radiation," *Construction and Building Materials*, vol. 230, p. 117035, 2020.

[71] S. Singh, D. Gupta, V. Jain, and A. K. Sharma, "Microwave processing of materials and applications in manufacturing industries: a Review," *Materials and Manufacturing Processes*, vol. 30, no. 1, pp. 1–29, 2015.

[72] P. R. Matli, R. A. Shakoor, and A. M. A. Mohamed, "Development of metal matrix composites using microwave sintering technique," *Sintering of Functional Materials*, 2018.

[73] N. Zhao, T. Zou, C. Shi, J. Li, and W. Guo, "Microwave absorbing properties of activated carbon-fiber felt screens (vertical-arranged carbon fibers)/epoxy resin composites," *Materials Science and Engineering: B*, vol. 127, no. 2-3, pp. 207–211, 2006.

[74] A. Benedetto and A. Calvi, "A pilot study on microwave heating for production and recycling of road pavement materials," *Construction and Building Materials*, vol. 44, pp. 351–359, 2013.

[75] P. Wan, Q. Liu, S. Wu et al., "A novel microwave induced oil release pattern of calcium alginate/nano-Fe3O4 composite capsules for asphalt self-healing," *Journal of Cleaner Production*, vol. 297, p. 126721, 2021.

[76] Y. Zhang, L. Yang, J. Li, Q. Wang, and B. Guo, "Influence of the particle sizes and densities of RAP on microwave heating efficiency," *Alexandria Engineering Journal*, vol. 61, no. 1, pp. 65–71, 2022.

Research Article

Physicomechanical Assessments and Heavy Metals' Leaching Potential of Modified Asphalt Binders Incorporating Crumb Rubber and Tin Slag Powders

Ali Huddin Ibrahim,[1] Mohd Rosli Mohd Hasan [iD],[1] Ashiru Sani,[2] Sharvin Poovaneshvaran,[1] Tracy Leh Xin Wong,[1] Megat Azmi Megat Johari,[1] Kok Keong Choong,[1] and Ramadhansyah Putra Jaya [iD][3]

[1]*School of Civil Engineering, Universiti Sains Malaysia (Engineering Campus), Nibong Tebal 14300, Pulau Pinang, Malaysia*
[2]*Department of Civil Engineering, Kano University of Science and Technology, Wudil 3244, Kano, Nigeria*
[3]*Department of Civil Engineering, College of Engineering, Universiti Malaysia Pahang, Gambang 26300, Kuantan, Pahang, Malaysia*

Correspondence should be addressed to Mohd Rosli Mohd Hasan; cerosli@usm.my

Industrial solid waste has been widely used as an alternative additive for bituminous material modification. This study aims to evaluate the basic properties and quantify the leaching potential of modified asphalt binders incorporating crumb rubber powder (CRP) from waste tires and tin slag (TS) for a local smelting company. Three percentages of CRP and TS, at 5, 10, and 15%, were considered. The conventional asphalt binder (PEN 60/70), CRP, and TS-based modified asphalt binders were analyzed for toxicity, softening point, penetration value, elastic recovery, torsional recovery (TR), and coatability index. The findings indicated that the addition of the waste materials led to no significant heavy metal content in the asphalt binder mix. Moreover, the basic and physical properties of the asphalt binders were also improved by 5, 10, and 15% of the waste, respectively. However, TS waste exhibited limited effects on all the parameters and had a 5% optimum dosage. The modified binders' results showed that the CRP modified asphalt binders had fewer heavy metals and responded more to elastic recovery and coatability.

1. Introduction

In Malaysia, the escalated usage of vehicles on roads generates a huge amount of waste tires at the end of their life cycle [1]. Up to mid-2017, there were 28,181,203 units of vehicles registered, as reported by the Malaysia Automotive Association (MAA) [2]. As a developing country, the huge increase in the generation of scrap tires is alarming. The disposal of waste tires poses a major environmental problem, as they have a long lifespan and possess nonbiodegradable properties. Disposal of waste tires is a challenging task as it will lead to scarcity of landfills capacity due to its large quantity [2, 3]. This issue can be overcome by recycling scrap tires to protect the environment from pollution [4, 5]. Since

the last few decades, recycled waste tires are being utilized as a modifier in asphalt paving mixtures, additives in Portland cement concrete, and lightweight fillers. In addition, the tires can also serve as the crash barrier, a bumper, and an artificial reef [3, 6, 7]. The utilization of waste tires is effective in overcoming the issue associated with solid scrap tire disposal, and the recycled tires such as crumb rubber can act as a good modifier for enhancing the properties and performance of asphaltic concrete [2, 8, 9]. The utilization of polymer-modified bitumen is a cost-effective and efficient alternative to improve the performance of asphalt pavements [10, 11].

Vehicle tire shreds are usually found in the range of 460 mm to 25 mm, and thus, the small sizes of shred and chip

eased the production of ground crumb rubber [12]. The wire and other metal contaminants are removed [12–14]. The applications of crumb rubber in asphalt paving mixtures are known as rubber asphalt in the USA. It consists of asphalt cement, reclaimed tire rubber, and additives. According to the reports, approximately 15% of the rubber components are integrated into the rubber asphalt blend. During the blending process, grounded rubber particles were mixed with hot asphalt cement, resulting in swelling of the rubber particles [15]. The particles size of CRP influenced the physical properties of modified binders. Studies reported that the particle size of crumb rubber, which is subjected to high temperature, was an influential factor in viscoelastic properties [16, 17].

On the other hand, tin slag is formed through the smelting process of tin. Recently, a company from Penang managed to produce 27,172 tonnes of tin metal, thus making Penang the largest tin producer in Malaysia. Malaysia is known as the third-largest tin metal supplier globally, leading in the production of tin metal and tin-based products, as well as custom tin smelting [18]. Cassiterite is reduced to form tin metal with carbon at a very high temperature (1200°C to 1300°C). Currently, the lack of commercial application of tin slag and its unsuitability for disposal in landfills has resulted in the accumulation of a large quantity of waste that poses a disposal concern for smelting plant companies. The TS generally consists of SiO_2, Al_2O_3, CaO, Fe_2O_3, and TiO_2. The elements such as Pb, Cr, and Mn in TS tend to be soluble in an acid environment [19]. With stringent environmental restrictions by the government and local authorities, treatment, and disposal issues for scheduled waste are getting more attention from manufacturers or industry authorities. Along with this, an alternative approach such as reusing or recycling industrial waste or by-products has been considered. The outcome of previous research shows that those products are feasible to be used in road pavement construction as binder modifiers with and without additives [20–24].

However, incorporating various industrial wastes into asphalt binders has compelled me to conduct related studies to ascertain that the heavy metals are present in the CRP and TS modified binders. The studies are to ensure its environmental sustainability through the use of asphalt pavement technology. This study is also partially intended to examine the basic and physical characteristics of CRP and TS modified binders. Therefore, this study mainly aims to evaluate the possibility of adding different industrial wastes (CRP and TS) as additives to bituminous materials.

2. Materials and Methods

2.1. Materials. The physical properties of conventional asphalt binder (PEN 60/70) used for the sample preparation in this study are shown in Table 1. The dosages of industrial waste that are used to modify asphalt binders, namely, crumb rubber powder (CRP) and tin slag (TS), are provided in Table 2. The CRP and TS industrial waste adopted were supplied by Malaysia's Pan Century Oleochemicals Sdn Bhd. and Penang's Malaysia Smelting Corporation Berhad

TABLE 1: The bitumen properties.

Physical properties	Results
Torsional recovery	0.5%
Softening point	50°C
Elastic recovery	83%
Penetration	65 dmm
Flash point	273°C

TABLE 2: Percentages of additives used.

Types of additives	Designation	Dosages (%)	Sample designation
Crumb rubber powder	CRP	5	5% CRP
		10	10% CRP
		15	15% CRP
Tin slag	TS	5	5% TS
		10	10% TS
		15	15% TS

(MSC). The physical appearance of the CRP is shown in Figure 1(a). The CRP is a processed waste tire, in which the size of the tire is reduced by grounding it into smaller particles. The distribution of particle size for both the CRP and TS is shown in Figure 2. TS was initially dried in an oven at $105 \pm 5^{\circ}$C for 24 hours and then grounded for 8 hours to obtain finer particles using a laboratory scale ball mill. The tin slag went through a $75\,\mu$m sieve to remove coarser particles, as shown in Figure 1(b). The tin slag chemical composition is shown in Table 3 [25]. All samples were prepared using a liquid antistripping agent at 0.1% Silane additive based on the binder weight.

2.2. Preparation of Samples

2.2.1. Preparation of the Sample for Toxicity Characteristic Leaching Procedure (TCLP) Test. Initially, the asphalt binder in galvanized iron containers was preheated at 160°C for 1 hour. Besides that, modified binders with different dosages (5%, 10%, and 15%) of CRP and TS were also prepared to compare the impact of various dosages on the quantity of detected heavy metals. Before testing, the preheated modified binder in each galvanized iron container was manually stirred for 1 minute to improve its consistency. Then, the sample was poured into a container and cooled to room temperature for 1 hour prior to the test. The toxicity of the conventional and modified asphalt binders was tested according to US EPA Method 1311, Toxicity Characteristic Leaching Procedure (TCLP) [26] by using the water from the purification system (Figure 3(a)) and an automatic rotary agitator as shown in Figure 3(b).

2.2.2. Preparation of the Sample for the Physical Property Tests. The TS and CRP modified binders were prepared using three dosages at 5%, 10%, and 15% by weight of asphalt binder. The incorporation of waste materials (TS that was passing $75\,\mu$m or CRP passing 1 mm) was incorporated in

(a) (b)

FIGURE 1: Physical appearance of industrial waste powders. (a) Crumb rubber powder. (b) Tin slag.
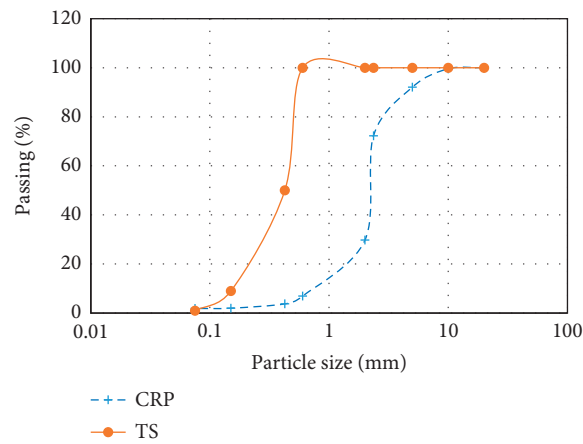
FIGURE 2: Particle size distribution of crumb rubber powder (CRP) and tin slag (TS).

TABLE 3: Chemical composition of tin slag.

CaO (%)	SiO$_2$ (%)	Al$_2$O$_3$ (%)	MgO (%)	FeO/Fe$_2$O$_3$ (%)	WO (%)	As (%)	Pb (%)	Cd (%)	TiO$_2$ (%)	Sn (%)	Zn (%)
16–20	28–32	10–13	2–4	13–18	20	<0.01	<0.01	<0.0001	4–6	<0.3	<0.14

(a) (b)

FIGURE 3: TCLP test assembly. (a) Water purification machine. (b) Automatic rotary agitator.

the binder via a wet process. Firstly, the conventional asphalt binder was preheated at a temperature of 160°C before blending. After that, the waste materials were incorporated into the binder for 30 minutes at a temperature of 160°C in a high-shear mixer. The waste materials were added gently into the binder to avoid clumping to produce a homogenous

modified binder. The mixing speed of the high-shear mixer to blend the waste material and binder was set at 1000 rpm.

3. Test Methods

3.1. Toxicity Characteristic Leaching Procedure (TCLP). The testing was initiated by preparing samples of bitumen, CRP, or TS mixed binder of about 100 g with each placing in a 2 L plastic bottle together with extractor fluid #1 used as leaching fluid. The buffer chosen for the extraction of fluid depends on the pH of the samples. The preparation of extraction fluid #1 was started by mixing glacial acetic acid (CH_3COOH) (5.7 mL) into 1 L Type II reagent water, followed with the addition of 1 N NaOH (64.3 mL), and diluted it to the volume of 2 L with final pH 4.93 ± 0.05. Type II reagent water was filtered by the New Human Power System water filter (Figure 3(a)). Referring to Figure 3(b), the plastic bottles were placed in an Automatic Rotary Agitator at 18 ± 2 h at room temperature. After agitation, the samples were filtrated with 0.7 μm glass microfiber filters. The filtered samples were collected and analyzed for 21 chemical elements. The concentrations (ppm) of chemical elements such as arsenic (As), beryllium (Be), calcium (Ca), cadmium (Cd), cobalt (Co), chromium (Cr), copper (Cu), iron (Fe), lithium (Li), magnesium (Mg), manganese (Mn), molybdenum (Mo), nickel (Ni), lead (Pb), antimony (Sb), selenium (Se), strontium (Sr), thallium (Ti), thallium (Tl), vanadium (V), and zinc (Zn) were determined by state-of-the-art equipment namely ICP-OES (Varian 715-ES ICP Optical Emission Spectrometer). The same approach was repeated for tin slag samples. Table 4 shows the United States Environmental Protection Agency (US EPA).

3.2. Basic Properties of Asphalt Binders. The asphalt binder basic tests were carried out using the penetration, softening point, elastic recovery, and torsional recovery tests. The penetration test was performed in accordance with ASTM D5 [28] to evaluate the differences in penetration grade and the consistency of asphalt binders. Likewise, the softening point test determined the temperature of the initial asphalt binder response as followed by the ASTM D36 procedure [29]. Moreover, the determination of temperature susceptibility of crumb rubber and tin slag modified asphalt binders was evaluated from the penetration index (PI), which was obtained from the penetration and softening point test. The calculation of penetration index is shown in Shell Bitumen Handbook as stated in the following equation:

$$PI = \frac{1952 - 500 \log(\text{Pen25}) - 20\, x\, \text{SP}}{50 \log(\text{Pen25}) - \text{SP} - 120}, \quad (1)$$

where Pen_{25} refers to the penetration at 25°C, and SP refers to the softening point temperature of modified asphalt binder.

The elastomeric characteristics of the asphalt binder and modified binders were ascertained via elastic recovery and torsional recovery. The elastic recovery test was done by following AASHTO T51 and ASTM D6084 [30, 31]. This elastic testing was conducted at 25°C according to ASTM

Table 4: Metals' hazardous waste parameters by the US EPA [27].

Metals	Regulatory level (ppm)
Arsenic (As)	5.0
Barium (Ba)	100.0
Cadmium (Cd)	1.0
Chromium (Cr)	5.0
Lead (Pb)	5.0
Mercury (Hg)	0.2
Selenium (Se)	1.0
Silver (Ag)	5.0

specification, in which the binder specimens were pulled apart in a ductilometer and held after reaching a specified elongation during the test. The specimens are then cut in the middle of the elongation, and the percent recovery of each specimen is determined [31].

The torsional recovery test is an inventive method in determining the elasticity in the asphalt binder. It was conducted following the ARRB AG: PT/T112 procedure [32] at 25°C. This test was performed by embedding a metal disc in a cup of asphalt, and the sample container was rotated at 180°. Then, the band was removed, and the specimen was left aside to recover for 30 seconds. The torsional recovery percentage (T_R) was calculated by the following equation:

$$T_R = \frac{A}{180} \times 100, \quad (2)$$

where A is recovered angle, in degrees.

3.3. Binder Coatability Test. The coatability of the asphalt mixtures was determined based on the aggregate absorption method in accordance with the AASHTO T 195 [33]. In this method, only coarse aggregate particles are considered. The short-term aged coated aggregate with a soaking time of 60 minutes was presumed that a completely coated aggregate would demonstrate high resistance towards the diffusion of water due to the presence of asphalt film that covered the aggregate surface. Otherwise, a coated aggregate could be prone to water absorption by allowing the water to diffuse into the partly coated aggregate [34–36].

This study determined the coatability of asphalt base binder and modified asphalt mixtures by the following procedures. Firstly, the 20 mm coarse aggregate was wet-sieved in order to remove the excessive fine particles. Then, the coarse aggregate was dried in an oven at a temperature of 105 ± 5°C for 24 ± 0.5 hours. Oven-dried coarse aggregate was sieved, and the portion retained on the 10 mm sieve size was used to prepare the sample. A 2,000 g batch sample consisted of 26% of aggregate between 20 mm and 14 mm, and 74% of aggregate with sizes ranging from 14 mm to 10 mm was prepared. Six individual batches were formed from coarse aggregate gradations following Marshall mix design, with three batches sample of 2,000 g subjected to preheating at a mixing temperature of 160°C for four hours, and the others were stored at the room temperature. The considerations have taken to their rheological behavior at mixing, and construction temperature, the base asphalt

binder, and modified asphalt binder were subjected to a high temperature of 163°C for at least 85 minutes to simulate the short-term aging process artificially. The aging process was conducted in accordance with ASTM D 2872 [37].

Mix design and the surface area distribution of the coarse aggregate fraction determined the required amount of binder. Equations (3) to (6) were used to compute the binder content and the output parameters such as absorption of loss mixture aggregate, absorption of aggregate, and coating index of each mixture. The input parameters used for the sample preparation are presented in Table 5. The amount of binder of 41.25 g was mixed with the 2,000 g of coarse aggregate fraction batch. The optimum binder content (OBC) of Pb was obtained from the Marshall mix design. The asphalt binders were subjected to heating for two hours. Then, the loose mixture was placed into a bucket mixer for 60 seconds before being transferred into a tray and heated in the oven for the next two hours. These allow for binder absorption and induce the short-term aging process during production simultaneously. Moreover, the loose mixture was cooled at room temperature overnight. Both aggregates and loose mixture were exposed to water for 60 minutes. Then, a dry towel was used to remove the excess water until the saturated surface dried (SSD) condition was achieved. The masses obtained for aggregate and loose mixture in SSD condition were recorded as $W_{agg-SSD}$ and $W_{loose-SSD}$, respectively.

$$\text{Binder content, } W_b = W_{agg} \times \frac{P_b}{100 - P_b} \times \frac{SA_{coarse}}{SST} \times \frac{1}{P_{s-coarse}}, \quad (3)$$

$$\text{Abs\%}_{loose} = \frac{W_{loose-SSD} - (W_{agg} + W_b)}{W_{agg} + W_b} \times 100, \quad (4)$$

$$\text{Abs\%}_{agg} = \frac{W_{agg-SSD} - W_{agg}}{W_{agg}} \times 100, \quad (5)$$

$$\text{coating index} = \frac{\text{Abs\%}_{agg} - \text{Abs\%}_{loose}}{\text{Abs\%}_{agg}} \times 100. \quad (6)$$

The surface area of mix design combined with aggregates is calculated by adopting methods from previous studies and past laboratory work experiences regarding aggregate gradation [38]. The calculation for surface area determination is shown in Table 6.

4. Results and Discussion

4.1. Effect of Crumb Rubber and Tin Slag on the Leaching Potential. The current study investigates the potential leaching of heavy metals from crumb rubber, tin slag, and conventional asphalt binder through TCLP experiments. The collected leachates of the samples were analyzed for the heavy metals by Inductively Coupled Plasma Optical Emission Spectrometry (ICP-OES). The initial TCLP test was performed on raw material, namely, crumb rubber powder, tin slag, and unmodified asphalt binder. Next, the

TCLP test was performed on crumb rubber powder and tin slag incorporated asphalt mixture. The TCLP test was conducted at two different stages to deliver a thorough correlation between the leaching of raw materials and the incorporation of raw material into asphalt mixtures. Along with this, the research findings indicated the effect of asphalt binder in reducing the leaching of heavy metals from the raw materials. Furthermore, the findings of TCLP analysis for crumb rubber powder, tin slag, and asphalt binder can be used to portray the mobility of heavy metals and replicate the leaching situation, as heavy metals elements were leached by acid rain.

The unmodified asphalt binder was tested as a control sample. The filtered samples or leachate solution was analyzed for the chemical elements using optical emission spectroscopy (ICP VARIAN 715-OES). The results from the leachate solution of the unmodified asphalt binder analysis implied that the chemical elements such as Arsenic (As), Beryllium (Be), Cadmium (Cd), Cobalt (Co), Copper (Cu), Lithium (Li), Lead (Pb), Strontium (Sr), and Thallium (Tl) were not detected. However, Ca, Cr, Fe, Mg, Mn, Mo, Ni, Sb, Se, Ti, V, and Zn were detected via the conducted tests. The experimental results of the TCLP for these materials in Table 7 were expressed in part per million (ppm). Zinc was detected with the highest concentration recorded as 62 ppm in crumb rubber powder, but it is still considered within the safe level compared to its maximum allowable limit of 250 ppm in Table 4. Chromium and selenium, which are more hazardous, were obtained at a concentration of 0.007 ppm and 0.235 ppm, respectively, for crumb rubber powder, while they were 0.003 ppm and 0.078 ppm for tin slag. Chromium was not detected in asphalt binder samples, yet selenium was detected at 0.134 ppm. Nevertheless, it is very much lower than the regulatory level according to the metals hazardous waste parameters by US EPA regulatory in Table 4 [27].

Meanwhile, the results in Table 8 show the detected metal elements concentrations for the samples of asphalt binder with the incorporation of crumb rubber powder at different concentrations. Generally, the trend of the experimental results showed that the increasing amount of crumb rubber powder caused a hike in certain heavy metal elements. A higher amount of heavy metals contamination for Ca, Fe, Mg, and Ti was detected in the filtered leachate solution for a higher portion of crumb rubber powder. This proved that incorporating asphalt binder mixed with crumb rubber powder does not facilitate or has no effect in reducing these heavy metal elements in the leaching process, which primarily comes from crumb rubber powder. In the case of selenium, it was found to be eliminated in bitumen mixed for 5%, 10%, and 15% added crumb rubber, but vanadium was slightly increased at 15% added crumb rubber in comparison to 5% and 10%. There was a fluctuation for Mo, Sb, and Zn, which could be occurred due to many factors such as the varying portion of chemical elements in the crumb rubber added into the specimens.

The metals considered as hazardous such as As, Cd, Cr, and Pb were evaluated to be below detectable limits, except Se that was obtained at 0.171 ppm but below 1 ppm limit.

TABLE 5: The amount of materials required for the sample preparation.

Parameters	Values
The optimum of binder content, Pb	5.0%
Coarse aggregate, W_{agg}	2,000 g
The surface area of the combined aggregate, SA_{coarse}	0.41 m^2/kg
The total surface area of mix design combined aggregate, SST	5.507 m^2/kg
Percentages of coarse aggregate retained on a 10 mm sieve, $P_{s\text{-coarse}}$	19%

TABLE 6: The determination of surface area.

Sieve size (mm)	Percent passing (%)	Surface area factor (m^2/kg)	Surface area (m^2/kg)
20	100	—	0.41
14	95	—	—
10	81	—	—
5	56	0.41	0.229
3.35	47	0.82	0.3854
1.18	26	1.64	0.4264
0.425	18	4.78	0.8604
0.15	10	12.29	1.229
0.075	6	32.77	1.9662
Total surface area of combination size aggregate			5.507

TABLE 7: Metal elements' concentrations on bitumen, crumb rubber powder, and tin slag leachate solution.

Metal elements	Bitumen (ppm)	Crumb rubber (ppm)	Tin slag (ppm)
Calcium (Ca)	0.538	26.050	19.341
Chromium (Cr)	—	0.007	0.003
Iron (Fe)	0.034	2.275	5.921
Magnesium (Mg)	0.116	1.020	3.369
Manganese (Mn)	—	0.035	0.466
Molybdenum (Mo)	0.077	0.108	0.256
Nickel (Ni)	—	0.035	0.034
Antimony (Sb)	0.074	0.045	0.051
Selenium (Se)	0.134	0.235	0.78
Titanium (Ti)	0.044	0.049	0.050
Vanadium (V)	0.005	0.011	0.046
Zinc (Zn)	0.152	61.81ACT5	0.495

TABLE 8: Metal elements' concentrations on CRP-modified bitumen leachate solution.

Metal elements	Bit. +5% CRP (ppm)	Bit. +10% CRP (ppm)	Bit. +15% CRP (ppm)
Calcium (Ca)	0.271	0.542	0.798
Iron (Fe)	0.045	0.064	0.367
Magnesium (Mg)	0.226	0.314	0.956
Molybdenum (Mo)	0.064	0.062	0.062
Antimony (Sb)	0.112	—	0.049
Selenium (Se)	—	—	—
Titanium (Ti)	0.046	0.047	0.093
Vanadium (V)	0.004	0.004	0.006
Zinc (Zn)	0.084	0.060	0.089

Other metals obtained below detectable limits consisted of Be, Co, Cu, Li, Mn, Ni, Sr, and Tl. The analysis was obtained in a minimum of Ca, Fe, Mg, Mo, Sb, Se, It, V, and Zn. The results showed that not only bitumen mixed sources of toxicity from crumb rubber were emanated but the bitumen itself also contributed to some of these toxic contaminants.

Table 9 shows the metal elements concentrations on bitumen added tin slag mixed leachate solutions. The experimental results show that a bigger portion of tin slag causes higher Ca, Fe, Mg, Se, and Ti contamination in the leachate solutions. Meanwhile, for Mo, Sb, V, and Zn, the fluctuations might be similar to what was mentioned earlier.

TABLE 9: Metal elements' concentrations on TS-modified bitumen leachate solution.

Metal elements	Bit. +5% CRP (ppm)	Bit. +10% CRP (ppm)	Bit. +15% CRP (ppm)
Calcium (Ca)	0.231	0.449	1.944
Iron (Fe)	0.045	0.064	0.367
Magnesium (Mg)	0.226	0.314	0.956
Molybdenum (Mo)	0.064	0.062	0.062
Antimony (Sb)	0.112	—	0.049
Selenium (Se)	—	0.127	0.168
Titanium (Ti)	0.046	0.047	0.093
Vanadium (V)	0.004	0.004	0.006
Zinc (Zn)	0.084	0.078	0.089

However, metal elements in bitumen added with tin slag mixed leachates solution are very low and below the regulatory level according to the metals hazardous waste parameters stated by US EPA, as shown in Table 4.

4.2. Basic and Physical Characterization of the Asphalt Binder

4.2.1. Softening Point, Penetration, and Elastic Recovery Results.
Results tabulated in Table 10 show that the asphalt binder's basic and physical properties are incorporated with crumb rubber powder and tin slag. The properties of all asphalt binders were assessed through penetration tests by evaluating their consistency and softening point. These tests were assisted in identifying the maximum service temperature; meanwhile, an elastic recovery test was used to determine the rate of the elastic response of asphalt binders. Table 10 demonstrates a reduction in penetration, while the softening point value increased with the increasing content of additive. This trend was acceptable on the crumb rubber modified asphalt binder except for the tin slag modified asphalt binder. There were no changes in the penetration and softening point for the tin slag modified asphalt binder, regardless of their concentrations. Nonetheless, the penetration and softening point of tin slag modified asphalt binder exhibited lower than the control asphalt binder. The increase in softening point is essential as the asphalt binder will be less temperature susceptible in resisting permanent deformation. The higher softening point and lower penetration value are due to the stiffening effect of additives. In addition, the different tin slag dosages have resulted in similar results for both the softening point and penetration value due to insufficient elastic response and stiffening effect of tin slag. Bitumen with imbalanced chemical compound and molecular weight distribution has presented a low penetration ratio and penetration index (PI) values resulting in high-temperature susceptibility. The asphalt binder was enhanced by reducing the temperature susceptibility, which led to a higher penetration index. As tabulated in Table 10, crumb rubber powder modified asphalt binders exhibited low susceptibility to temperature compared to the control asphalt binder as the crumb rubber content increased. Nevertheless, the tin slag modified asphalt binders are prone to temperature difference since the penetration index is much lower than the control asphalt binder due to the effects of softening point.

The incorporation of crumb rubber powder has a significant influence on the behavior of modified asphalt binders. The crumb rubber powder-based modified asphalt binder shows a linear increase for all types of rubberized asphalt binder. Elastic recovery findings were comparable to rubberized bitumen ductility outcomes as it demonstrates the high elasticity of modified asphalt binder and its recovery after deformation, enhancing the resistance behavior towards permanent deformation. The outcome of the test presented that a lower percentage of recovery indicated a better recovery. The elastic recovery findings improved for all concentrations of crumb rubber powder from 92.3% for unmodified asphalt binder to 54%, 37%, and 32% for 5%, 10%, and 15% for crumb rubber powder modified asphalt binders, respectively. The crumb rubber powder has significantly improved the elastic recovery and indicated that the asphalt binder could recover after removing a certain amount of strain load. This is caused by the natural elastic behavior of the crumb rubber powder, which is also an elastomer. However, the tin slag modified asphalt binders do not portray any elastic recovery since the findings are comparably similar to the control sample. This is because tin slag does not possess an elastic behavior as it is not an elastomer or plastomer. Conclusively, it inferred that the addition of crumb rubber powder significantly affected the basic properties of asphalt binder, while tin slag showed the opposite due to its inelastic behavior.

4.2.2. Torsional Recovery (TR).
Results for torsional recovery of asphalt base binder modified with CRP and TS at 5%, 10%, and 15% dosages are presented in Tables 11 and 12, respectively. The incorporation of CRP and TS as additives in asphalt binder changes the recovery percentage at 5%, 10%, and 15% compared to the control binder. The torsional recovery percentage of the binder with the incorporation of CRP in Table 11 portrayed a significant improvement in the elasticity of the asphalt binder at all percentages. Moreover, the highest and the least percentage recovery difference observed compared to the conventional asphalt binder were 9% and 1.7%, respectively. The addition of TS in the asphalt binder, as shown in Table 12, showed a contrary pattern as compared to CRP. The torsional recovery differences of 5%, 10%, and 15% modified TS binders in the conventional asphalt binder have identical values with 0.5% due to their similar torsional recovery angle observed.

TABLE 10: Basic properties of asphalt binders.

Properties	Control sample	Crumb rubber content (%)			Tin slag content (%)		
		5%	10%	15%	5%	10%	15%
Penetration, dmm	65	58	54	42	56	57	57
Softening point, °C	50	53	56	61	49	48	45
Penetration index	−0.574	0.217	0.957	2.062	−2.255	−2.255	−2.255
Elastic recovery, %	92.3	54	37	32	91.67	91	91.67
Ductility, cm	>100	>100	>100	>100	>100	>100	>100

TABLE 11: Torsional recovery results of CRP modified binders.

Asphalt binder	Recovered angle (°)	Torsional recovery (%)	% (differences) T_R
Control	1	0.6	—
5% CRP	4.2	2.3	1.7
10% CRP	11.1	6.1	5.5
15% CRP	17.2	9.6	9.0

TABLE 12: Torsional recovery results of TS modified binders.

Asphalt binders	Recovered angle (°)	Torsional recovery (%)	% (differences) T_R
Control	1	0.6	—
5% TS	2.0	1.1	0.5
10% TS	2.0	1.1	0.5
15% TS	2.0	1.1	0.5

Conclusively, it deduced that the incorporation of CRP and TS, which was influencing the formation of crystalline network lattice in the binder structure, resulted in returning the pointer of the apparatus to its initial position due to controlled recovery force.

4.2.3. Coatability Index. The coatability results for the conventional asphalt mixture (HMA) and wastes modified asphalt mixtures of CRP and TS are shown in Table 13. Subsequently, the averaged absorption of the three trials with loose mixes and the bare aggregates was tested, and the coating indexes were computed. The conventional HMA findings are compared with wastes modified asphalt mixtures. The coatability testing for the mixtures was conducted by using three different dosages at 5%, 10%, and 15% (CRP and TS), respectively. The results of asphalt added with CRP and TS were different from those of the controlled sample. The coating index of the mixture with CRP showed better performance at 5% dosage; meanwhile, TS performed better at 10% dosage. Moreover, the absorption of the aggregate particles was decreased due to the improvement in coating index by the modified asphalts. However, a low marginal difference was observed between different percentages of TS. The mixtures containing 15% CRP and TS showed the highest absorption rate corresponding to the lowest coating index. This indicates that absorption and coatability rate was dependent on the dosages and chemical compositions of waste materials. Likewise, the CRP exhibits more elastic and bonding characteristics than the TS. The results show reasonable trends in the variable percentages of CRP and TS in asphalt mixture compared to HMA.

TABLE 13: Coatability test results of the control and waste-modified asphalt mixtures.

Specimen	Water absorption of loose mix (%)	Coating index
Control	0.22	88.2
5% CRP	0.04	97.6
10% CRP	0.11	94.5
15% CRP	0.13	93.1
5% TS	0.09	95.3
10% TS	0.08	96.0
15% TS	0.14	93.0

5. Conclusion

This current study demonstrated the effects of differences in percentages of CRP and TS on the leaching potential, basic, and physical properties, as well as the coatability of asphalt binder. The obtained findings concluded that the quantity of CRP and TS waste materials in bitumen impacts the metal concentration present in mixtures with leachate solutions. Moreover, the higher percentage portion of CRP and TS resulted in a higher increment of the metals content. The existence of metals in bitumen mix was a minor concern due to their low quantity and minimum toxicity. Therefore, this study portrayed that CRP and TS metals content presents an insignificant source of hazard towards the environment and groundwater.

Furthermore, the basic properties of CRP and TS modified binders significantly improved the physical properties (softening point, penetration, elastic recovery, and coatability) of the conventional asphalt binder and modified binder. The modified binders with CRP

demonstrated a better improvement compared to the base asphalt binder and TS.

Torsional recovery results with CRP incorporation showed an obvious improvement inelastic response of the asphalt binder at all percentages compared to the base asphalt binder and TS samples. In addition, the TS showed an identical elastic response across the percentages considered.

Data Availability

The data used to support the findings of this study are available from the corresponding author upon request.

Disclosure

Any opinions, findings, and conclusions expressed in this manuscript are those of the authors and do not necessarily reflect the view of USM.

Conflicts of Interest

The authors declare that they have no conflicts of interest.

Acknowledgments

References

[1] S. Kumar and A. L. Thiruvangodan, *Waste tyre management in Malaysia*, PhD thesis, Universiti Putra Malaysia, Seri Kembangan, Malaysia, 2006.

[2] Paultan.Org, "Vehicle registrations in Malaysia hit 28.2 million units," 2017, https://paultan.org/2017/10/03/vehicle-registrations-in-malaysia-hit-28-2-million-units.

[3] M. S. Senin, S. Shahidan, S. R. Abdullah, N. A. Guntor, and A. S. Leman, "A review on the suitability of rubberized concrete for concrete bridge decks," *IOP Conference Series: Materials Science and Engineering*, vol. 271, no. 1, 2017.

[4] M. G. Mohamed and H. A. Laz, "Tire hazardous, disposal, and recycling," *Journal of Applied and Industrial Sciences*, vol. 2, no. 2, pp. 63–74, 2014.

[5] N. E. Khamsan, N. Bidin, S. Islam et al., "Recycling of pneumatic scrap tyre into nano-crumb rubber by pulsed laser ablation in different pH media," *Journal of Physics: Conference Series*, vol. 1027, no. 1, 2018.

[6] X. Shu and B. Huang, "Recycling of waste tire rubber in asphalt and portland cement concrete: an overview," *Construction and Building Materials*, vol. 67, pp. 217–224, 2014.

[7] V. Gopinath, A. M. Vijaya, and D. Prasannan, "An overview of recycling of crumb-rubber in asphalt and concrete structures," *International Journal on Applications in Civil and Environmental Engineering*, vol. 2, no. 4, pp. 17–22, 2016.

[8] M. Sulyman, M. Sienkiewicz, and J. Haponiuk, "Asphalt pavement material improvement: a review," *International Journal of Environment and Sustainable Development*, vol. 5, no. 5, pp. 444–454, 2014.

[9] K. Yan, H. Sun, L. You, and S. Wu, "Characteristics of waste tire rubber (WTR) and amorphous poly alpha olefin (APAO) compound modified porous asphalt mixtures," *Construction and Building Materials*, vol. 253, Article ID 119071, 2020.

[10] V. S. Punith, S. N. Suresha, S. Raju, S. Bose, and A. Veeraragavan, "Laboratory investigation of open-graded friction-course mixtures containing polymers and cellulose fibers," *Journal of Transportation Engineering*, vol. 138, no. 1, pp. 67–74, 2011.

[11] K. Yan, Z. Hong, L. You, J. Ou, and M. Miljković, "Influence of ethylene-vinyl acetate on the performance improvements of low-density polyethylene-modified bitumen," *Journal of Cleaner Production*, vol. 278, 2021.

[12] F. A. Aisien, F. K. Hymore, and R. O. Ebewele, "Application of ground scrap tire rubbers in asphalt concrete pavements," *Indian Journal of Engineering and Materials Sciences*, vol. 13, no. 4, pp. 333–338, 2006.

[13] D. Lo Presti, "Recycled Tyre Rubber Modified Bitumens for road asphalt mixtures: a literature review," *Construction and Building Materials*, vol. 49, pp. 863–881, 2013.

[14] Opus International Consultants Ltd, "Removing barriers to the use of crumb rubber in roads," NZ Transport Agency research report 578 Contracted research organization, Opus International Consultants Ltd, Wellington, New Zealand, 2015.

[15] B. George and P. E. Way, *Asphalt-Rubber Standard Practice Guide*, Rubber Pavement Association, Tempe, AZ, USA, 2011.

[16] S. Liu, W. Cao, J. Fang, and S. Shang, "Variance analysis and performance evaluation of different crumb rubber modified (CRM) asphalt," *Construction and Building Materials*, vol. 23, no. 7, pp. 2701–2708, 2009.

[17] N. S. Mashaan, A. H. Ali, M. R. Karim, and M. Abdelaziz, "A review on using crumb rubber in reinforcement of asphalt pavement," *Science World Journal*, vol. 2014, Article ID 214612, 2014.

[18] "The boon and bane of rising tin prices," 2018, https://www.theedgemarkets.com/article/boon-and-bane-rising-tin-prices.

[19] A. Rustandi, F. W. Nawawi, Y. Pratesa, and A. Cahyadi, "Evaluation of the suitability of tin slag in cementitious materials: mechanical properties and leaching behavior," *IOP Conference Series: Materials Science and Engineering*, vol. 299, no. 1, 2018.

[20] A. M. Rodríguez-Alloza, J. Gallego, I. Pérez, A. Bonati, and F. Giuliani, "High and low temperature properties of crumb rubber modified binders containing warm mix asphalt additives," *Construction and Building Materials*, vol. 53, pp. 460–466, 2014.

[21] W. Huang, P. Lin, N. Tang, J. Hu, and F. Xiao, "Effect of crumb rubber degradation on components distribution and rheological properties of terminal blend rubberized asphalt binder," *Construction and Building Materials*, vol. 151, pp. 897–906, 2017.

[22] L. Han, M. Zheng, and C. Wang, "Current status and development of terminal blend tyre rubber modified asphalt," *Construction and Building Materials*, vol. 128, pp. 399–409, 2016.

[23] A. Razmi and M. M. Mirsayar, "Fracture resistance of asphalt concrete modified with crumb rubber at low temperatures," *International Journal of Pavement Research and Technology*, vol. 11, no. 3, pp. 265–273, 2018.

[24] H. Yu, Z. Leng, F. Xiao, and Z. Gao, "Rheological and chemical characteristics of rubberized binders with non-foaming warm mix additives," *Construction and Building Materials*, vol. 111, pp. 671–678, 2016.

[25] M. A. W. Yusof, *Investigating the potential for incorporating tin slag in road pavements*, PhD thesis, University of Nottingham, Nottingham, UK, 2005.

[26] "Method 1311, toxicity characteristic leaching procedure," 2015, https://www.epa.gov/sites/production/files/2015-12/documents/1311.pdf.

[27] "Hazardous waste characteristics, a user-friendly reference document," 2016, https://www.epa.gov/sites/production/files/2016-01/documents/hw-char.pdf.

[28] ASTM D5, *Standard Test Method for Penetration of Bituminous Materials*, American Society for Testing Materials, Conshohocken, PA, USA, 1997.

[29] ASTM D36, *Standard Test Method for Softening point of Bitumen (Ring-and-ball Apparatus)*, American Society for Testing Materials, Conshohocken, PA, USA, 1995.

[30] AASHTO T51, *Standard Method of Test for Ductility of Asphalt Materials*, The American Association of State Highway and Transportation Officials, Washington, DC, USA, 2009.

[31] ASTM D6084, *Standard Test Method for Elastic Recovery of Asphalt Materials by Ductilimeter*, American Society for Testing Materials, Conshohocken, PA, USA, 1997.

[32] ARRB AG:PT/T122, *Torsional Recovery of Polymer Modified Binders*, Australia Road Research Board, Sydney, Australia, 2006.

[33] AASHTO T 195, *Standard Method of Test for Determining Degree of Particle Coating of Asphalt Mixtures*, The American Association of State Highway and Transportation Officials, Washington, DC, USA, 2011.

[34] A. Jamshidi, *Rheological properties of asphalt binders, performance and sustainability of warm-mix asphalt incorporating sasobit®*, PhD thesis, University Sains Malaysia, George, Malaysia, 2013.

[35] R. Velasquez, G. Cuciniello, D. Swiertz, R. Bonaquist, and H. Bahia, "Methods to evaluate aggregate coating for asphalt mixtures produced at WMA temperatures," in *Proceedings of the CTAA Annual Conference Proceedings-Canadian Technical Asphalt Association*, vol. 57, p. 225, Vancouver, Canada, November 2012.

[36] F. Yin, E. Arambula, D. Newcomb, and A. Bhasin, "Workability and coatability of foamed warm-mix asphalt," in *Proceedings of the Asphalt Pavements-International Conference on Asphalt Pavements, ISAP 2014*, vol. 1, pp. 721–730, Raleigh, NC, USA, June 2014.

[37] ASTM D 2872, *Standard Test Method for Effect of Heat and Air on a Moving Film of Asphalt (Rolling Thin-Film Oven Test)*, American Society for Testing Materials, Conshohocken, PA, USA, 1997.

[38] M. R. M. Hasan, Z. You, H. Yin, M. O. Hamzah, S. Chen, and F. Gong, "Assessments of potential service characteristics of ethanol and ethanol-NaHCO$_3$ foamed WMA mixtures," *Journal of Materials in Civil Engineering*, vol. 31, no. 6, Article ID 04019079, 2019.